Automated Dry Fiber Placement and Resin Infusion for Fabrication of Composite Aerostructures

Farid Ehsani

A thesis

in

The Department

of

Mechanical, Industrial & Aerospace Engineering

Presented in Partial fulfillment of the requirements

for the Degree of Master of Applied Science

(Mechanical Engineering)

Concordia University

Montreal, Quebec, Canada

December 2022

Concordia University

School of Graduate Studies

This is to certify that the thesis prepared

By: **Farid Ehsani**

Entitled: **Automated Dry Fiber Placement and Resin Infusion for Fabrication of**
                                  Composite Aerostructures

and submitted in partial fulfillment of the requirements for the degree of

Master of Applied Science (Mechanical Engineering)

Complies with the regulations of this University and meets the accepted standards with respect to originality and quality.

Signed by the final examining committee:

_____Examiner

Dr. Ramin Sedaghati

_____Examiner

Dr. Mehdi Hojjati

_____Supervisor

Dr. Suong V. Hoa

_____Supervisor

Dr. Farjad Shadmehri

Approved by:

_____

Dr. Sivakumar Narayanswamy, MASc Program Director

Department of Mechanical, Industrial & Aerospace Engineering

_____

Dr. Mourad Debbabi, Dean

Faculty of Engineering and Computer Science

Date: _____

Abstract

Automated Dry Fiber Placement and Resin Infusion for Fabrication of Composite Aerostructures

Farid Ehsani

This dissertation targets the development of the Automated Dry Fiber Placement (ADFP) process in combination with Vacuum Assisted Resin Infusion (VARI), which allows producing high-performance aerostructures (i.e., fuselage panels, etc.) at a reduced cost in comparison with conventional composite manufacturing techniques. Using Vacuum Assisted Resin Infusion (VARI) at high temperature, epoxy resin can be infused into the bed of dry fibers made by Automated Dry Fiber Placement to make the composite laminate.

The resin flow rate depends on the permeability of the dry fiber preform, which is dependent on the preform fiber volume fraction. Automated Dry Fiber Placement (ADFP) allows the capacity to control the fiber volume fraction in terms of gaps between the tows. So, reducing the fiber volume fraction of preforms by introducing gaps into the preform pattern can increase the through the thickness permeability. On the other hand, introducing gaps in the pattern results in a drop in the mechanical properties of the laminate (such as compressive modulus and strength). An optimum gap size may provide a significant gain in the through the thickness permeability with minimum loss in compressive properties.

In this thesis, firstly, process challenges in ADFP and VARI processes, including the formation of various defects, are identified, and solutions to overcome them are introduced. Second, process parameters for ADFP and VARI are introduced. Thirdly, this thesis investigates the effect of the increasing gap size in the preforms layup on the through the thickness permeability of the preform and compressive properties of the laminate. Finally, in this thesis, four fuselage panels were fabricated using ADFP and VARI at high temperature (inside oven), and the quality of obtained laminates was analyzed.

Keywords:

Automated dry fiber placement, Dry fiber, Resin infusion, Transverse permeability, Gap, Compressive properties, Fuselage Demonstrator

Acknowledgements

Table of Content

List of Figures

List of Tables

Chapter 1. Introduction

Aerospace is a reputed industry in Montreal with $31 billion in revenues and annual sales of more than $15 billion. Montreal is reported as the world's 3rd largest center of aerospace and the only area in the world where an entire aircraft can be assembled from locally manufactured components. This potential has offered close to 60,000 job opportunities in Quebec, mainly in the advanced industries [1], [2].

Rising needs for composite structures in different industries, such as automotive, biomedical and energy, especially aerospace, make automated manufacturing techniques attractive. For instance, in 2015, composite materials consisted of 53% of the total weight of Airbus aircraft and had doubled from 2010 (Figure 1)[3]. This high demand for polymer-matrix composites (PMC) advocates the development of automated manufacturing techniques for different applications. In particular, the Automated Fiber Placement (AFP) process can be addressed as a new approach for manufacturing large-scale complex composite structures like wing skins and spars for Airbus A350 XWB [4]. Compared to traditional techniques, it has many advantages, such as reducing material waste, increasing the production rate, and reducing costs. Although AFP requires lower technician times than conventional methods like hand layup, the materials used for the AFP process are costly.

Conventionally, in the aviation industry, pre-impregnated fibers with resin (prepreg) are deposited using AFP machines (gantry or robotic) and then after making layup, they are transferred into autoclave for consolidation. Using this developed and mature process, composite structures can be manufactured with high quality compatible with aerospace industry standards. For instance, Bombardier Aviation uses Coriolis AFP systems to manufacture bulkheads and three fuselage skins assembled into the A-220 fuselage as the CSeries aircraft [5]. However, there are some disadvantages to be pointed out. First, prepreg materials are expensive materials with a limited working/shelf life. Second, the need for autoclave consolidation makes the process significantly more energy-consuming than curing inside the thermal oven [6]. The AFP infrastructure with high capital expenditure is usually cost-prohibitive to produce smaller components and offers limited flexibility to tackle complex geometries. From this point of view, there is a need to develop intermediate PMC processing options between hand layup and the conventional AFP process.

Recently, dry fiber materials were developed and introduced as an out-of-autoclave replacement for prepreg materials. Unlike pre-impregnated materials (prepreg), dry fiber materials have no matrix inside their structures; however, they can consist of substances to keep the fibers together and increase resin infiltrating in infusion [7], [8]. Taking advantage of dry fibers could lead the industry to a method that saves material costs and energy consumption. Automated Dry Fiber Placement (ADFP) can fabricate complex preforms (e.g., preforms with cut-outs) with the ability to steer fibers, which is more accessible than prepregs due to the lack of the matrix inside the microstructure. Dry fiber preforms made by ADFP can be impregnated by resin transfer molding (RTM) process, such as vacuum-assisted resin infusion (VARI), as an out-of-autoclave process, without requiring high investment for equipment and training technicians. Due to low-cost equipment and high-quality results obtained from VARI, these methods are desirable in composite manufacturing [9].
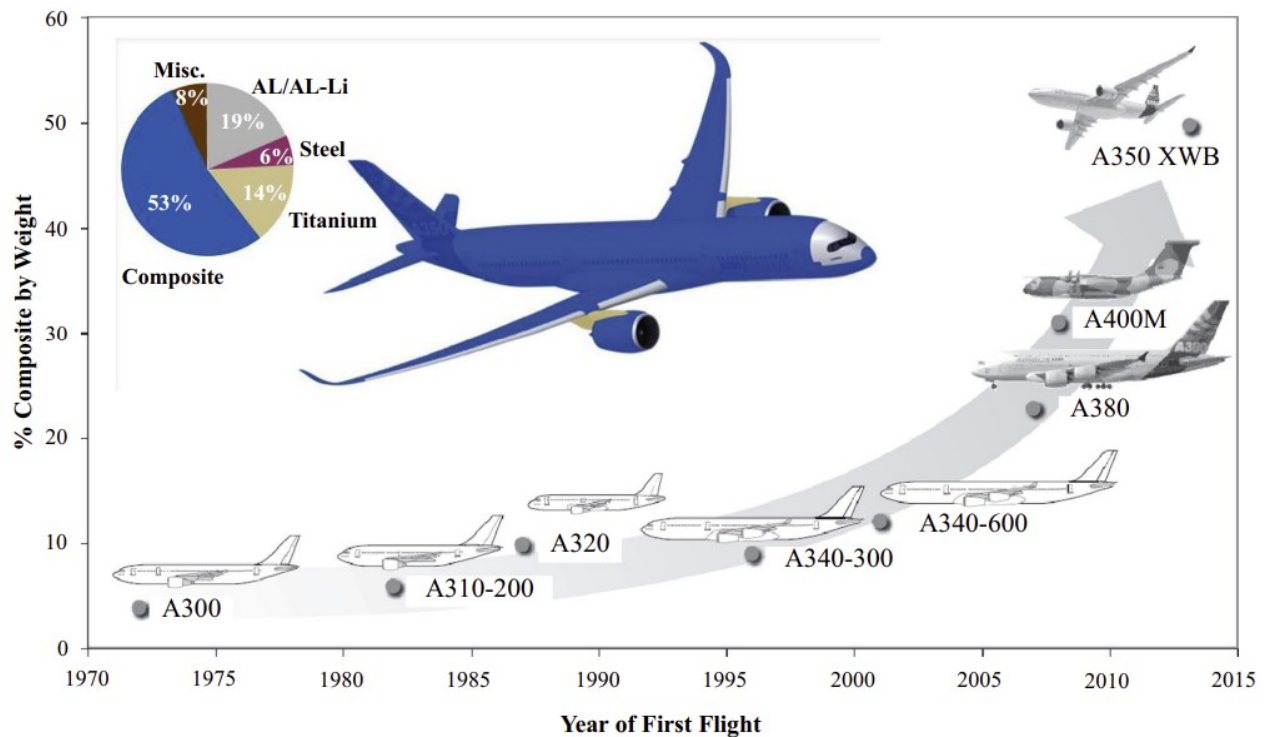
Figure 1. Use of composite materials in Airbus aircraft [3]

However, using AFP-made preforms can be challenging in vacuum infusion. Since a compaction load is applied on the preforms for depositing in the AFP process, they have low permeability, making impregnation difficult. Permeability is the fiber's attribute that shows the flow's ease through the fiber reinforcement, in which the fiber bundle's anisotropic behavior results

in different permeabilities magnitude in different directions [10]. The AFP machine can introduce gaps of various sizes between tows, reducing the fiber content and increasing permeability. However, these gaps could reduce the mechanical strength of laminate since fiber content is lower than the same architecture without gaps.

This thesis targets developing the Automated Dry Fiber Placement (ADFP) process in combination with infusing resin into a dry perform using Vacuum Assisted Resin Infusion (VARI), which allows producing high-performance aerostructures (e.g., fuselage panels, etc.) at a much lower price in comparison with conventional autoclave processes. However, several scientific challenges must be addressed here; mechanical behaviors of ADFP-made laminates, geometrical stability of dry fiber preforms, thickness spring back over time, binder effects on preform architecture and performance, low permeability, etc.

Chapter 2. Literature Review

2.1 Automated Fiber Placement

Interest in composite structures in the aerospace industry has increased due to their high performance and durability of composite structures which have led to the development of automated manufacturing techniques. These methods can significantly save labor time and decrease material scrap. Automated tape laying (ATL) and automated fiber placement (AFP) are two main automated processes which are utilized to manufacture composite structures [11]–[13]. Figure 2 shows the increasing interest in the AFP and ATL process by increasing the number of publications over time. Usually using AFP and ATL, prepreg materials are laid down on the flat or curved surface, controlling the feeding rate, tape tension and temperature. Although the ATL process is similar to AFP, ATL employs wide prepreg tapes (typically 3-in to 12-in) in comparison to the AFP tapes, which have narrow widths (1/8-in to 1/2-in) [14]. A study by Lukaszewicz et al. [15] showed that the estimated productivity of AFP as a function of part size and speed for a simple flat part would be higher than ATL due to optimized layup time and better cutting system. However, considering the error correction and material filling can reduce the productivity up to 50 % for AFP.
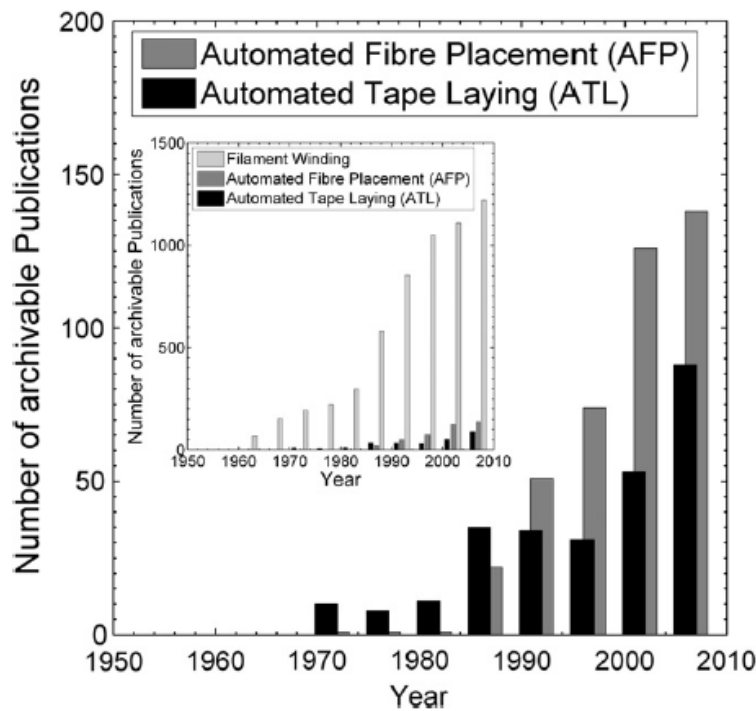
Figure 2. Annual publication on ATL and AFP [15]

4

2.1.1 Automated Dry Fiber Placement

Choosing the autoclave method for composites structures curing has resulted in manufacturers investing large amounts of capital in the autoclave curing process. Using heat and pressure in autoclave methods leads to high fiber volume fraction. However, the high operational costs associated with autoclaves raised the idea of developing automated methods which can save energy and cost related to the autoclave. As composite materials usage has significantly increased in the aerospace industry, some out-of-autoclave (OOA) techniques have been developed to reduce operation costs. Witik et al. [6] conducted a detailed economic and environmental analysis to compare autoclave curing and other selected OOA processes. Considering a 400 x 400 x 4 mm carbon fiber reinforced panel, five below material/curing methods were compared.

1. Autoclave processing with unidirectional carbon fiber prepreg (Auto PP).
2. Thermal oven curing with a carbon fiber OOA prepreg system (Therm PP).
3. Microwave oven curing with a carbon fiber OOA prepreg system (Micro PP).
4. Thermal oven curing with liquid resin-infused carbon fiber non-crimp fabric (Therm inf).
5. Microwave oven curing liquid resin-infused carbon fiber non-crimp fabric (Micro inf).

Figure 3 shows the result of cost modelling based on studied parameters, including equipment, tools, labor, energy, consumables and materials. It indicates that methods using prepreg materials have a considerable share of materials in total cost. Also, equipment cost is high in the autoclave process, among other techniques.
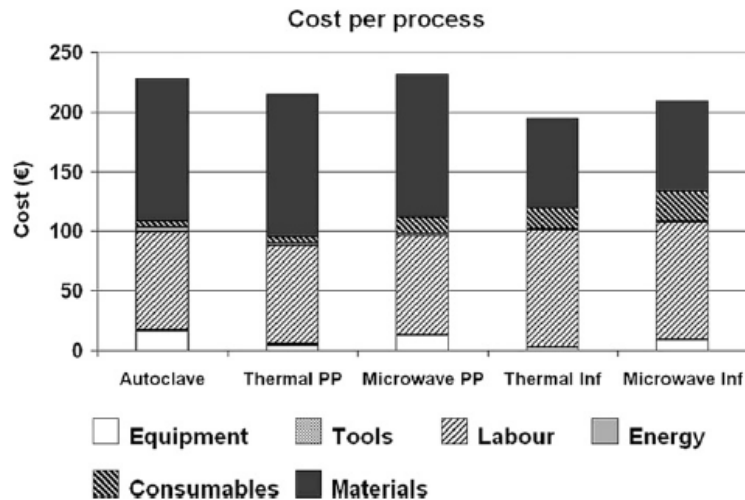
Figure 3. Total production costs per panel for all methods (in Euro) [6]

Research by Gruber et al. [16] compared OOA processes (e.g., thermoplastic in situ consolidation, thermoset AFP with oven curing, vacuum-assisted resin transfer molding, etc.) with prepreg AFP/autoclave consolidation. The objective was to find an optimized out-of-autoclave process for fabricating a sizeable composite part like the RLV liquid hydrogen tanks. Figure 4 indicates that VARTM has the lowest cost among other methods in terms of material and equipment costs. However, VARTM only provides vacuum pressure in the final cure, which is lower than autoclave pressure.
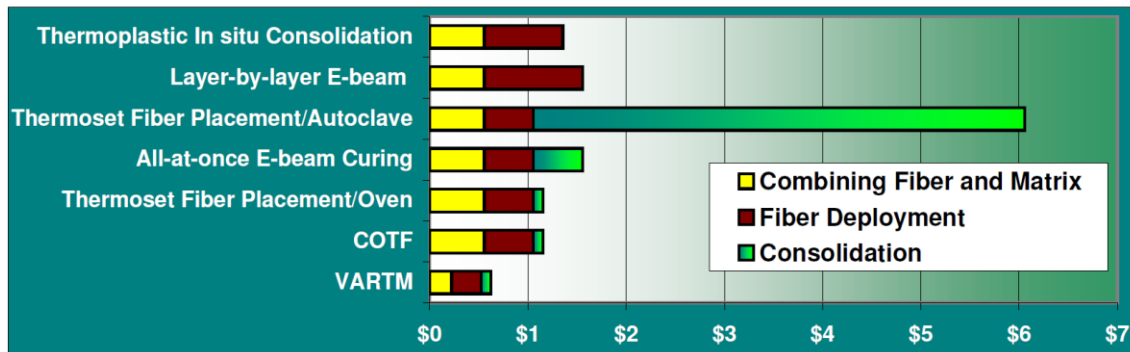
Figure 4. Comparison of the cost of material and equipment acquisition amortized for ten Reusable Lunch Vehicles LH2 (millions of dollars) [13]

Automated dry fiber placement (ADFP) not only requires low-cost materials but also eliminates the need for autoclave curing, which results in energy savings compared to the automated placement of prepregs/autoclave process. As preforms made by ADFP need to be impregnated by resin, combining the ADFP with resin transfer molding methods (RTM) provides a possibility of the OOA method. The Ph.D. thesis by Veldenz [16] indicates that the infusion method has low equipment cost and the ability to fabricate complex geometries. On the other hand, AFP/prepreg method has lower geometrical flexibility and uses materials with limited shelf time (see Table 1)

Table 1. Comparison between advantages and disadvantages of prepreg AFP and infusion methods [17]

	(a) Prepreg AFP	(b) Infusion of textiles
Advantages	Automated process	Low initial investment and tooling costs
	High quality laminate	Out-of-autoclave process
	High repeatability	Can achieve complex geometries
Disadvantages	Requires autoclave	Disposable consumables
	Limited geometrical flexibility	Labour intensive process
	Limited shelf life and frozen storage	High precursor material waste

A study performed by Liu et al. [7] investigated the results of the combination of fabrication of dry fiber by automated fiber placement (AFP) with vacuum assisted resin infusion (VARI). This study presented the ADFP and VARI as an alternative proposal to the manual hand-layup process for manufacturing high-performance composite structures out-of-autoclave. It shows that ADFP provides less porosity of 0.60%, better surface flatness with a coefficient in thickness variation of 3.75%, compared to 8.11% for manually lay-up laminates, and 8.5 % higher fiber content. Figure 5 demonstrates that laminates made by ADFP have compacted fibers in their structure compared to manual hand-layup. However, the ADFP prolongs the infusion time by 107.71% due to lower permeability which needs a solution to reduce the infusion time.
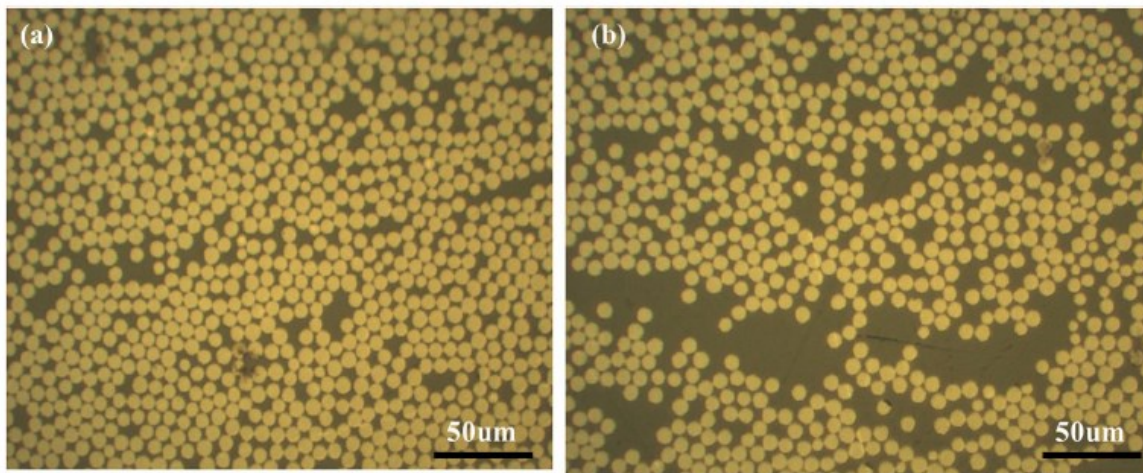
Figure 5. Metallographic photos of (a) ADFP-based laminate and (b) manually lay-up laminate [7]

Due to the long infusion time, without further research and development in ADFP, dry fibers cannot be considered alternatives for prepregs materials. Characterization of available dry fiber materials helps the manufacturer to use proper process parameters to utilize them. Additionally, identifying the process parameters of the AFP and correlating them with the quality of the cured laminate could be effective in developing automated dry fiber placement (ADFP). Veldenz et al. [18] proposed a material selection method of dry fibers for AFP using the analytical hierarchy process to encourage industries to adopt these materials. They compared five dry fiber materials based on the five primary criteria (procurement, raw material characteristics, AFP deposition process, consolidation process, and laminate characteristics). This method demonstrated that Solvay dry fiber material had the highest priority among available materials. Table 2 shows the

different defect types observed during AFP deposition using dry fiber materials, which could help the manufacturer to use these materials.

Table 2. Common defects observed in the AFP [19]

Observed fault types	
• Fiber fluff	• Overlap
• Binder residue inclusion	• Gap (>2 mm)
• Twisted tow	• Shearing
• Fiber folding	• Loose fibers on the surface

2.2 Permeability

"Permeability is a characteristic of the bed of fibers that indicates the ease (or difficulty) for the resin to penetrate the bed of fibers" [10]. Permeability characteristic is principally a function of fiber volume content which depends on the fiber architecture and can be used in Darcy's law equation to predict the flow rate[10], [20]–[23]. Permeability is measured by flow rate measurement through a bed of fiber (either saturated or unsaturated) under pressure difference. Due to the anisotropic behavior of fiber, the permeability of a preform along the fiber, in-plane permeability, is higher than the permeability transverse to the preform, out-of-plane permeability. Usually, high out-of-plane permeability is essential to prevent delamination by ensuring the last layers are impregnated and bonded.

A benchmark exercise by Yong et al. [23] indicated that the out-of-plane permeability measurement of a preform, which is normal to the plane of fibers, i.e. out-of-plane or through the thickness, is more complex because of the shorter distance for the resin to travel. It also compared different methods used in scientific studies, including saturated and unsaturated, for three specified target fiber volume fractions (46%, 50%, and 54%). Figure 6 shows the scatter of participants' data on out-of-plane permeability measurement of a biaxial ±45° E-glass fiber non-crimp fabric. It can be seen that the target fiber volume fractions were not reached precisely due to the differences in the preform layup and used cavity height among studies. Also, it shows the considerable scatter in each permeability zone, confirming the permeability measurement's complexity.
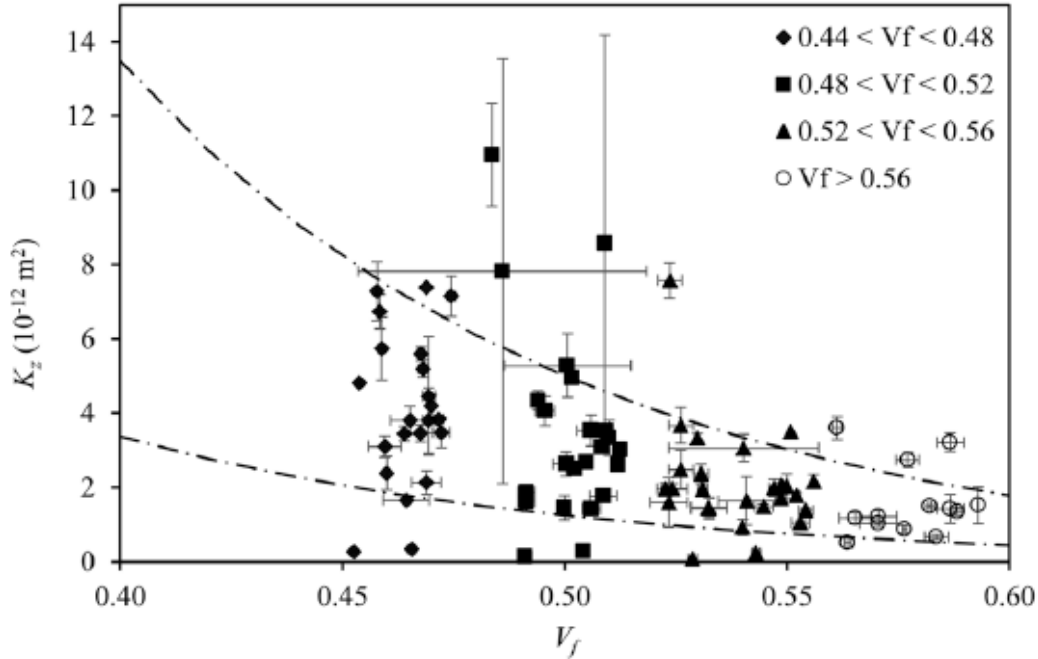
Figure 6. Out-of-plane permeability - fiber volume fraction (Dashed lines indicate a band of values where the ratio between the upper and lower bound is 4) [23]

Some experimental study has been done to measure the out-of-plane permeability of dry preforms made by ADFP. Belhaj et al.[20] characterize the out-of-plane permeability of ADFP preforms using nominal (no space between fiber tows), open (spacing of 2 mm every five fiber tows) and overlap patterns (reducing the displacement of 2 mm every five fiber tows). Table 3 indicates that overlapping tows on the tool reduce the out-of-plane permeability and provides more resistances against the flow. Also, fiber sliding can partially fill the channel during the vacuum compaction, which leads to permeability reduction in preforms with the open pattern. Therefore, these preforms have similar permeability with nominal patterns but higher than overlap patterns.

Table 3. Out-of-plane permeability of ADFP preform with nominal, open, and overlap patterns [20]

	Nominal preform		With open pattern		With overlap pattern	
	$V_f = 54\%$	Under vacuum	$V_f = 54\%$	Under vacuum	$V_f = 54\%$	Under vacuum
Thickness (mm)	1.5	1.8	1.4	1.7	1.6	1.9
Permeability K (m^2)	1.44×10^{-12}	5.15×10^{-12}	1.49×10^{-12}	5.21×10^{-12}	1.06×10^{-12}	3.15×10^{-12}
Fiber volume fraction V_f (%)	54	45	54	44	54	46.5

Aziz et al. [22] measured the out-of-plane permeability of dry preforms made by ADFP using two Prism TX1100 tapes, 6.35 and 12.7 mm wide, with a target 0.2 mm gap size between the tapes. Also, they created a geometrical model of dry fiber preforms validated by the experimental results to study the effect of gap size on the out-of-plane permeability. Figure 7 demonstrates the effect

of gaps on the out-of-plane permeability using the developed geometrical model. It also shows the effect of alternating the gap size by introducing 0.2 mm gaps between these gaps, which reduced the permeability of 0.3- and 0.4-mm gap width and increased the permeability of the 0.1 mm gap.
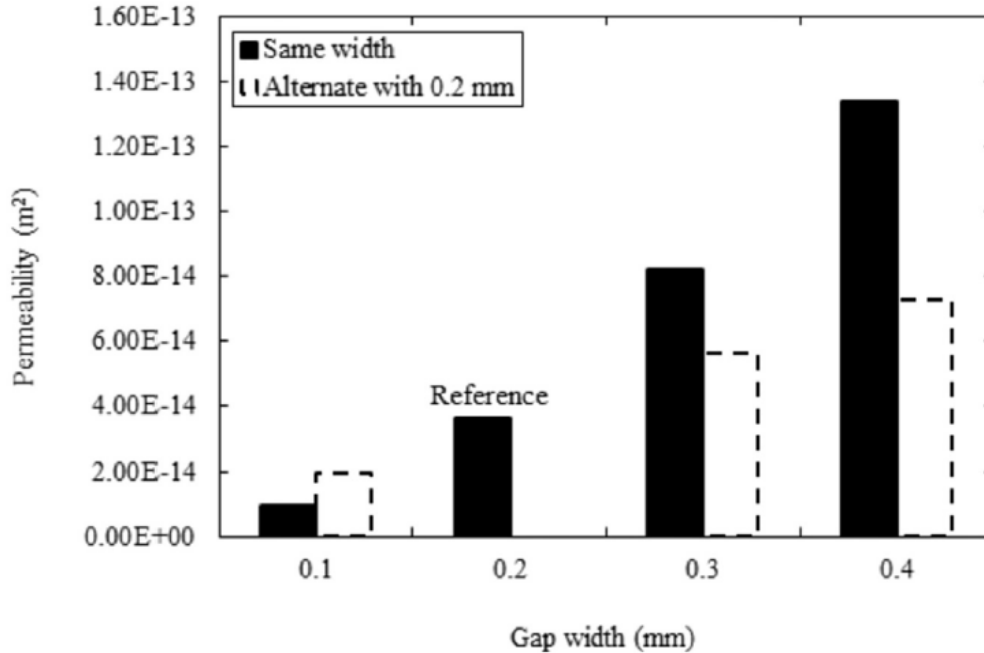
Figure 7. Comparison of permeability simulation results for different gap sizes [22]

In this work, X-ray Computed Tomography (X-CT) analysis was used to show the variability of the gaps performed by the AFP machine. Table 4 indicates that CFD simulations predicted the out-of-plane permeability of preforms made by 12.7 mm wide tapes (Preform B) about 90% lower than preforms made by 6.35 mm wide tapes (Preform A). However, the experimental values show that the average permeability of Preform B is about twice of Preform A. It is noteworthy that an unpaired two-tail t-test with criteria of 0.05 demonstrates that there is no significant statistical difference in the experimental values. Using images taken by the X-CT machine, the average gap widths in the 45, 0, 90, and -45 were calculated for both preforms. It was observed that the % gap for preform A was overestimated in the CFD model as it was about 2.1 times lower. This difference in the calculated % gap by CFD and the measured % gap by X-CT can explain the difference in the measured and simulated permeability. Therefore, modifying the model using the % gap measured by X-CT improved the simulations of permeability.

Table 4. Comparison of experiment and simulation result of permeability of the dry fiber with different width [22]

Preform sample	Tape width (mm)	% Gaps		Permeability [m²]					%Error (Exp vs. Design)	%Error (Exp vs. X-CT)
		Design	X-CT	Experiment			CFD (Design)	CFD (X-CT)		
				Test	Average	Unpaired t-test p-value				
Preform A	6.35	3.1	1.5	8.51×10^{-14} 7.66×10^{-14} 8.75×10^{-14}	8.31×10^{-14}	0.07	3.87×10^{-13}	7.47×10^{-14}	366	-10
Preform B	12.7	1.5	3.5	2.52×10^{-13} 1.09×10^{-13} 1.94×10^{-13}	1.85×10^{-13}		3.65×10^{-14}	2.04×10^{-13}	-80	10

Lionetto et al. [24] measured the out-of-plane permeability of a preform made by TX1100 dry fiber using unsaturated flow for validating the resin infusion simulation of a stiffened laminate made by ADFP. A single ultrasonic transducer was used in the permeability measurement setup to track the thickness flow front during a vacuum-assisted resin infusion. In this study, the in-plane permeability of the preform was measured by recording the flow front using a video camera on top of the setup. Table 5 shows the measured permeabilities in principle directions for the TX1100 preform. It demonstrates that out-of-plane permeability order is way lower than in-plane permeabilities.

Table 5. Permeabilities of the TX1100 preform [24]

Permeability	TX1100 Preform
K_1 (μm^2)	2.81 ± 0.55
K_2 (μm^2)	0.38 ± 0.43
K_3 (μm^2) [18]	0.043 ± 0.009

2.3 Vacuum Assisted Resin Infusion (VARI)

The resin infusion process is considered an inexpensive liquid transfer molding process that has been used in the industry for a long time. The governing equation for the resin flow in all Liquid Composite Molding (LCM) processes like Vacuum Assisted Resin Transfer Molding (VARTM) is Darcy's Law which relates the flow rate and the pressure drop within the media where liquid flow through. Seemann's composite resin infusion process (SCRIMP [25]) is one of the favored VARTM methods. In this method, a layer of distribution media (i.e., flow mesh, mesh media) is added to the setup to improve the in-plane flow efficiently through the VARTM process. This layer allows the resin to impregnate the fiber bed quickly and reduces manufacturing time [26]. Glancey [26] explained that unlike in-plane flow in RTM and VARTM, flow is three-

dimensional in SCRIMP and fiber permeability characterization in all directions and distribution media permeability is essential (see Figure 8).
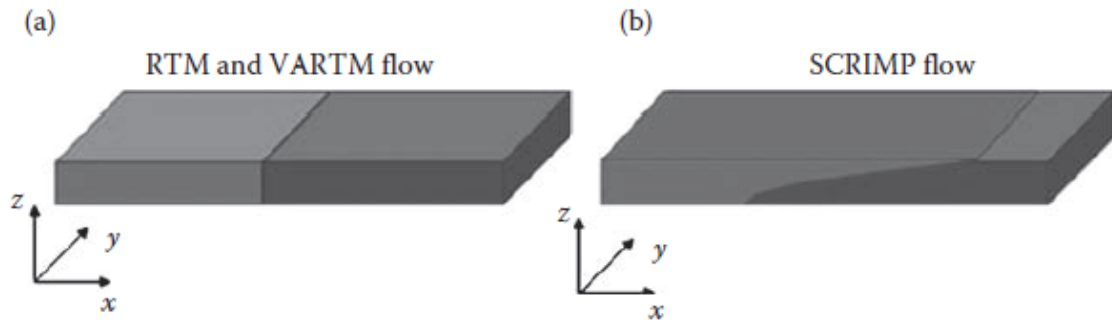
Figure 8. Flow front pattern in (a) RTM and VARTM (b) SCRIMP [26]

A study by van Oosterom et al. [9] compared six standard VARTM methods based on process parameters and physical and mechanical properties of the finished parts. They demonstrated that a preform infused with Seemann's composite resin infusion process (SCRIMP) had very good thickness homogeneity among all other common vacuum-assisted resin infusion methods with void contents below 0.2%. It also presented the vacuum-assisted process (VAP), which has a similar setup to SCRIMP and utilizes a permeable membrane in addition to SCRIMP. In this method, the membrane layer creates an inner chamber holding the resin in and extracting gasses and air to go outside the setup through the outer chamber formed by the vacuum bag. This paper demonstrated that using the VAP method can fill the same laminate geometry 13% faster than the SCRIMP method. This research studied six standard infusion methods by comparing process parameters, including infusion time, laminate and pot pressure, laminate thickness, resin mass in the reservoir at the inlet, and laminate void formation (see Table 6).

Table 6. Process parameters of infusion methods [9]

	VARTM	SCRIMP	DBVI	CAPRI	PI	VAP
Infusion time (s)	3426	634	2075	1010	1201	551
Resin mass (g)	302	367	490	279	384	352
Max laminate pressure (Bar)	0.949	0.881	0.985	0.410	1.024	0.859
Max relaxation (mm)	0.594	0.420	0.907	0.062	1.921	0.466
Final pressure inlet (Bar)	0.569	0.562	0.793	0.124	0.947	0.140
Final pressure mid (Bar)	0.472	0.553	0.792	0.116	0.868	0.139
Final pressure outlet (Bar)	0.347	0.552	0.789	0.110	0.699	0.134
Post-cure thickness inlet (mm)	3.18	3.10	3.34	2.83	3.76	2.96
Post-cure thickness outlet (mm)	3.02	3.06	3.13	2.80	2.98	2.97

A study by Hubert et al. [27] showed that distribution media layer existence in the setup increases the exothermic temperature by 16.4 C for a 28 mm thick panel. It also demonstrated that the distribution media changes the residual stress distribution in the C-shaped laminate manufactured using VARTM (Figure 9 and Figure 10).
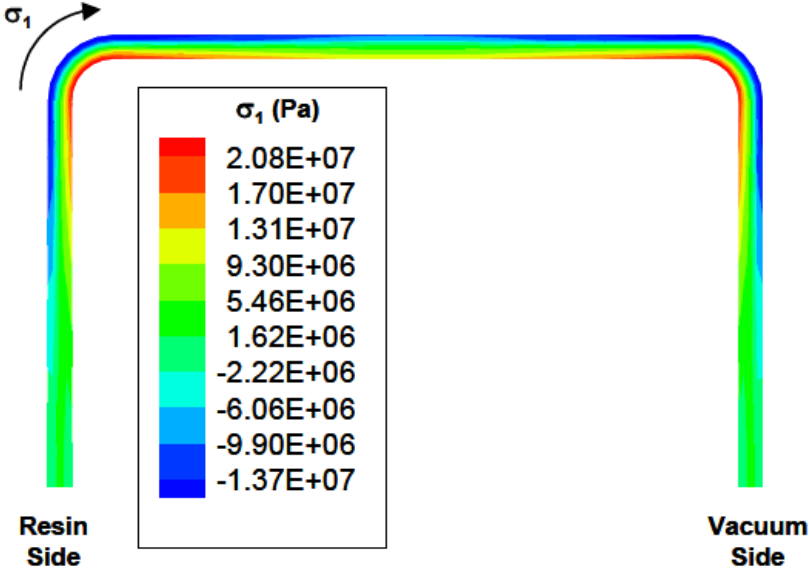
Figure 9. Longitudinal stress distribution at the end of cure for the C-shaped laminate infused without the distribution media [27]
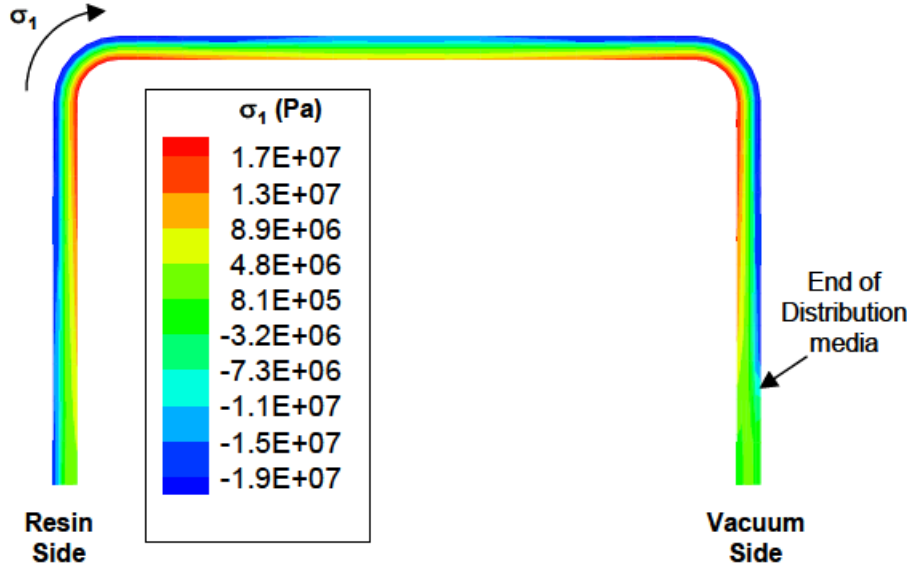
Figure 10. Longitudinal stress distribution at the end of cure for the C-shaped laminate infused with the distribution media [27]

2.4 Mechanical Evaluation of Laminate made by ADFP and VARI

Using dry fiber materials needs to have comparable outcome quality to prepreg materials. Dell'Anno et al. [8] showed promising tensile and in-plane shear properties of laminate made by ADFP using Porcher and Hexcel tapes. Table 7 shows the mechanical performance evaluation of laminates made by ADFP and infusion using HiTape and Porcher dry fibers. Results demonstrate that Solvay's resin gives better transverse tensile strength and modulus.

Moreover, they suggested that through-the-thickness reinforcing by tufting can overcome delamination failure. Due to out-of-plane loads caused by the lack of fibers along the Z direction, the matrix should tolerate the out-of-plane loads.

Table 7. Mechanical performance of ADFP carbon/epoxy laminates [8]

Test	Property	Hexcel tape HexFlow RTM6	Hexcel tape Prism EP2400	Porcher tape Cycom 890RTM
Tensile 0°	Modulus (GPa)	142 ± 3	143 ± 7	135 ± 5
	Strength (MPa)	2,160 ± 100	2,200 ± 190	2,220 ± 150
	Ultimate strain (%)	1.44 ± 0.13	1.45 ± 0.05	1.53 ± 0.08
Tensile 90°	Modulus (GPa)	7.2 ± 0.1	7.8 ± 0.3	7.8 ± 0.5
	Strength (MPa)	33.3 ± 2.4	47.2 ± 7.9	62.1 ± 4.1
	Ultimate strain (%)	0.46 ± 0.03	0.41 ± 0.28	0.83 ± 0.06
In-plane shear	Modulus (GPa)	3.8 ± 0.3	4.1 ± 0.5	4.2 ± 0.3
	Strength (MPa)	63 ± 1.3	61.6 ± 2.5	68.3 ± 0.5

In a master dissertation by Gharabegi [28], the mechanical properties of carbon/epoxy laminates made by ADFP/VARI were compared with laminates made by conventional autoclave/prepreg and out of autoclave prepreg. Tensile, compression, short beam shear, open hole tension (OHT), and open hole compression (OHC) tests were considered for the comparison. For the ADFP/VARI process, preforms made by Hexcel's HiTape IM7 dry fiber were infused using the Solvay Prism EP2400 epoxy system. The chosen materials for the baselines are Hexcel's HexPly IM7 8552 for autoclave prepreg and Cytec's IM7 5320-1 for OOA prepreg. The significant difference between laminates made by ADFP/VARI and the conventional process is compressive strength which is closely dependent on the epoxy system. Figure 11 illustrates that the laminate made by ADFP/VARI had 17% and 35% lower strength than autoclave prepreg in OHC and compression 0°, respectively.
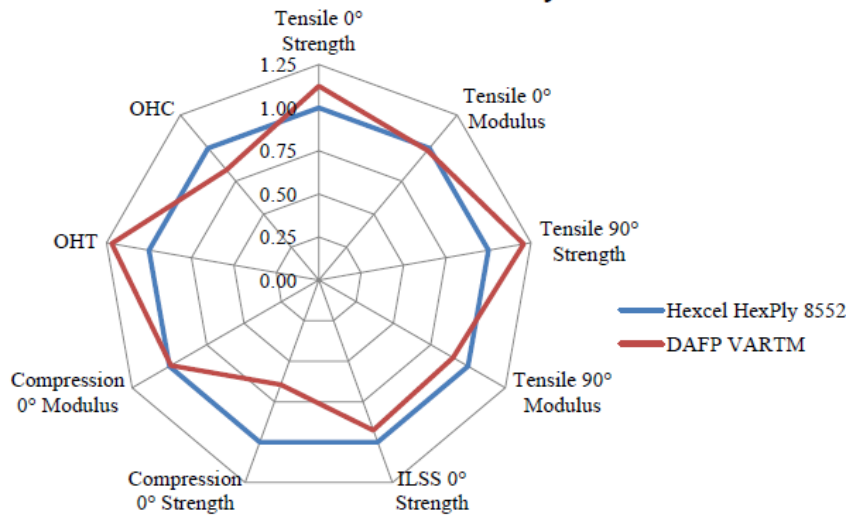
Figure 11. Comparison of laminates made by ADFP/VARI and autoclave prepreg in mechanical performance [28]

Also, Figure 12 shows that the laminate made by ADFP/VARI had 24% and 46% lower strength compared to OOA prepreg in OHC and compression 0°, respectively. It was mentioned that using old epoxy to infuse the ADFP preforms, which might have cross-linking before curing, is the main reason, as compressive properties are highly influenced by the epoxy system [28].
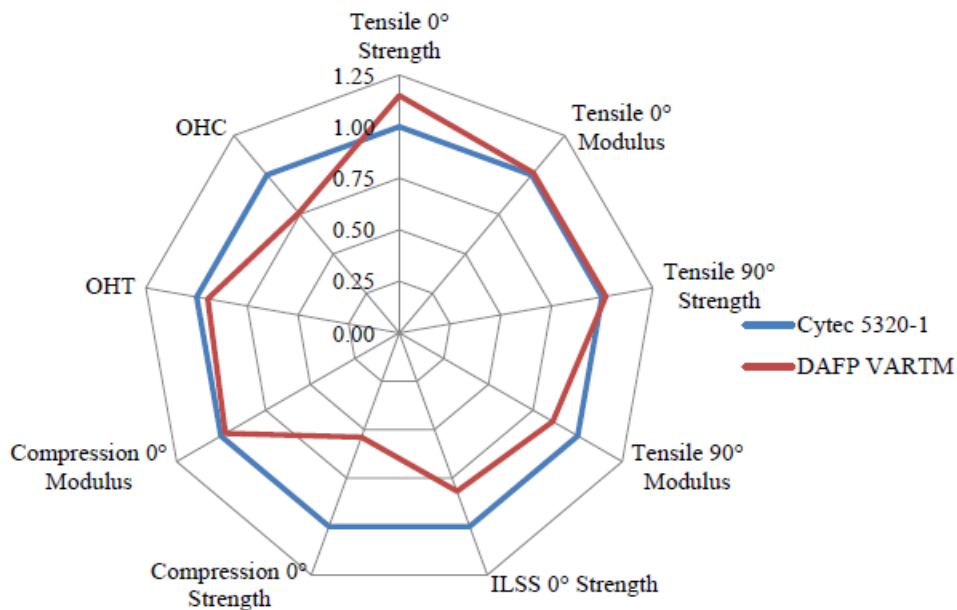
Figure 12. Comparison of laminates made by ADFP/VARI and OOA prepreg in mechanical performance [28]

Also, Belhaj et al.[20] demonstrated that open pattern ADFP preforms present higher plastic deformation than overlap and normal preforms (see Figure 13), even if they have higher out-of-plane permeability.
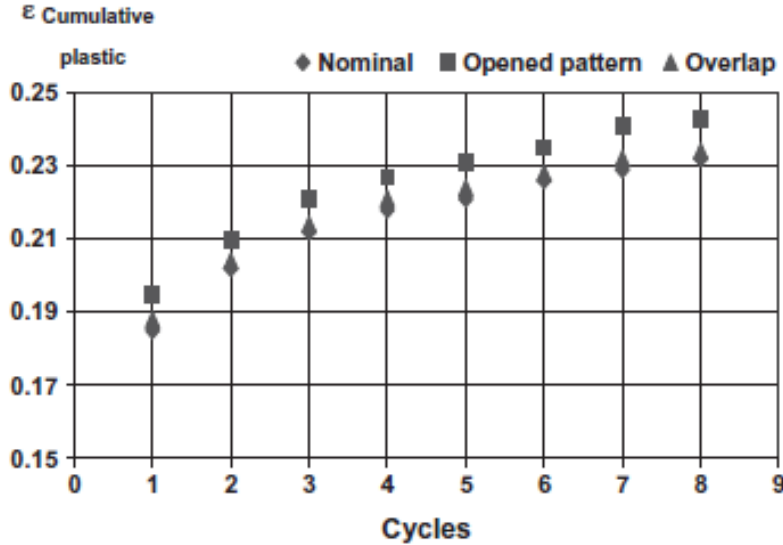
Figure 13. Plastic deformation of nominal, opened and overlapping pattern preforms [20]

2.5 Objectives

Although the combination of Automated Dry Fiber Placement (ADFP) and Vacuum Assisted Resin Transfer Molding Infusion (VARTM) has been developed in the literature, they are limited to manufacturing small flat panels without looking into the effect of AFP control on the processability of this method. The important key in manufacturing is the production rate, so, in VARTM, the production rate is dependent on the flow rate, which depends on the permeability of the dry fiber preform. Using the AFP machine provides the ability to make different fiber architectures by reducing the fiber content, introducing gaps between tows, or increasing the fiber content, overlapping tows. This ability allows the manufacturer to control the permeability of the preform as it is correlated to the fiber volume fraction. However, it should be noted that mechanical properties of the laminate depend on the fiber volume content. Reducing the fiber volume contents leads to a drop in the mechanical properties.

This thesis aims to study the characterization of preforms made by ADFP, using HGT-assisted AFP, and laminates infused by VARI at high temperature to manufacture a large-scale fuselage panel demonstrator with high quality. To address the objective, this thesis is organized in

the following sequence. To address the objective, this thesis is organized in the following sequence.

First, available dry fiber materials are presented and compared. Material substances can play a key role in the AFP consolidation, infusion process and curing after impregnation. ADFP and VARTM methods, process parameters in each process, and challenges and defects in each method are then introduced. Also, different VARTM setups are experimentally compared. Moreover, the effects of tailoring different gap sizes, using AFP, into the layup of the preform on its out-of-plane permeability are explained. Compression tests are performed to show the effect of introducing gaps on the mechanical properties. These mechanical tests can indicate the weight of the gap's advantage, like higher permeability, over disadvantage, like lower mechanical properties. Four 76 cm by 76 cm (30-by-30-inch) fuselage demonstrators were fabricated using ADFP and VARTM. The effects of introducing the gaps and using different VARTM setups are analyzed by fabricating these demonstrators. Finally, the quality of demonstrators is analyzed based on the defined procedure to measure the void content, fiber content, fiber waviness, thickness uniformity, and degree of cure.

Chapter 3. Material and Method

This chapter describes automated dry fiber placement and vacuum-assisted resin transfer molding. The selected materials, process parameters, defects, and challenges have been discussed in each process. Permeability is also explained as a preform parameter which could affect the processability of this method, especially in infusion.

3.1 Automated Dry Fiber Placement

Robotic AFP machines have a robotic arm that holds the head, a feeding system, and a user interface controller. Generally, thermoset and thermoplastic materials are two kinds of materials in which AFP heads are designed to process. Depending on the customer's requirement, an AFP machine would be designed with different heating systems (e.g., laser heating system, hot gas torch, etc.)
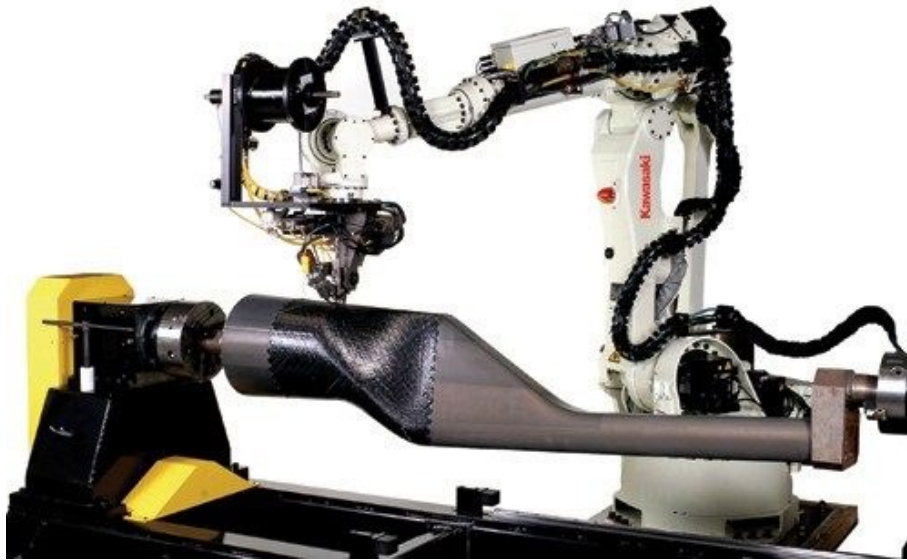
Figure 14. Concordia composite center AFP machine [29]

In the case of AFP machine heads available in Concordia Center for Composites (CONCOM) lab, Figure 14, there are two heads designed for thermoplastic and thermoset materials, which are not intended to deposit dry fiber tapes. Although the available thermoset head can deposit four tapes simultaneously on the mold, the thermoplastic head is chosen for using dry fiber tape, see Figure 15. The reason is that the thermoplastic head provides better controllability than the thermoset head, specifically in the heating system, as only one tape being deposited. The thermoplastic head of the AFP machine at CONCOM has a hot gas torch (HGT) heating system.

In our case, HGT temperature and flow rate are two important process parameters that play the main role in providing the necessary stickiness for the material to lay down on the tool.
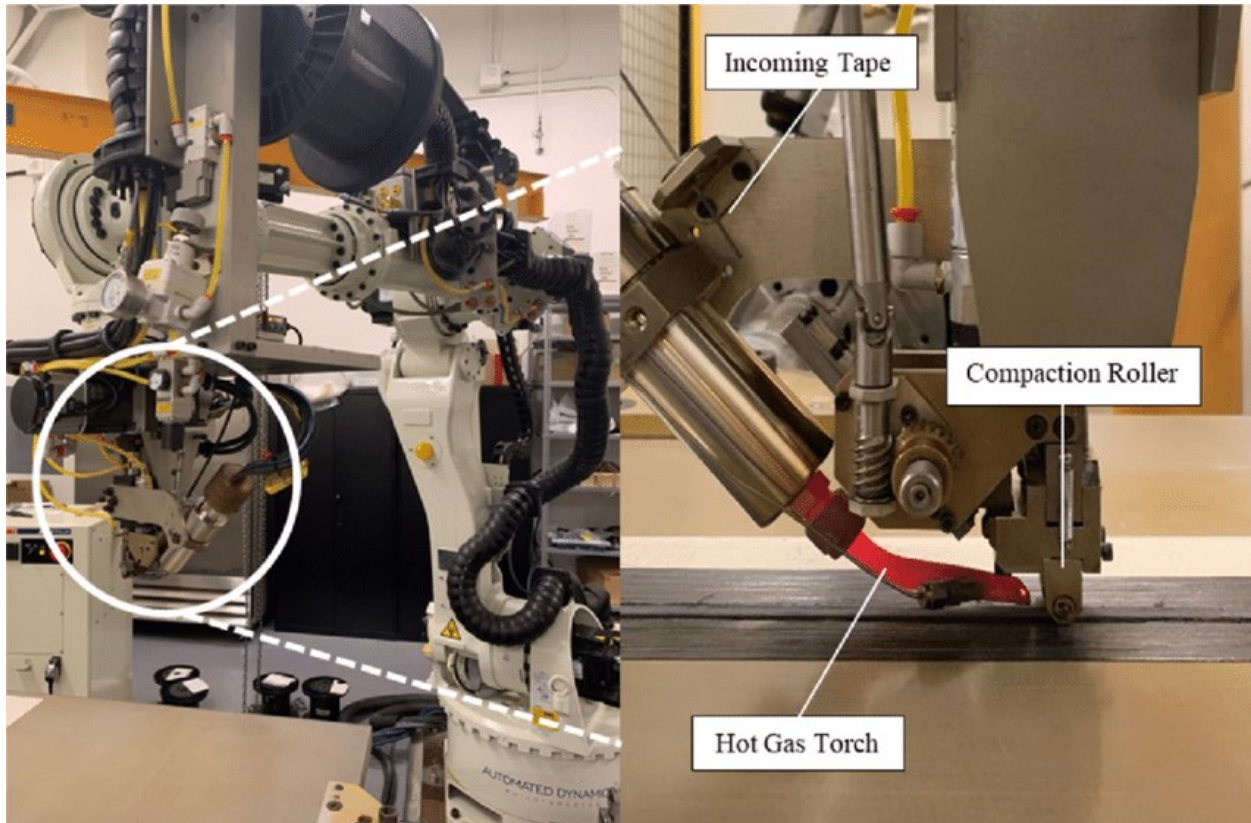
Figure 15. CANCOM AFP thermoplastic head [30]

In this thesis, flat panels were fabricated as trials to study defects, challenges, and bottlenecks [31]. As mentioned before, this process is considered the combination of AFP and VARTM; thus, the experimental part is also divided into two different parts. However, the AFP process can affect the infusion process, which will be explained in section 3.2.

3.1.1 Material Selection

Unlike pre-impregnated materials (prepreg) widely used for the AFP process in the aerospace industry, dry fiber materials are recently introduced to this field. These materials have no matrix inside their structures; however, they consist of a substance, called binder, which acts like glue to stick them to the preform substrate [7], [8]. Also, some of the available dry fibers, like Solvay TX1100, contain a veil layer that provides channels for resin infiltrating, in other words, it improves permeability for infusion [7], [19]. Using these materials can help the manufacturer to reduce energy consumption since the autoclave is removed from this process. Also, the production cost is lower than prepreg material due to the lack of a matrix layer.

Currently, there are several suppliers for this type of material, and this project took advantage of three suppliers, as mentioned in Table 8.

Table 8. Dry fiber Materials [32]

No.	Supplier	Material name	Nominal fiber density, g/cm^3	Nominal areal weight, g/m^2 [18]	Nominal tape width, mm(in)	Binder type [18]
1	Hexcel	Hitape IMA/IM7	1.79	140	6.35(1/4)	Epoxy-based
2	Cytec Solvay	TX 1100 IMS65	1.78	196	6.35(1/4)	Thermoplastic based
3	Teijin	Tenax E HTS40 X030	1.76	126	6.35(1/4)	Epoxy-based

The addition of binder into the epoxy system can cause changes in the cure kinetics of the epoxy system. The reaction heat of the epoxy system mixed with the binder is higher than neat epoxy system, and also adding binder can reduce the processing time of the epoxy resin [33]. To define the mechanism of dry fiber's substances, dry fiber tapes are looked at under the 3D microscope, model VHX 5000 Keyence. Based on the photographs from three available dry tapes, the difference between veil structure and binder structure, binder content and different binder structure can be understood. As in Figure 16, Solvay material has CYCOM 7720 RTM preform binder on the top surface and a thermoplastic veil layer on the bottom. CYCOM 7720 RTM is compatible with Cytec engineered materials epoxy resin systems, e.g., PRISM EP2400. Fabrics coated with this binder must be injected on a tool heated to 100 – 130°C [34].
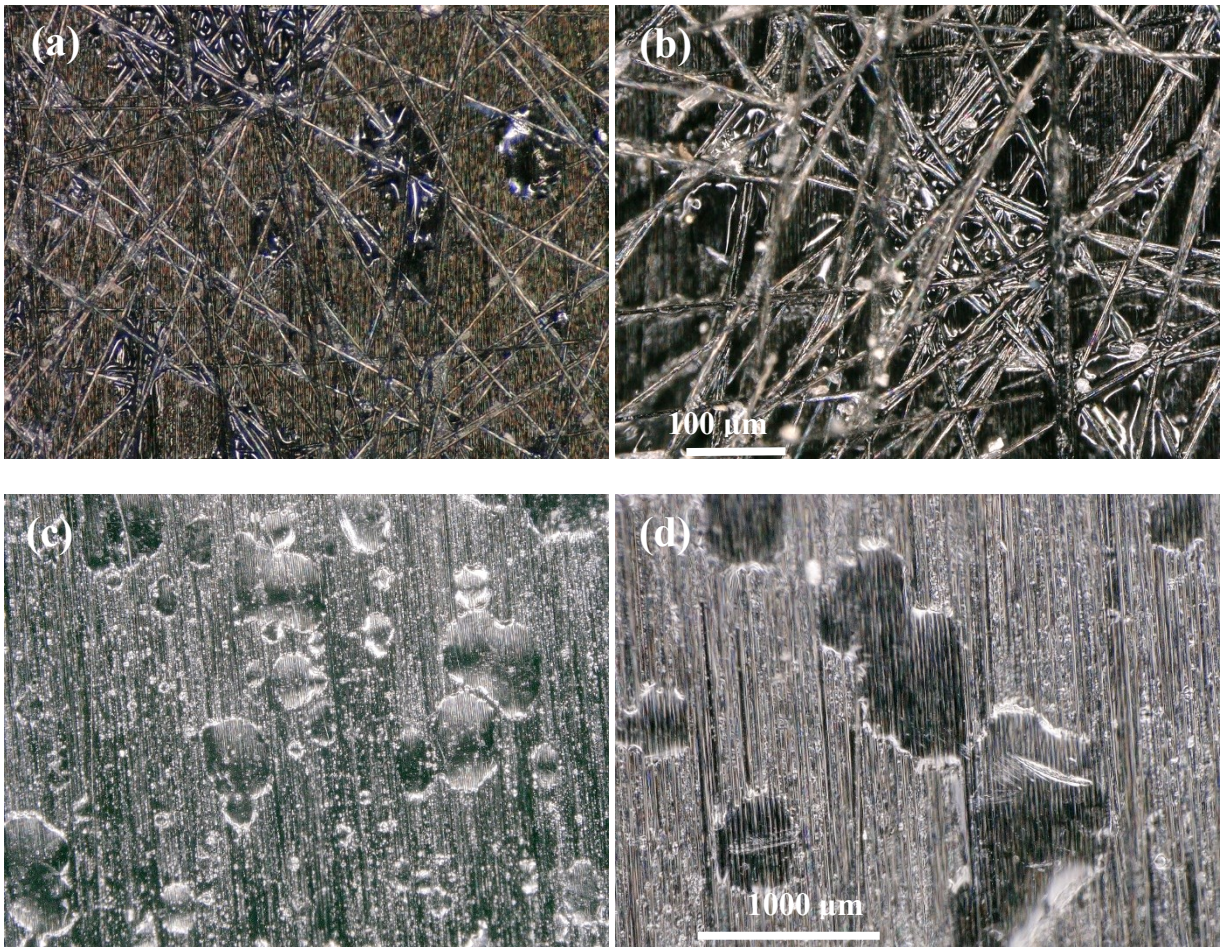
Figure 16. Veil layer on Solvay (a) 200x; (b) 300x - binder spots on Solvay (c) 200x; (d) 500x [32]

Figure 17 shows the thermoplastic binder on Hexcel's HiTape IM7, which requires 300-150-175°C (350°F) temperature to be activated to adhere the fibers. Also, Figure 18 presents the epoxy-based binder on the surface of Teijin Tenax E HTS40 dry fiber.
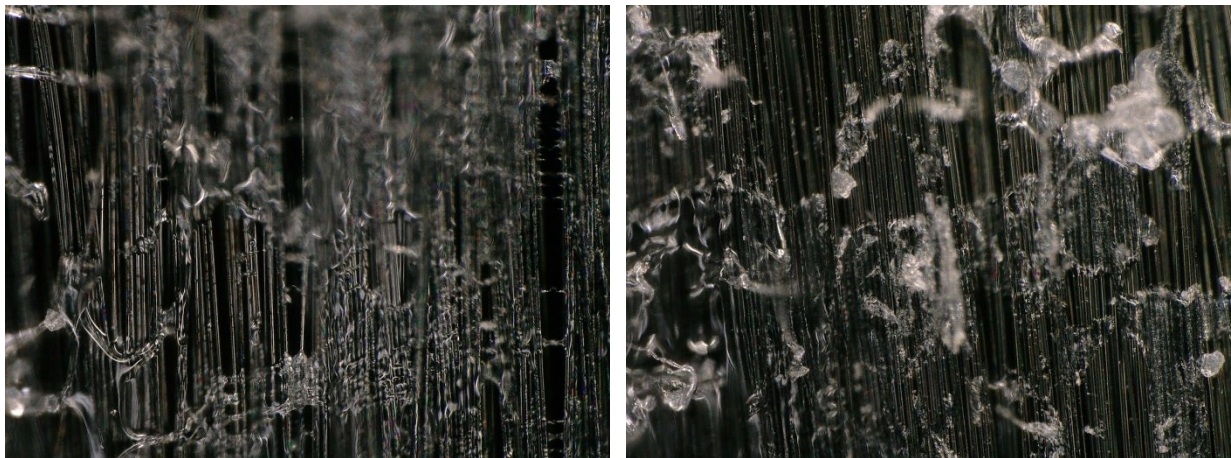
Figure 17. Binder spots on HiTape - 500x (both side)
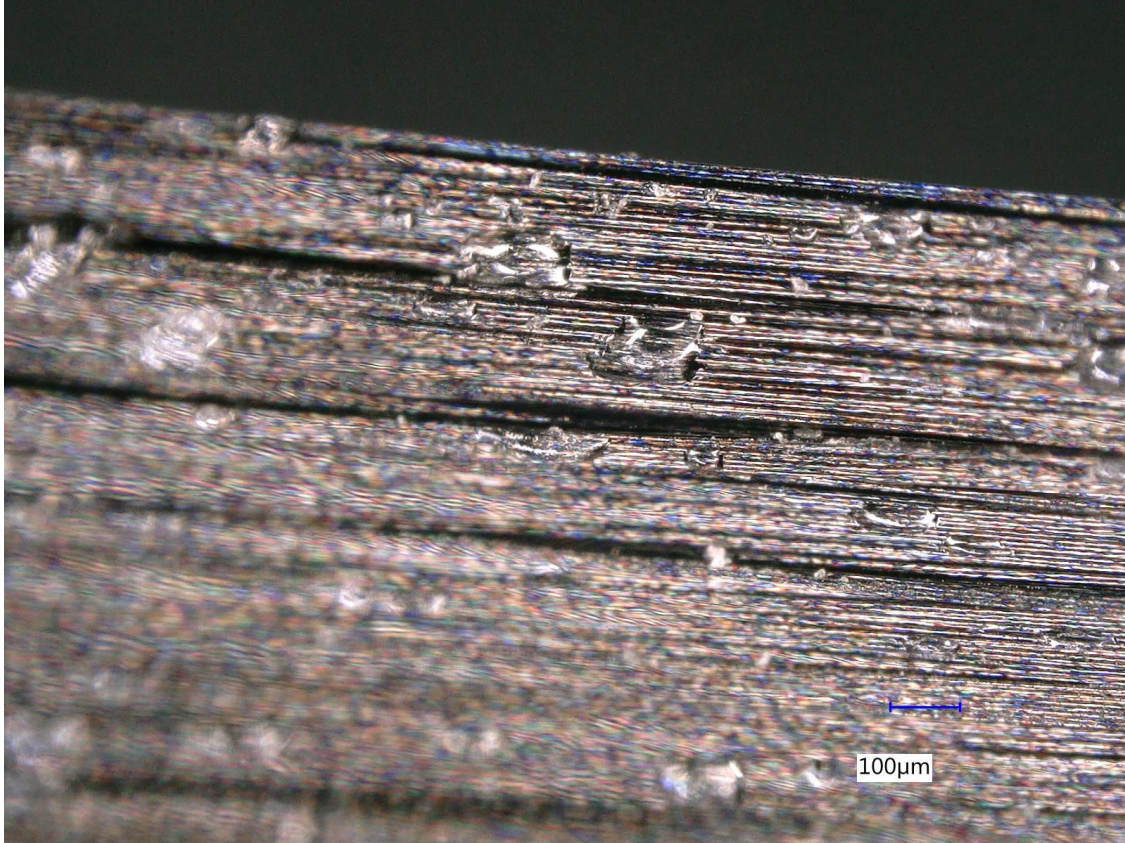
Figure 18. Binder spots on Teijin - 50x (Back side)

According to the dry fibers' micrographs, Figure 16 - Figure 18, the binder level is higher in the Solvay material, which endorses the stiffness of laminate made by this material compared to other materials in the trial. Also, we can understand the difference between the veil and binder structure. Another hypothesis is that suppliers use different processes to add the binder into the fibers, like spraying or embedding. It is noteworthy that Teijin has the lowest binder level among all available materials, which supports its fragility.

The dry fiber tape used in this study to fabricate preforms for permeability measurement, compression tests and fuselage demonstrators was Solvay TX 1100 IMS65. However, Hexcel's HiTape IM7 and Teijin Tenax E HTS40 were used to study their AFP process parameters and compare them with Solvay dry fiber.

3.1.2 Process Parameters

In the AFP process, process parameters must be defined after specifying the machine's coordinate system, tool geometry, and layup pattern. While process parameters are sometimes available for some materials, unfortunately, in the case of dry fiber materials, there are few

available references. Moreover, the process parameters can vary depending on the type of machine and heating system used in the process. Consequently, the "trial and error" approach is used to understand the effect of each parameter on depositing material.

In addition to the HGT temperature and flow rate explained before, the compaction force of the roller can significantly affect the depositing process. Usually, compaction load is used to stick the fiber to the substrate, increasing fiber content and infusion time. However, there is a bouncing effect for dry fibers, unlike prepreg which has matrix in their structures. The bouncing effect can cause peel off issue, which will be discussed in 3.1.3.

Although the feeding rate can be set using the machine user interface, the optimized value should be obtained as a low feeding rate has no meaning in industrial manufacturing. Also, increasing the feed rate does not let dry fibers stick to the mold. Since dry fibers are softer materials than thermoplastics, pulling fibers without sufficient tension causes roll up. The AFP machine user interface can be programmed to deposit materials in different layups and patterns, such as introducing gaps of various sizes between tows.

Consequently, HGT temperature and flow rate, compaction load, feed rate, and nozzle distance to roller can be considered process parameters.

3.1.3 Defects and Challenges

- **Rolls up**

In some cases, after performing 1-2 tows, the subsequent tows could not stick to the surface and made frays, see Figure 19, which are caused by rolls up. Also, rolls up may appear due to the roller tackiness, which causes fibers to stick to the roller instead of substance. Using Teflon shrinkage tapes on the roller makes it slippery and non-sticky, which can solve the issue as demonstrated in Figure 20. Also, applying the optimized temperature and flow rate for the HGT can be the other solution.

Figure 19. Rolls up in the 2nd deposited tow
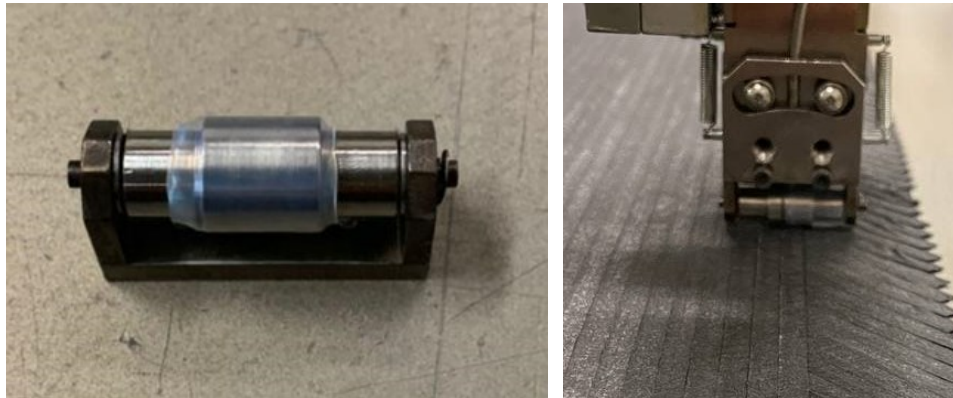
Figure 20. Teflon shrinkage tape on the roller [32]

- **Peel off (Edge lifting)**

In some cases, edges start to lift after depositing more than six plies due to a lack of bond at the edges (Figure 21). Although the tension in the roller is set at zero, there might be internal friction which causes tension in the depositing tow. Also, more plies are deposited, softer substance will be, and consequently, lift-up appears in the edges of the preform. Clamping edges to hold the tows or staggered layup can avoid this challenge, see Figure 22.
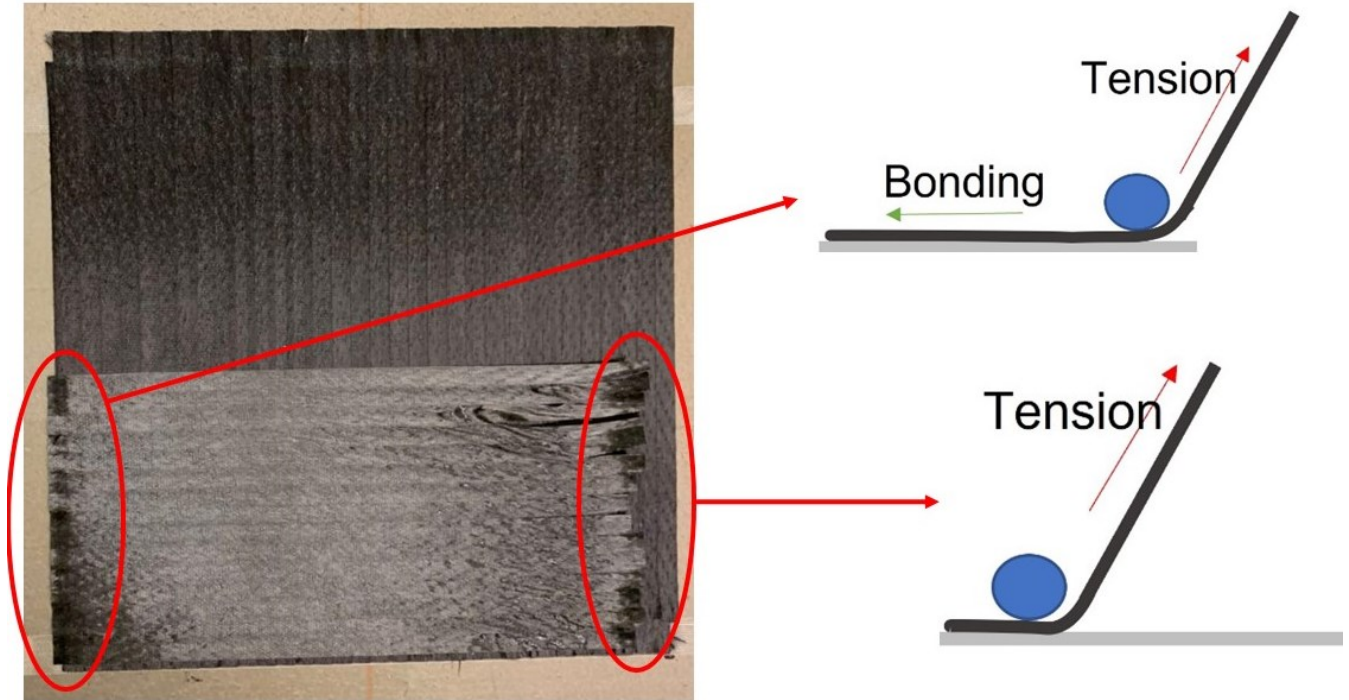
Figure 21. Lack of bonding at the edge causing edge lifting
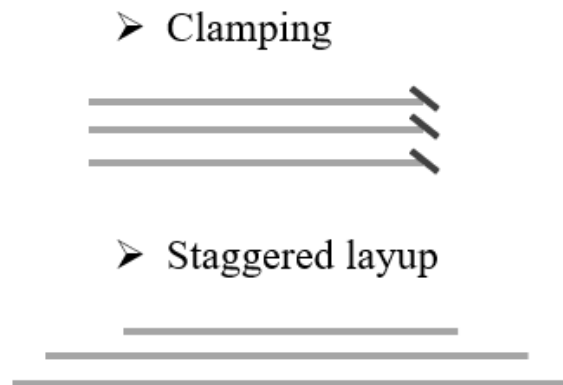
Figure 22. Solutions for edge lift

- **Misalignment and Waviness**

Due to machine errors in defining the path, there are misalignments, especially in the last layers. The only way to avoid this issue is to control the temperature to stick the material to substance appropriately without any movement afterward. For example, the waviness of the edge was the first challenge with the AFP process in the 1st trial, which started after laying 8 plies due to the dry fiber fluffiness, see Figure 23. The idea to solve this issue was to make two separate 6 plies preforms and put them together for infusion.

Figure 23. Misalignment

Although each AFP process parameter might separately cause a defect, these parameters depend on each other, as illustrated in Figure 24. For example, increasing the HGT temperature might result in rolls up, which needs the temperature to be reduced. Also, reducing the temperature might prevent fiber from sticking to the substrate. Thus, optimizing a group of parameters is necessary to control discussed defects.
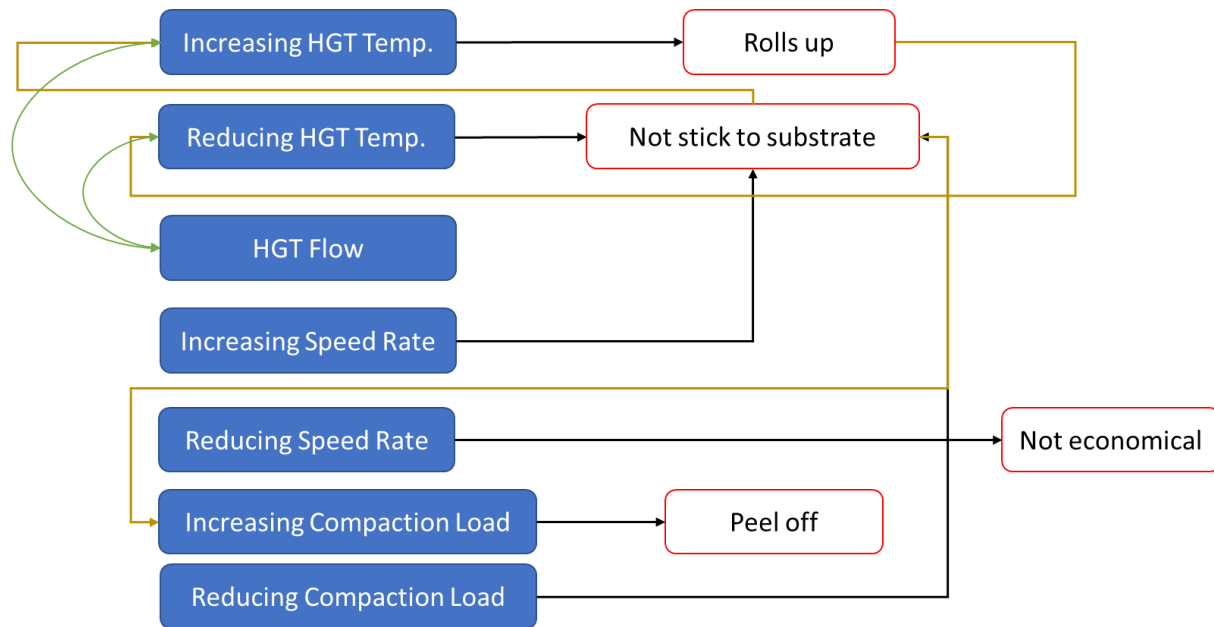
Figure 24. AFP parameters' effect on defects [32]

3.2 Permeability

The need for Liquid Composite Molding (LCM) has raised due to the ease of this process, high product quality and low void content [23]. The governing equation in these processes, which includes VARI, is Darcy's law, described below:

$$\vec{u} = -\frac{1}{\mu}.[K].\nabla p \quad [10] \tag{1}$$

In this equation, $\vec{u}$ describes a vector for flow velocity, μ is dynamic fluid viscosity, K is a permeability matrix that indicates the directional permeability of fibers, and ∇p is the pressure gradient.

Permeability is the fiber's attribute that shows the flow's ease through the fiber reinforcement, which has different magnitudes in different directions because of the fiber bundle's anisotropic behavior [10]. Permeability is related to the fiber's alignment in the preform structure and, more importantly, fiber volume fraction V_f which can be calculated using Darcy's law [22]. The permeability matrix includes three principal components of K_x, K_y, and K_z corresponding to the fiber axis.

The permeability of fibers is categorized into two, in-plane (K_x and K_y) and out-of-plane (K_z) (e.g., transverse, through the thickness). Usually, simulations and experiments are easier for the in-plane permeability than the out-of-plane, as composite structures are manufactured as thin layers [23]. The out-of-plane permeability measurement is challenging due to the short distance for the resin to flow and the lower magnitude for permeability value to in-plane ones. To overcome this challenge, out-of-plane permeability is usually measured independently from in-plane permeability. Performs with high out-of-plane permeability can be impregnated and bonded easily to prevent delamination in the last layers.

Out-of-plane permeability can be measured by either steady flow through a saturated preform or transient flow for an unsaturated preform by tracking the time and flow front in the thickness under pressure difference, see Figure 25. Also, the flow direction is usually considered in only z-direction to simplify the effect of in-plane permeabilities. A benchmark published in 2021 showed 26 measurements from different labs for through the thickness permeability. Among these studies, 21 used the saturated 1D method, three used unsaturated 1D, three used unsaturated 3D and only 1 used the saturated 3D method, which can explain the complexity of tracking flow front in the fiber reinforcement thickness for measuring the transient flow rate.
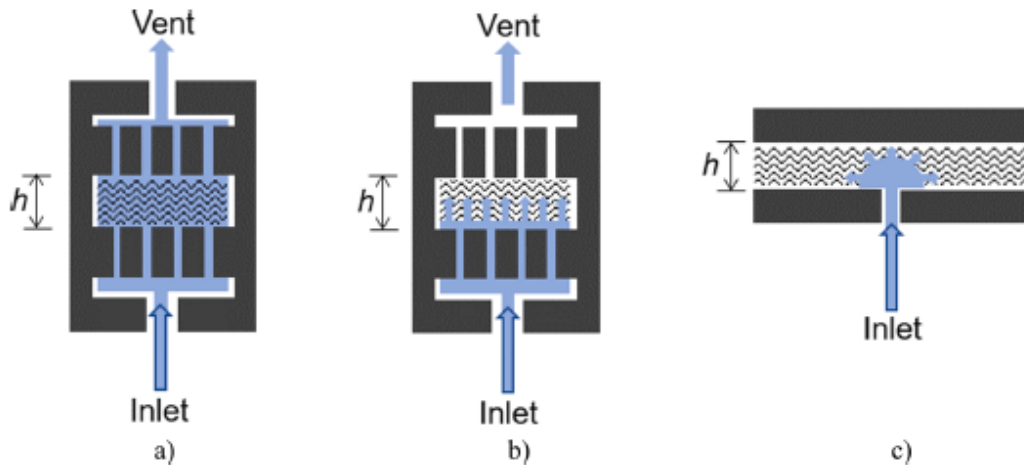
Figure 25. Schematic of flow type in the out-of-plane permeability measurement (a) saturated 1D flow, (b) unsaturated 1D flow, (c) unsaturated 3D flow [23]

3.3 Vacuum-Assisted Resin Infusion

Resin transfer molding (RTM) has been used in the aerospace industry for manufacturing complex components with high quality, lower costs, and inexpensive equipment [9]. Among all kinds of RTM methods, vacuum-assisted resin infusion (VARI) is considered one of the cheap and easy-to-operate methods that can prevent complex mold manufacturing and high injection pressure. Different developed VARI types provide a pressurized chamber to compact the stack up under the vacuum bag and flow the resin inside the structure [35].

This thesis employed two infusion setups to fabricate carbon/epoxy laminates using three epoxy systems. First, Seemann's composite resin infusion process (SCRIMP), see Figure 26; second, vacuum-assisted process with the membrane (VAP), see Figure 27. On the one hand, in SCRIMP, one vacuum chamber is introduced to the setup consisting of a layer of distribution media to accelerate the in-plane flow front and achieve a shorter infusion time. Since the setup configuration is simple and the operational temperature is lower, it does not require much equipment and has a faster preparation time. On the other hand, the VAP membrane provides two chambers, the outer for applying pressure and extracting gas and the inner for resin infusion, by adding a membrane layer, see Figure 28. Generally, a membrane is an air-permeable layer that acts as a filter and lets air and gas pass through it; however, it is a resin barrier and contains the resin inside the chamber [36].
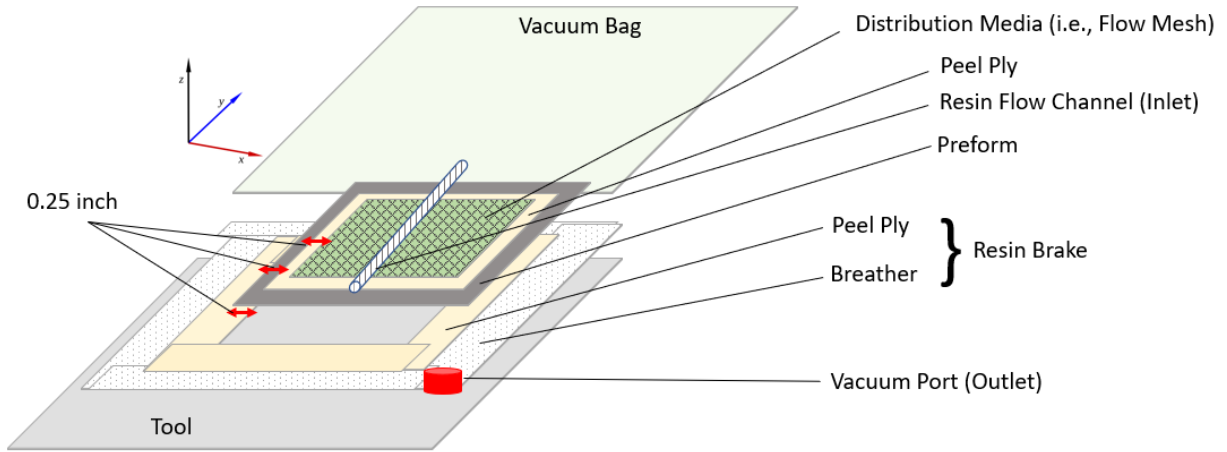
Figure 26. Explosive view of SCRIMP setup [37]
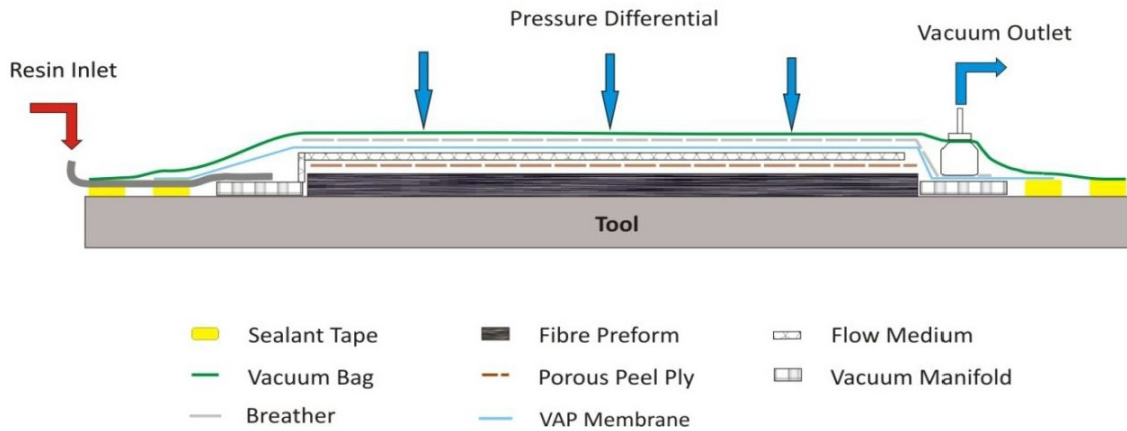
Figure 27. VAP membrane setup [38]

The Vacuum Assisted Process (VAP), patented by European Aeronautic Defence & Space Co. (EADS, Amsterdam, The Netherlands), uses a semipermeable membrane to separate the vacuum outlet from the surface of the part, creating a vacuum gradient and in-situ degassing across the entire part surface rather than at the part edges only. ∎
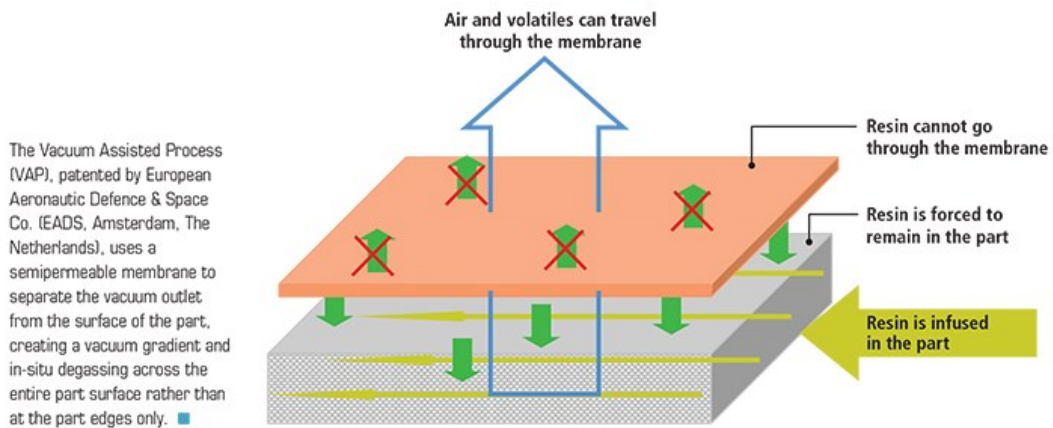
Figure 28. Chambers in VAP process [39]

3.3.1 Material Selection

In this project, room temperature and hot infusion, one at 25°C and another at a high temperature (120 °C), were employed to study the difference in impregnation and processability.

Regarding room temperature, Araldite®LY 8601 (Resin) / Aradur® 8602 (Hardener), a two-component, low-viscosity epoxy system designed for VARTM, RTM and SCRIMP, was used. The neat resin properties can be found in Table 9.

Table 9. Araldite®LY 8601 / Aradur® 8602 system properties [40]

Property	Value
Mixed Viscosity, cP (at 25 °C)	175
Gel time, minutes (at 25 °C)	70
Tensile Strength, MPa (ksi)	54.5 (7.9)
Compressive Strength, MPa (ksi)	106.2 (15.4)
Compressive Modulus, GPa (ksi)	2.1 (305.4)
Flexural Strength, MPa (ksi)	75.8 (11.0)
Flexural Modulus, GPa (ksi)	2.2 (322.6)
Tg by DMA, °C (°F)	73 (164)

For compression test samples' infusion, the epoxy resin used was EPON Resin 862/Curing agent W, whose neat resin properties can be found in Table 10. According to the technical datasheet of EPON Resin 862/Curing agent W resin system, the resin system pot was preheated at less than 60 °C, and it was infused into a heated mold inside an oven at 100 °C, see Figure 29. Afterwards, the curing cycle for 8 hours at 121 °C was selected, followed by cooling to room temperature for 24 hours, illustrated in Figure 30.
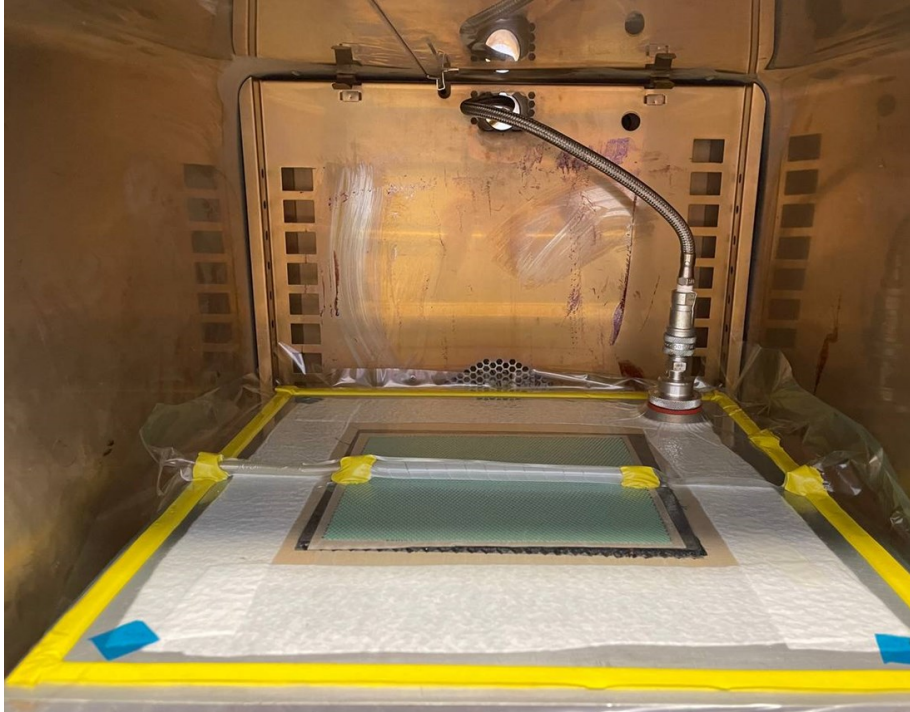
Figure 29. Heated tool inside the oven for compression samples infusion
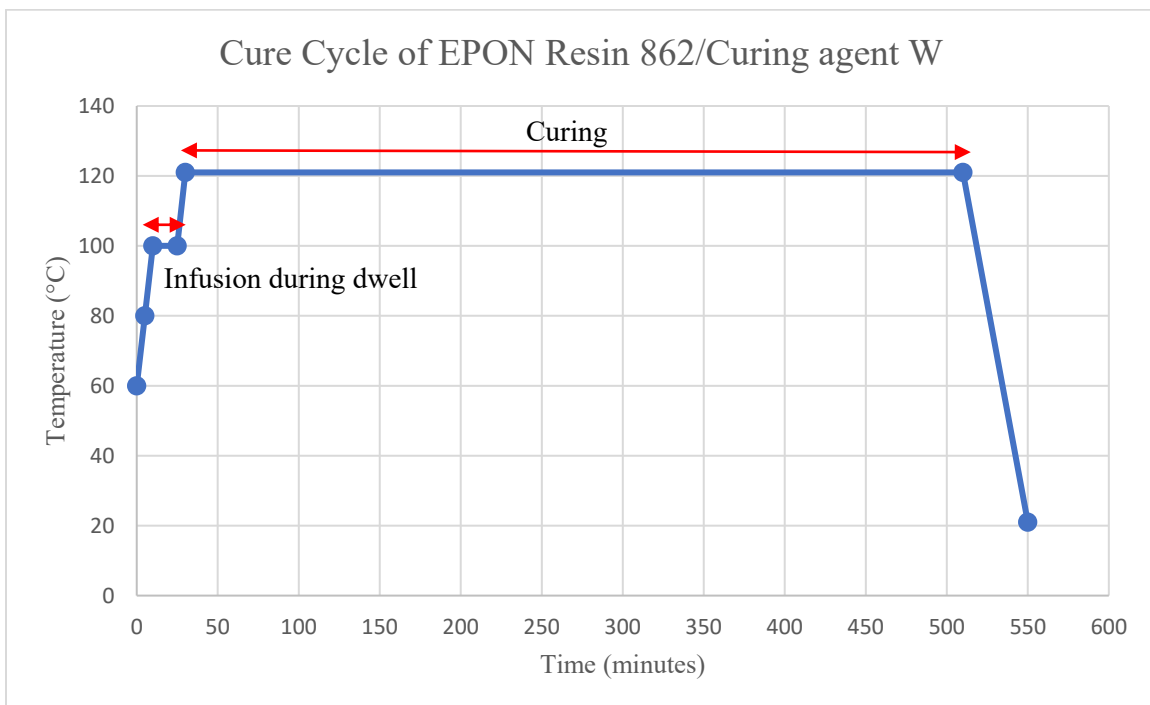
Figure 30. Cure Cycle for EPON Resin 862/Curing agent W resin system

Table 10. EPON Resin 862/Curing agent W system properties [41]

Property	Value
Viscosity @ 25 °C, P	21-23
Gel time @ 177 °C, minutes	15
Tensile Strength, MPa (ksi)	82.7 (12)
Tensile Modulus, GPa (ksi)	3.2 (457)
Flexural Strength, MPa (ksi)	124.1 (18)
Flexural Modulus, GPa (ksi)	3.1 (455)
Tg, °C (°F)	133.9 (273)

For fuselage panel demonstrators' infusion, the epoxy resin used was PRISM™ EP2400 resin system by Solvay. The resin properties are described in Table 11. This liquid epoxy resin is a single part with low viscosity and 180°C (356°F) curing, ultimately leading to omitting post-processing like using an autoclave. The EP2400 viscosity sweep as a function of temperature in a range from 60 °C to 180 °C and isothermal viscosity profiles were presented by Solvay. Figure 31 shows that it takes 10 hours to reach 300cP viscosity at 100ºC.

Table 11. PRISM™ EP2400 system properties [42]

Property	Value
Tensile Strength, MPa (ksi)	95 (13.8)
Tensile Modulus, GPa (ksi)	3.4 (490)
Flexural Strength, MPa (ksi)	164 (23.8)
Flexural Modulus, GPa (ksi)	3.6 (520)
Tg, °C (°F)	179 (354)
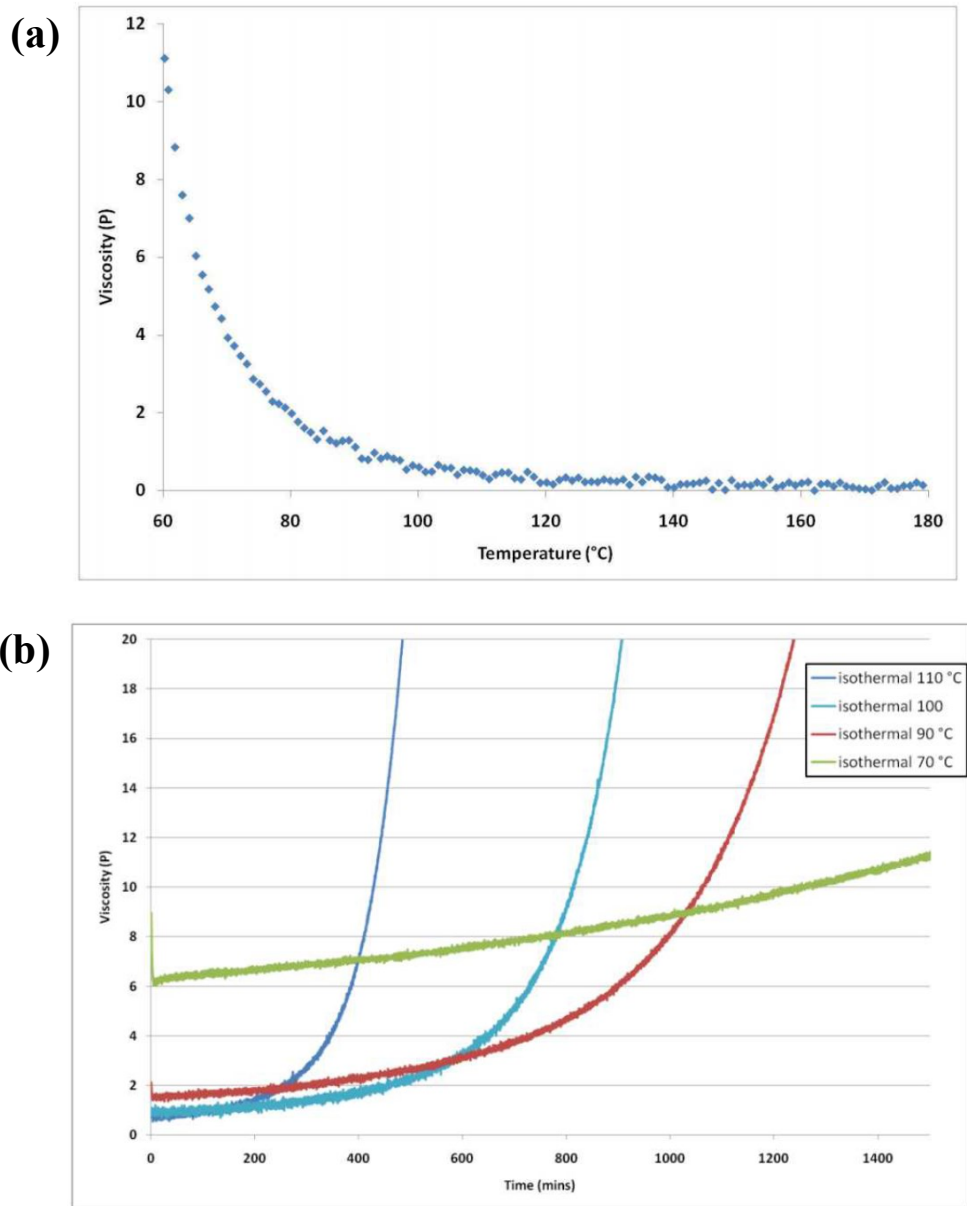
Figure 31. PRISM EP2400 (a) viscosity sweep to 180°C at 2°C/min (b) Isothermal viscosity profiles [42]

The curing cycle of the PRISM™ EP2400 resin is described in Figure 32.
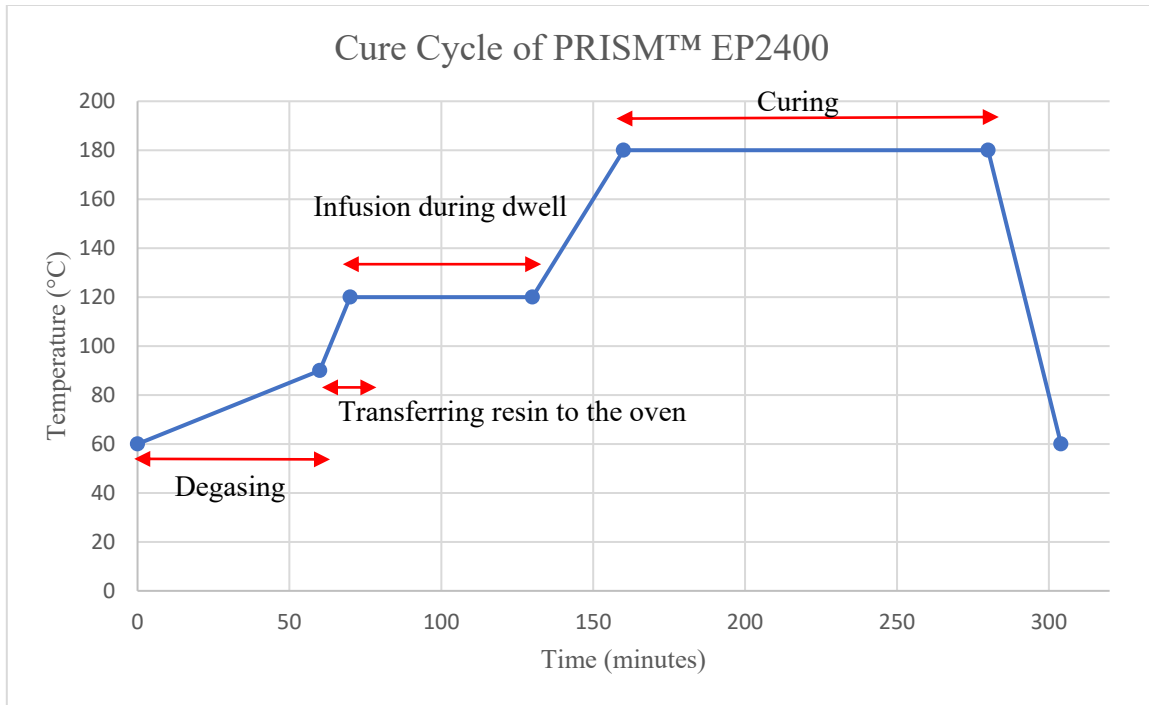
Figure 32. Cure Cycle for Solvay PRISM™ EP2400 resin (for the 1st and 2nd demonstrators)

3.3.2 Process Parameters

The VARI's most important parameters are permeability of the preform and resin viscosity. It was discussed that using AFP allows the manufacturer to deposit or steer the fibers in complex geometry. However, the impregnation time of preform made by AFP increases relatively compared to manual hand layup due to the applied compaction on preform [7]. The other process parameter is epoxy viscosity which is dependent on the temperature. Usually, suppliers provide the viscosity-temperature profile, which can help the manufacturer to choose the proper cycle for the infusion and curing based on the epoxy's viscosity profile.

3.3.3 Defects and Challenges

- **Bag bridging**

Wrinkles absorb a noticeable amount of resin, prevent resin penetration through the fiber, and make resin-rich areas (see Figure 33). The outer peel ply was trimmed to stop the resin from flowing outside the preform, which was unsuccessful. The second experimental solution was cutting the outer peel ply layer along the tube to prevent the resin flow outside the preform. However, the results were not promising. So, a layer of the air-permeable membrane was added to the setup. This membrane aids the removal of air; however, it keeps and restricts the resin from flowing underneath.
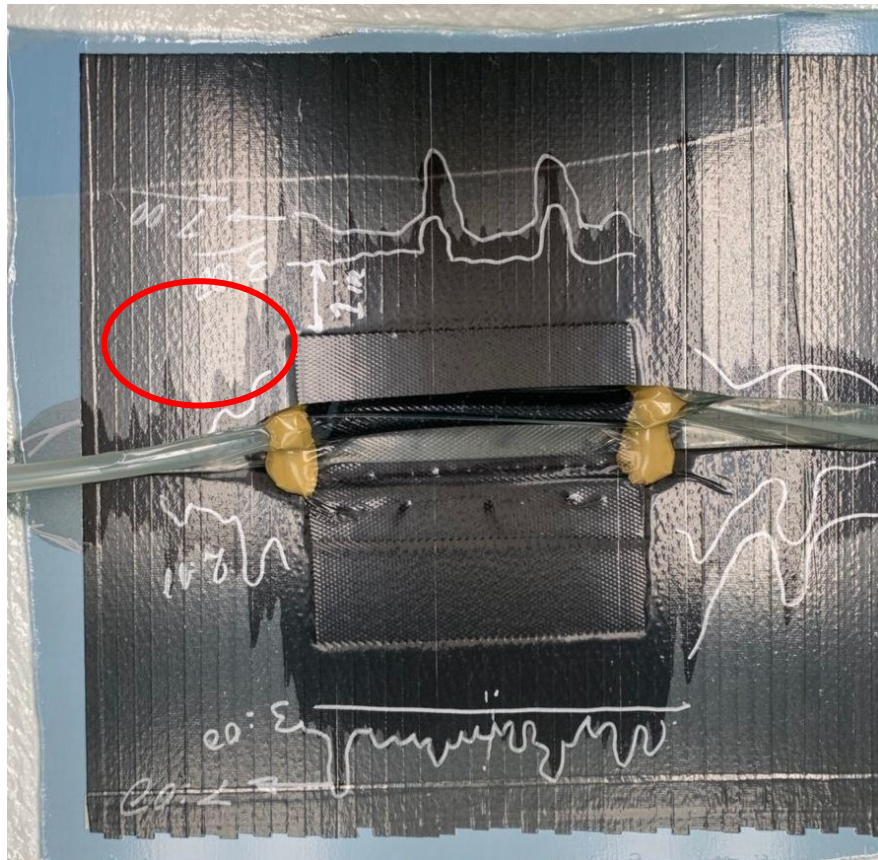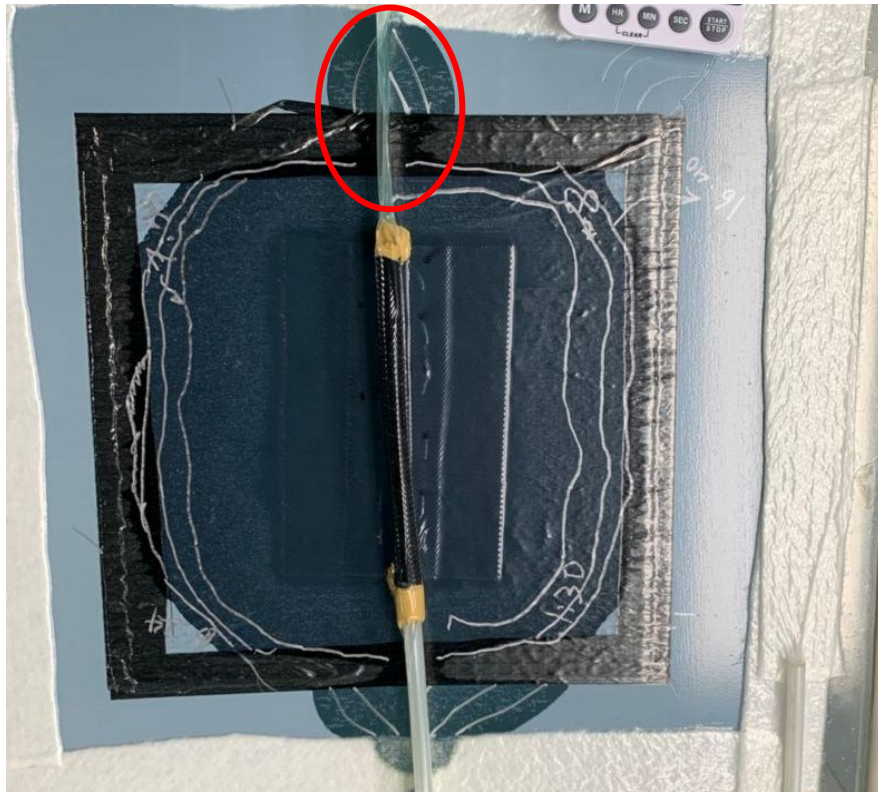
Figure 33. Wrinkles along the tube

- **Vacuum lost**

The vacuum bag chamber lets the resin go inside the fiber and provides uniform pressure on the panel to cure after infusion. Therefore, it is important to keep the vacuum during curing, and any leakage can cause damage to the final performance. For instance, for the first fuselage demonstrator, Figure 34, due to the unbounding of the vacuum bag sealant, the resin could not travel inside the panel completely, and some portion of the panel remained dry. Double bagging vacuum infusion or VAP membrane infusion setups can prevent this since they can keep the vacuum pressure and avoid leaking. In the double bagging setup, two vacuum bag chambers are constructed. The outer chamber reduces the chance of leaks and keeps the rigidity of the inner chamber [9].
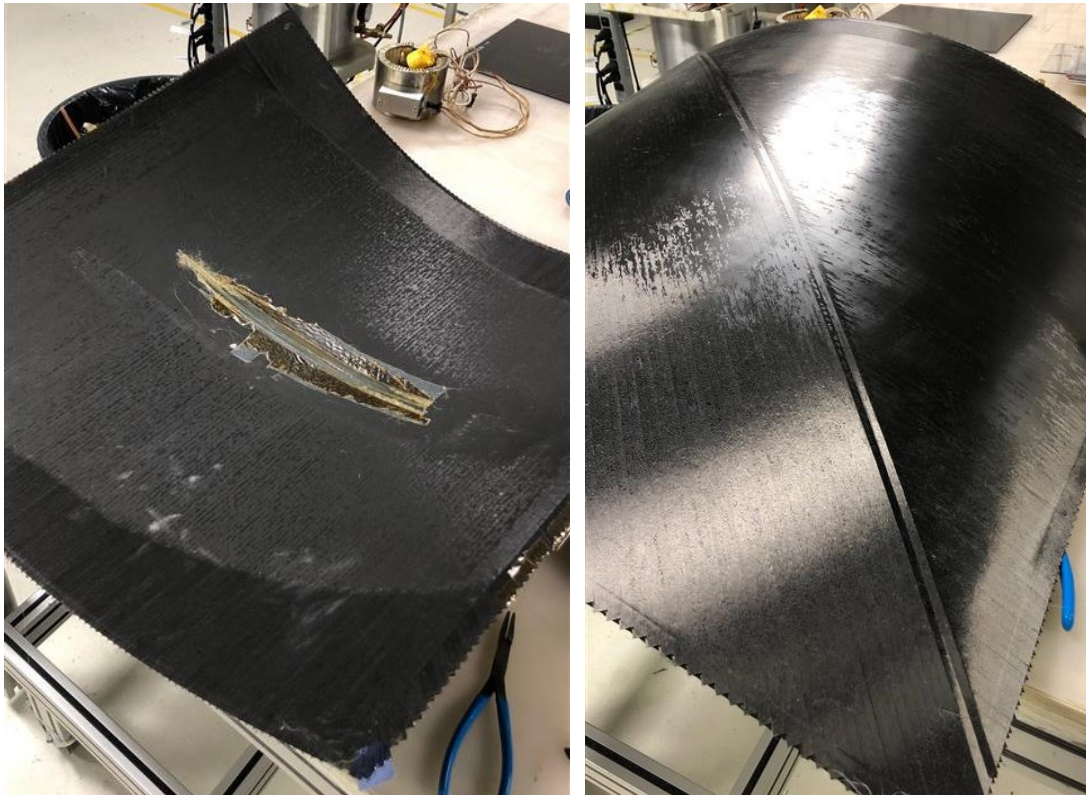
Figure 34. Uncured fuselage demonstrator due to the vacuum lost

Chapter 4. Characterization of Preforms and Laminates made by ADFP and VARI

Part of this chapter is submitted as a paper entitled "Effect of gaps on preform and laminate made by automated dry fiber placement and resin infusion" for consideration for publication in Composite Part A" journal [37].

4.1 Out-of-Plane Permeability

Using AFP-made preforms can be challenging in vacuum infusion. This is because a compaction load is applied on the preforms during the deposition in the AFP process, which results in the preforms' low permeability and makes impregnation more difficult and more prolonged. In this thesis, considering the importance of the out-of-plane permeability of preforms made by ADFP, the out-of-plane permeability of different preform patterns made by ADFP was measured to show the effect of introducing gaps between tows using the AFP machine.
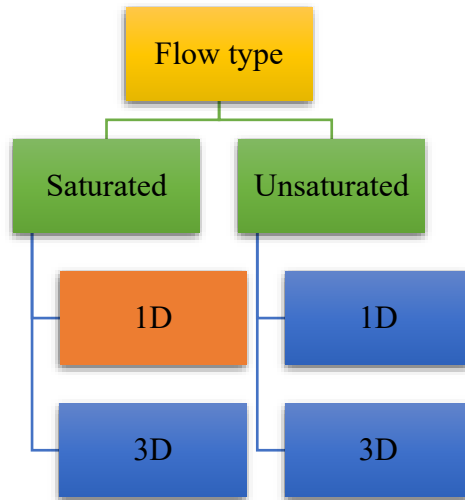
Figure 35. Different flow types in the out-of-plane permeability measurement

The fluid used in these measurements was Dow Corning Xiameter PMX-200 100 cSt silicone fluid which provides stable viscosity compared to any other type of resin. Therefore, based on the saturated 1D method, Figure 35, Darcy's law can be converted to the following equation to measure the out-of-plane permeability:

$$K_z = \frac{-\mu \cdot Q \cdot h}{\Delta p \cdot A} = -\frac{\mu \cdot (^m/_{\rho \cdot t}) \cdot h}{\Delta p \cdot A} \qquad (2)$$

In which μ is the fluid viscosity, Q is the volumetric flow rate, h is the preform thickness, Δp is the pressure difference between both sides of the preform, A is the section area of the preform, m is the collected fluid weight in the outlet, ρ is the fluid density, and t is the experiment time in steady state. In the steady state method, monitoring the flow rate and pressure difference and keeping the flow running through the saturated preform is essential for measuring the out-of-plane permeability as soon as Q and Δp are constant [23].

This research used McGill University structures and composite materials laboratory setup for the out-of-plane permeability measurement. Figure 36 shows the porous distribution plates with large holes in the setup to clamp the preform between them and run the flow from the bottom to the top. As preforms have thickness variation, the cavity height can be adjusted to prevent any local pressure due to clamping. Additionally, the differential pressure is measured by using the pressure sensor at the inlet and placing the outlet in the atmospheric pressure. Finally, the steady flow rate can be calculated using a scale to measure the output flow weight from saturated preform and convert it to a volumetric rate using the flow density and time.
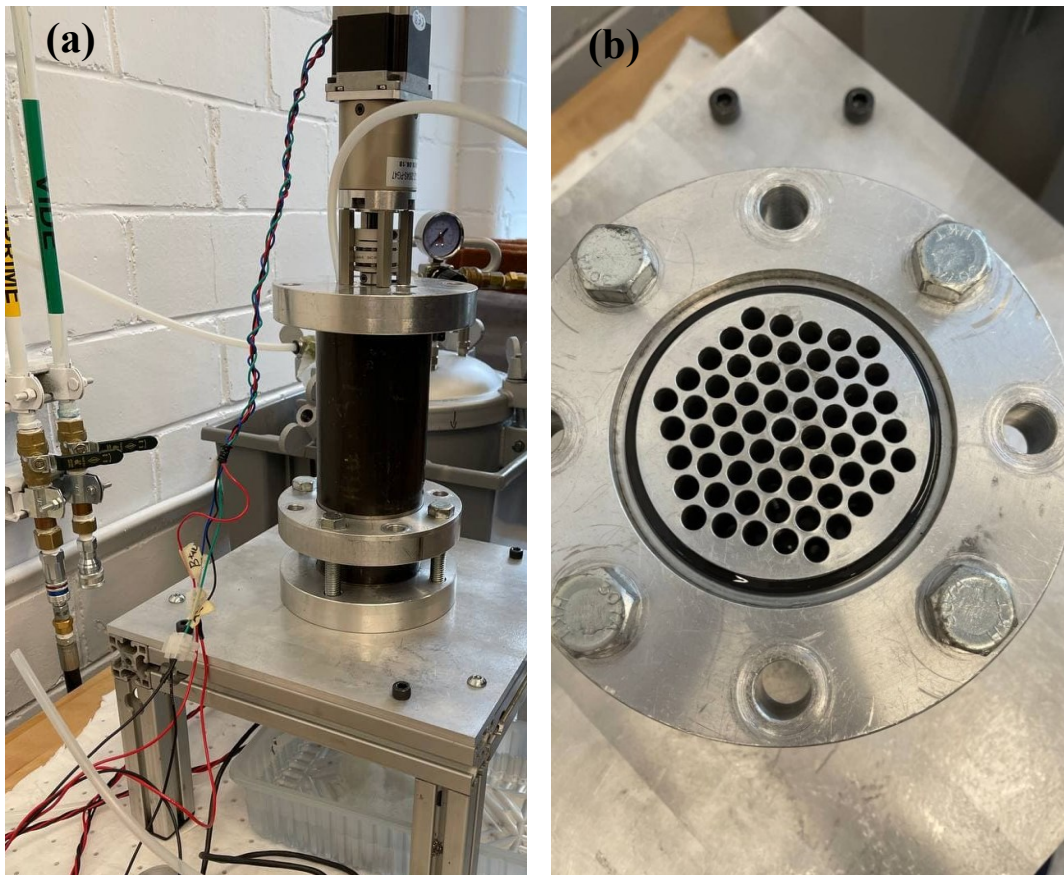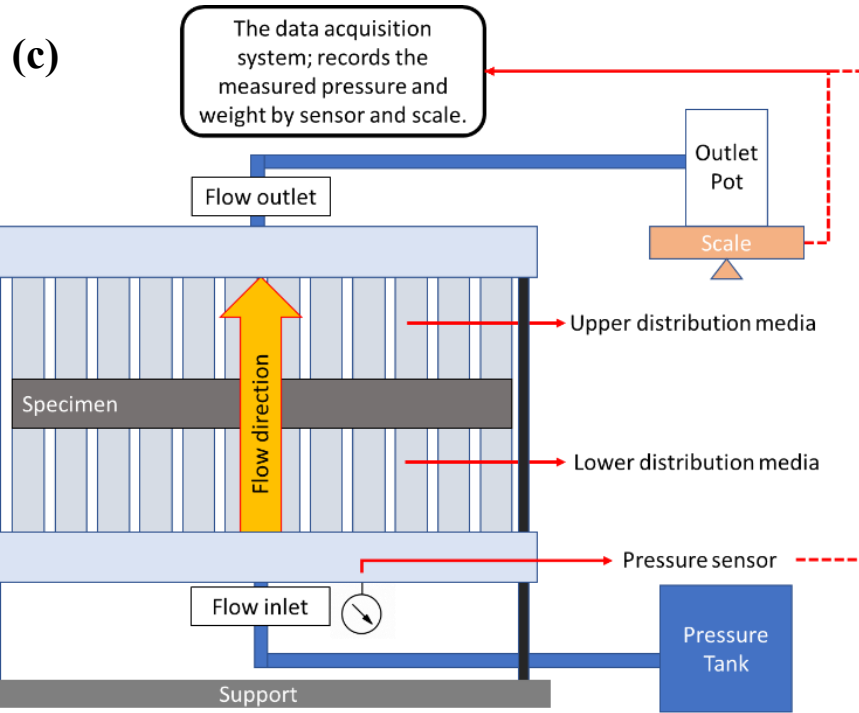
Figure 36. (a) Out-of-plane permeability setup (b) porous distribution media (inlet) (c) setup schematic [37]

4.1.1 Design of Experiments and Sample Preparation

Table 12 shows four flat 203.2 × 203.2 mm (8 × 8 inch) preforms in different patterns with the stacking sequence of [0, 45, 90, -45] considered for preparing specimens for investigating the effect of gap size on the out-of-plane permeability. Firstly, a preform was made as the reference with no gaps between adjacent tows (A). The following two preforms had gaps between tows in all four layers with gap sizes of 0.4 and 0.8 mm (B and C). The last one consisted of gaps between adjacent tows in two layers of stack up with gap sizes of 0.4 mm (D).

Table 12. Test plan for permeability test

Pattern	Gap Size (mm)	Layers with gap	Total number of layers	Injection pressure (gauge) (psi)	Number of Samples
A	No gap	-	4	15	3
B	0.4	All layers	4	15	3
C	0.8	All layers	4	12	3
D	0.4	Two layers	4	15	3

Following the setup described in the method, these preforms were trimmed into 76.2 mm (3 inches) diameter circular samples to be placed in the setup. To cut the specimen, a cutter clamp, see Figure 37, was used to make three circular shape samples out of flat preform using the cutter

under a mechanical press. In the setup's circular fixture, the flow passes through the specimen in the thickness direction from the bottom inlet to the top outlet.
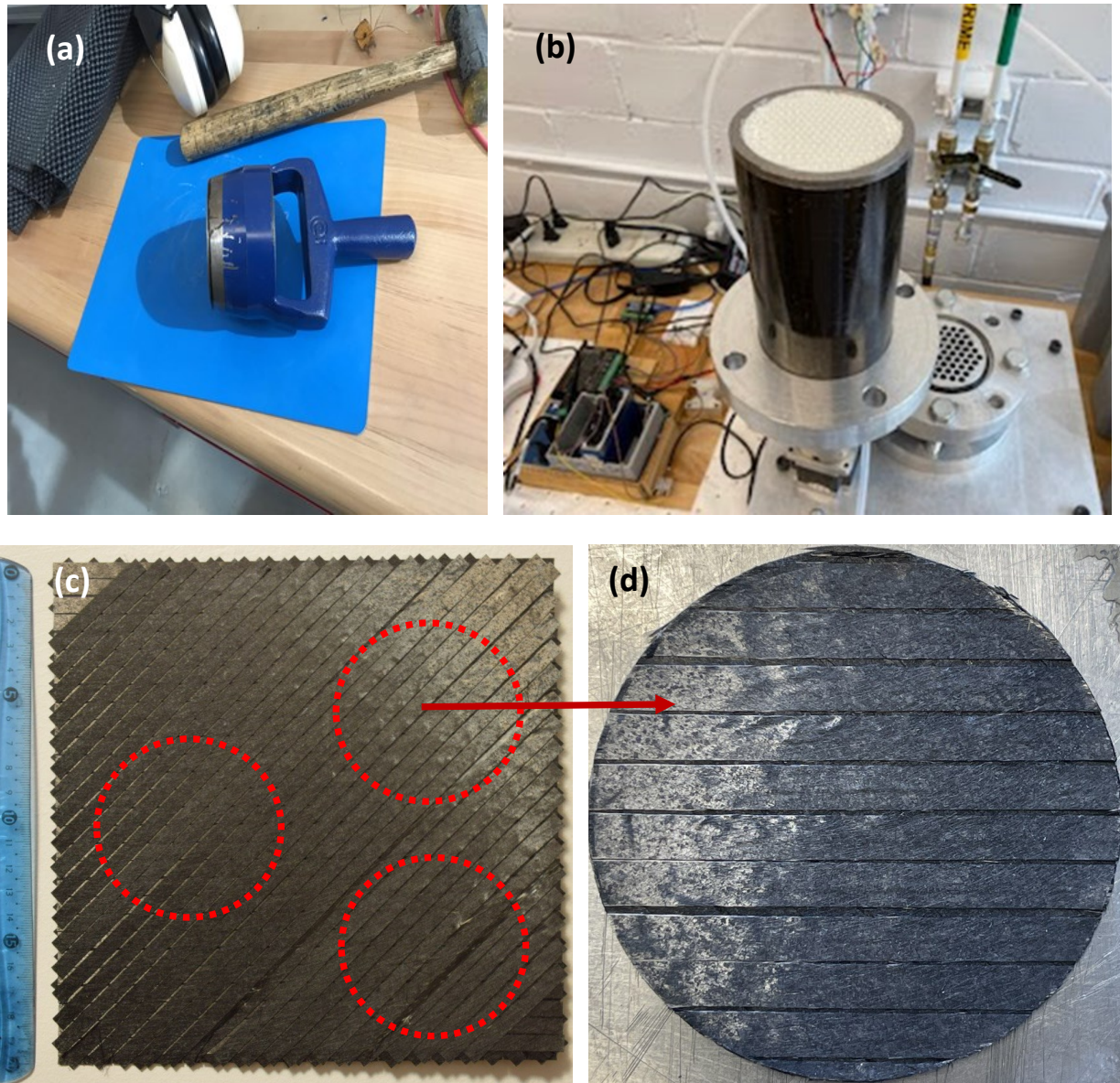
Figure 37. (a) Cutter punch (b) placing the sample inside the permeability setup (c) ADFP preform [37] (d) specimen [37]

4.1.2 Results

Table 13 presents the results for the out-of-plane permeability of preforms A, B, C and D. The thickness was measured using a micrometer, and the fiber volume fraction was calculated using equation (3). In this equation, m is specimen weight, A is the cross-sectional area, h is specimen thickness, and ρ is fiber density. The specimen weight and thickness were measured

using a scale with a precision of 0.0001 g and a micrometer with an accuracy of 0.001 mm. Also, the cross-sectional area and fiber density were considered constant for all the specimens. The pressure sensor used also had a precision of 0.00001 psi. The scale used for measuring the weight of collected oil in the outlet had a precision of 0.1 g.

Since most parameters were measured to obtain the permeability, the measurement error was also calculated by logarithmic differentiating of equation 2 based on variables and using the tools' precision for each variable's absolute error, see equations (4-7). It was observed that thickness measurement has the most influence.

$$V_f = \frac{m}{Ah\rho} \tag{3}$$

$$\ln K_z = \ln\frac{\mu.Q.h}{\Delta p.A} = \ln\frac{\mu.m.h}{\Delta p.A.\rho.t}$$
$$= \ln\mu + \ln m + \ln h - \ln\Delta p - \ln A - \ln\rho - \ln t \tag{4}$$

$$\xrightarrow{\Delta} \frac{dK_z}{K_z} = \frac{d\mu}{\mu} + \frac{dm}{m} + \frac{dh}{h} + \frac{d(\Delta p)}{\Delta p} + \frac{dA}{A} + \frac{d\rho}{\rho} + \frac{dt}{t} \tag{5}$$

μ, A and ρ are constant.
$\xrightarrow{\hspace{2cm}}$

$$\frac{dK_z}{K_z} = \frac{dm}{m} + \frac{dh}{h} + \frac{d(\Delta p)}{\Delta p} + \frac{dt}{t} \tag{6}$$

$$error = \frac{\Delta K_z}{K_z} = \frac{\Delta m}{m} + \frac{\Delta h}{h} + \frac{\Delta(\Delta p)}{\Delta p} + \frac{\Delta t}{t} \tag{7}$$

$$\frac{\Delta K_z}{K_z} = \frac{0.1\ g}{18.2\ g} + \frac{0.001\ mm}{0.900\ mm} + \frac{0.00001\ psi}{14.8085\ psi} + \frac{0.1\ s}{300\ s} = 0.006995 \approx 0.70\ \% \tag{8}$$

Equation (8) shows the error calculation for the 1st sample of pattern A.

Table 13. Out-of-plane permeability test result

Pattern	Gap Size (mm)	Thickness (mm)	Fiber Volume Fraction (%)	Permeability (μm²)	Error (%)
A1		0.858	58.13	0.012	0.70
A2	No gap	0.842	58.42	0.011	0.24
A3		0.847	58.19	0.009	0.31
Average ± SD		0.849 ± 0.007	58.25 ± 0.12	0.011 ± 0.001	
B1	0.4	0.795	56.56	0.221	0.22
B2		0.796	56.96	0.194	0.16

B3		0.811	57.26	0.171	0.17
Average ± SD		**0.801 ± 0.007**	**56.93 ± 0.29**	**0.195 ± 0.020**	
C1		0.773	53.43	0.535	0.21
C2	0.8	0.783	51.92	0.653	0.18
C3		0.771	54.46	0.531	0.20
Average ± SD		**0.776 ± 0.005**	**53.27 ± 1.04**	**0.537 ± 0.057**	
D1		0.791	59.55	0.030	0.19
D2	0.4	0.813	57.76	0.018	0.24
D3		0.805	57.39	0.018	0.21
Average ± SD		**0.803 ± 0.009**	**58.23 ± 0.94**	**0.022 ± 0.005**	

It can be observed that the permeability difference between different gap sizes obtained by the silicone oil injection has significant differences, see Figure 38 (a). Also, it should be noted that increasing the gap size affected the estimated fiber volume fraction, and consequently, a lower fiber volume fraction resulted in higher out-of-plane permeability. In addition to the gap size, introducing the gaps to the layers can also be effective too. It means having gaps in more layers with the same gap size results in higher permeability, as illustrated in Figure 38 (b).

(a) Out-of-Plane Permeability - Gap Size
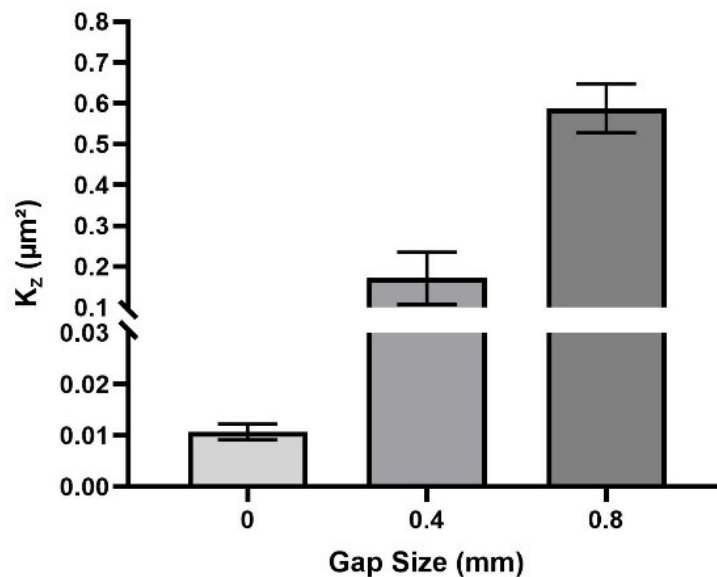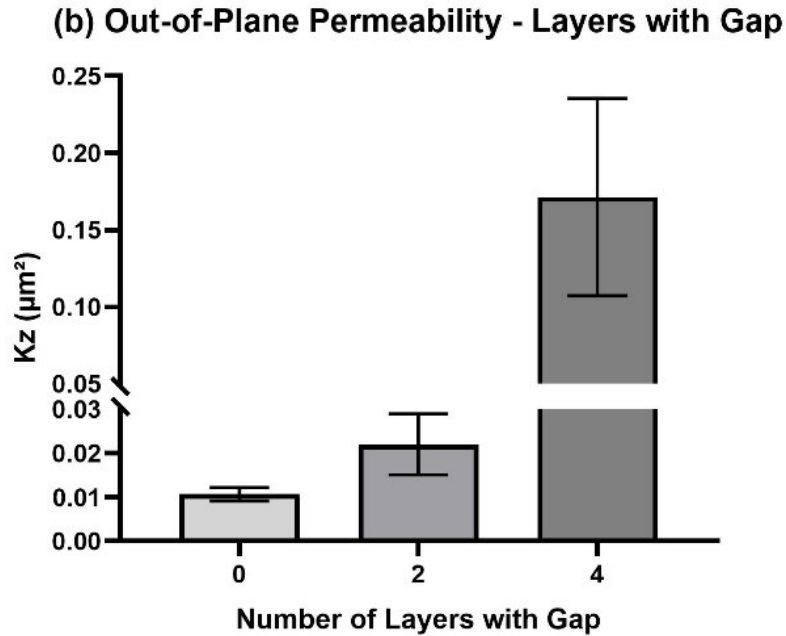
Figure 38. (a) Out-of-plane permeability - gap size [37] (b) Out-of-plane permeability – layers with 0.4 mm gap size

4.2 Compression Test

4.2.1 Design of Experiments and Sample Preparation

Dry preforms with a dimension of 203.2 × 203.2 mm (8 × 8 inch) and the stacking sequence of [0, 45, 90, -45]s had been laid up by ADFP. Once preforms had been made, they were infused using the high-temperature SCRIMP method to study the correlation between gap size and mechanical properties of the laminate.

Following the gap patterns in the permeability measurement, Table 14 describes the gap patterns in this step where reference (A) had no gap between tows, pattern (B) had 0.4 mm gaps between tows in all layers and pattern (B) had 0.8 mm gaps between tows in all layers.

The compressive test was performed to evaluate the effect of gap size on the mechanical performance of laminate made by ADFP and VARI. Compared to the tensile test, it could raise more challenges, like buckling during the test, as it introduces a compressive load to the material [43]. Also, since introducing gaps between tows could improve the impregnation of stack up and reduce the fiber content, the compression test can clarify the contribution of the epoxy in fiber bonding and mechanical performance. The compression test performed adhered to the American Society for Testing and Materials (ASTM) compression test standard, ASTM D 3410.

Table 14. Test plan for compression test [37]

Pattern	Gap Size	Layers with gap	Total number of layers	Number of repeats
A	No gap	-	8	5
B	0.4 mm	All layers	8	5
C	0.8 mm	All layers	8	5

Using a diamond saw, five specimens were cut from each of the above laminates to 140 mm (5.5 inches) in length and 26 mm (1 inch) in width, illustrated in Figure 39 (a). The gage thickness also was measured using a micrometer for each specimen. Using recorded stress and strain values from the load cell and unidirectional strain gauge, model C2A-06-125LW-350 from Micro-Measurements, compressive modulus and compressive strength of laminates were determined. All specimens had two strain gauges installed back-to-back, one on both sides, to check if buckling would occur, see Figure 39 (b) [44].
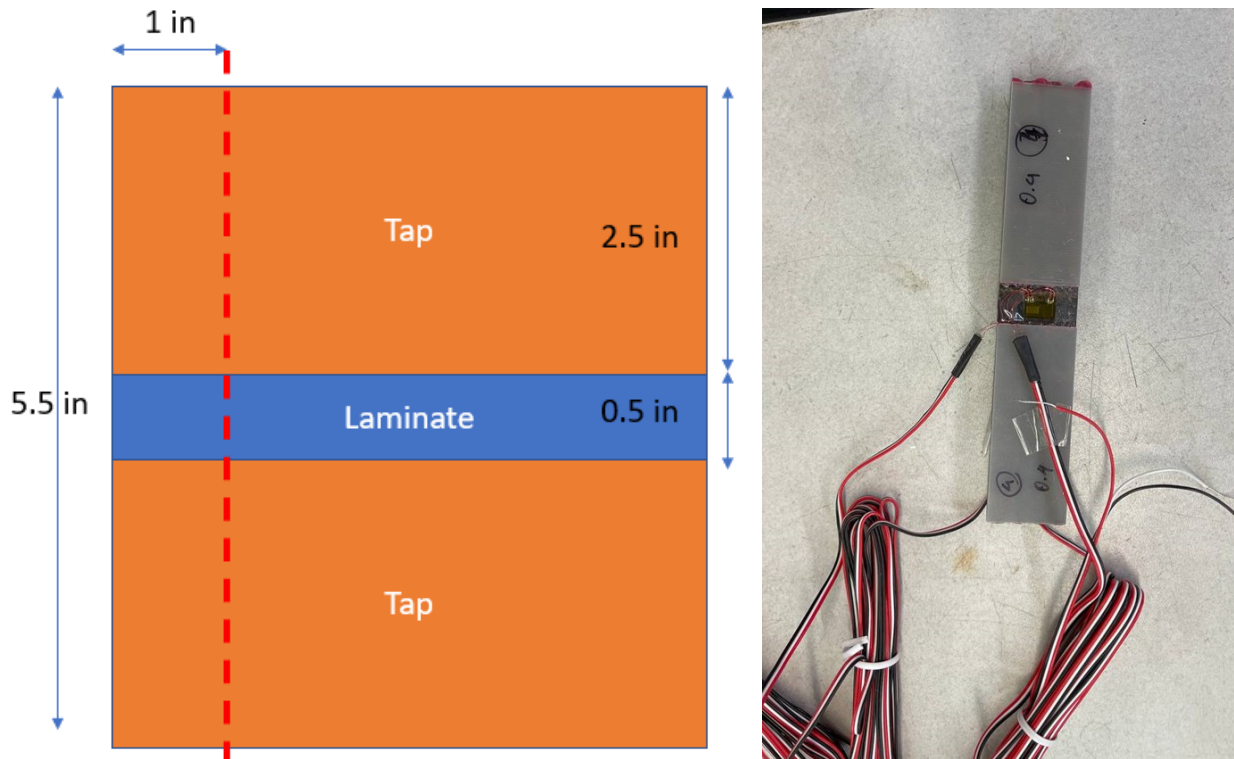
Figure 39. (a) Schematic of laminate cutting for compression specimen (b) Strain gauges installed on a specimen[37]

The difference between the stress-strain slope on both sides is determined by "Percent Bending", and it should be below the maximum allowable of 10% as per standard at the average longitudinal strain equal to 2000 $\mu\epsilon$. Equations (9) and (10) describe the percent bending and

average strain in which ϵ_1 indicates strain from the first gage and ϵ_2 indicates strain from the second gage.

$$B_y = Percent\ Bending = \frac{\epsilon_1 - \epsilon_2}{\epsilon_1 + \epsilon_2} \times 100\ [44] \tag{9}$$

$$\epsilon_{ave} = \frac{\epsilon_1 + \epsilon_2}{2}\ [44] \tag{10}$$

4.2.2 Quality Analysis

- **Microscopic Analysis**

As it was explained in the DoE section, three laminates without gap (A), with 0.4 mm gap in all layers (B) and with 0.8 mm gap in all layers (C) were fabricated. Thickness and weight of preforms were measured before infusion. After infusion, the laminates' weight and thickness were measured (see Table 15) to calculate the fiber volume fraction using equation 3.

Table 15. Laminate properties [37]

Pattern	Gap Size (mm)	Preform Thickness (mm)	Laminate Thickness (mm)	Preform Weight (g)	Laminate Weight (g)	V_f (%)	Infusion time (s)
A	0.0	1.619 ± 0.037	1.562 ± 0.030	69.146	92.472	58.1	940
B	0.4	1.572 ± 0.035	1.469 ± 0.021	64.987	85.370	56.2	810
C	0.8	1.567 ± 0.038	1.537 ± 0.027	62.308	86.291	54.1	650

Using ImageJ software, the gap size for 15 points in each layer of preforms inside the gage area was measured to obtain the variation of the gap sizes. Also, the gap size for 15 points in each layer of laminates made for compression study was measured using the optical microscope to compare the gap variation before and after infusion-curing. Although 0 mm, 0.4 mm, and 0.8 mm gap sizes were set in the AFP machine for patterns A, B, and C, respectively, Table 16 shows that the achieved average gap size is not precise.

Table 16. Gap variation in preform and laminate made for compression tests [37]

Pattern	Programmed Gap Size (mm)	Actual Gap Size Preform (mm)	Actual Gap Size Laminate (mm)
A	0	0.114 ± 0.131	0.051 ± 0.096
B	0.4	0.485 ± 0.231	0.354 ± 0.228
C	0.8	0.740 ± 0.232	0.618 ± 0.174

It is noteworthy that selected points for gap variation measurement of pattern A consisted of non-zero and zero gaps (overlaps are not considered). However, due to machine imprecision and low tension in dry fiber, overlaps may also be there in the preform A, which can not be recognized with 2D images taken by the digital single-lens reflex (DSLR) camera. Figure 40 illustrates that the average gap size is reduced after infusing and curing the preform in all the patterns. This reduction in the gap size after infusion and curing can be because of fiber migration due to the resin flow, which can move fibers. Also, vacuum pressure during the infusion and curing process is another possible reason which closed these gaps channels by applying pressure on the preform.
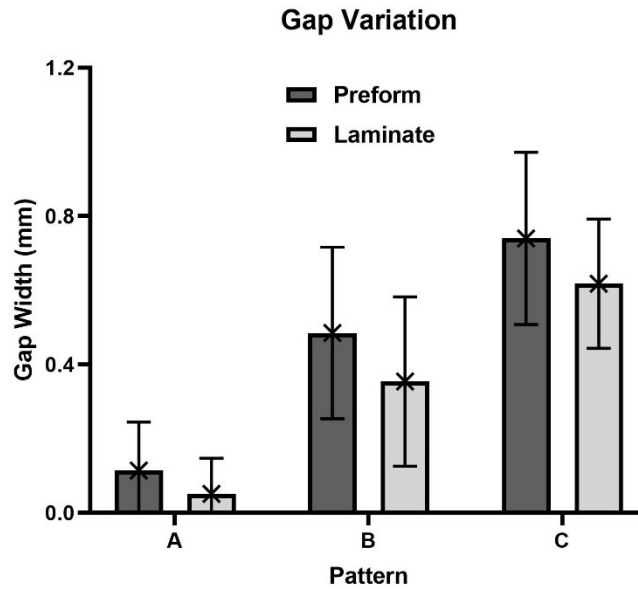
Figure 40. Gap size variation in preform and laminate for three patterns [37]

Figure 41 shows the expected gap size in each layer of micrograph samples for patterns B (0.4 mm gap) and C (0.8 mm gap), in which the first and last layers, 0° layers, have normal views. Figure 41 (c) demonstrates that gaps in the fourth and fifth layers of a sample with pattern B were

0.169 and 0.575 mm, respectively. However, they were supposed to be equal to 0.566 mm (normal value of 0.4 mm in a 45° plane).

*Gap size in the ±45° layers in cross-section view was calculated by dividing the gap size in the normal view by cos(±45).
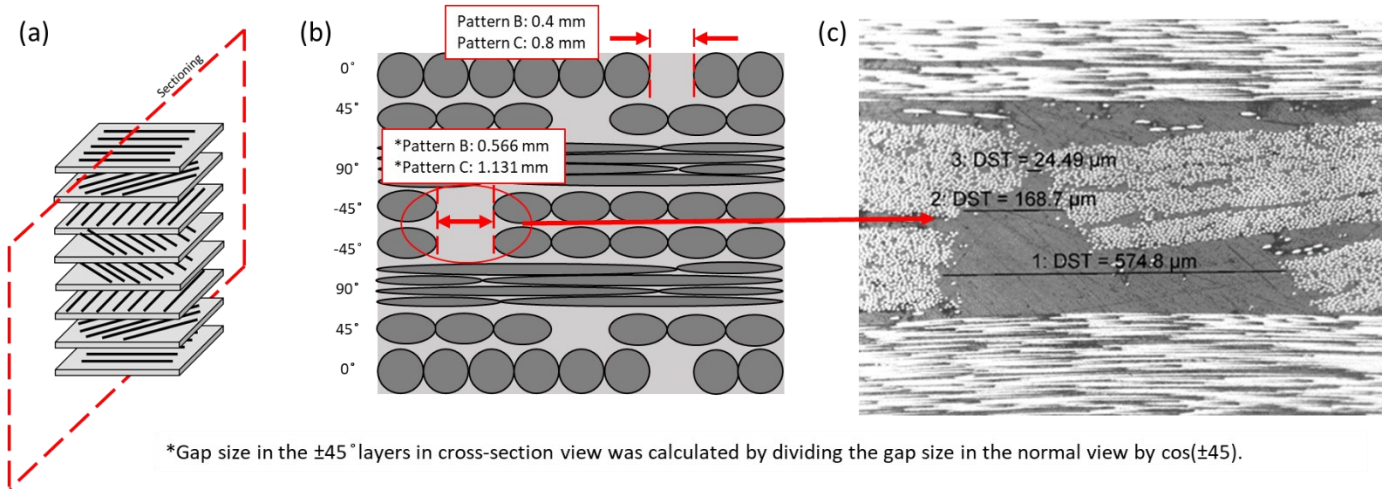
Figure 41. Schematic of gap sizes in the cross-section view of the laminate (a) laminate with sequence of [90, -45, 0, 45]s (b) gaps sizes in the laminate cross-section for pattern B and C (c) gaps in layers 4 and 5 (-45°) of a sample from pattern B (0.4 mm) (* DST: discrete sine transform) [37]

As gaps are introduced in the fiber architecture in two patterns (B and C), it was expected to have lower void content as impregnation increased due to more channels inside the fiber. However, introducing gaps made concerns about creating fiber waviness as the flow rate was higher in preforms with gaps.

So, ten samples from each laminate pattern were cut to study the void content and check the fiber waviness due to epoxy flow. The void content of each micrograph was measured using ImageJ software by specifying the voids' contrast and distinguishing them by fiber and epoxy (see Figure 42). It was observed that increasing the gap size results in lower void content, as void content is described in Table 17. Also, no significant fiber waviness was observed in each pattern.

Table 17. Void and gap content of laminates [37]

Pattern	Gap Size (mm)	Void Content (%)
A	No gap	1.58 ± 0.03
B	0.4	0.99 ± 0.07
C	0.8	0.88 ± 0.01
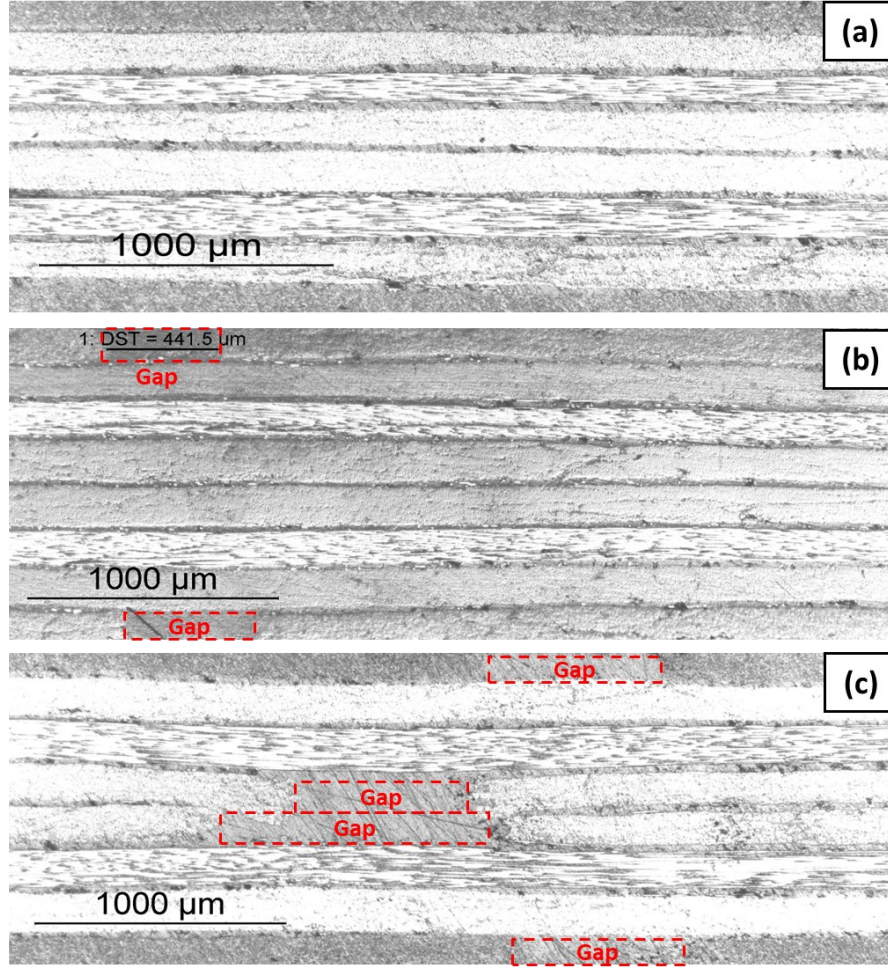
Figure 42. Micrography for laminate (a) without gap, (b) with 0.4 mm gap, (c) with 0.8 mm gap [37]

- **DSC**

The differential scanning calorimetry (DSC) test was used to verify the cure completeness and measure the epoxy system's glass transition temperature. Also, the degree of cure is calculated by measuring the released heat. The residual heat of reaction for the samples of the laminates (A), (B), and (C) was measured by DSC tests (see Figure 43). Table 18 shows the calculated degree of cure for samples using equation (11) and the total heat of reaction for the EPON 862 resin obtained from Ref [45]. The degree of cure for all fabricated laminates was in the range of 99.73 – 99.84 %; therefore, all samples were properly cured.

$$\alpha = \frac{\int_{t_0}^{t_1} h}{H_T} = 1 - \frac{H_{res}}{H_T} \ [10], [46] \tag{11}$$

In the above equation, α is the degree of cure, h is specific heat flow in (W/g), H_{res} is the residual heat of reaction in J/g, and H_T is the total heat of reaction in J/g.

Table 18. DSC test results for laminates A, B and C

Pattern	Glass Transition Temperature (°C)	Residual Heat of Reaction (J/g)	Total Heat of Reaction (J/g)	Degree of Cure (%)
A	143.50	0.6480	341 [45]	99.81
B	144.38	0.4971	341	99.85
C	142.73	0.4382	341	99.87
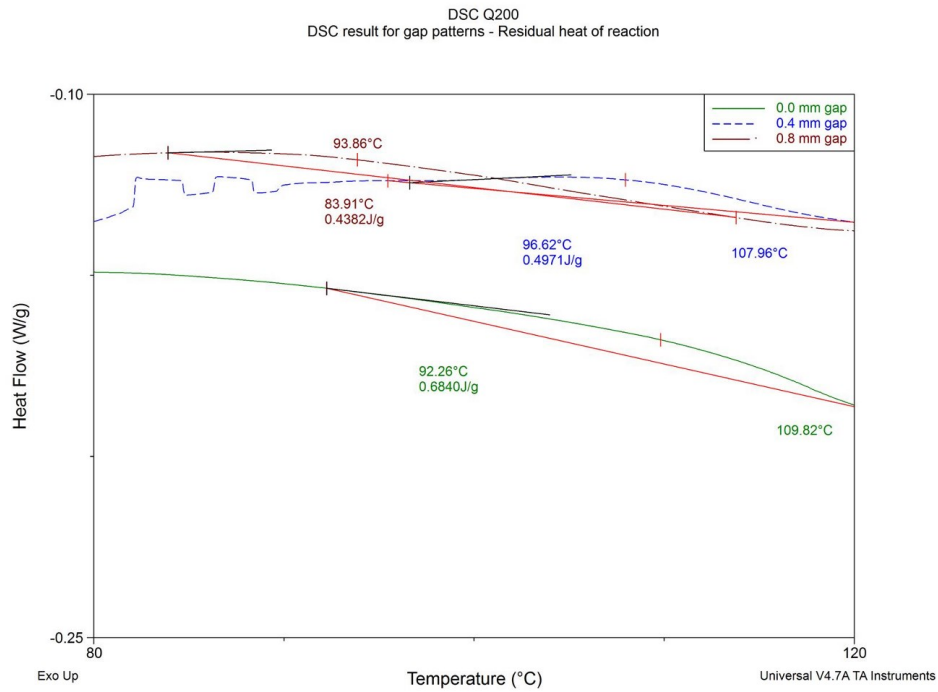
Figure 43. 1st heat in the DSC result for the three patterns
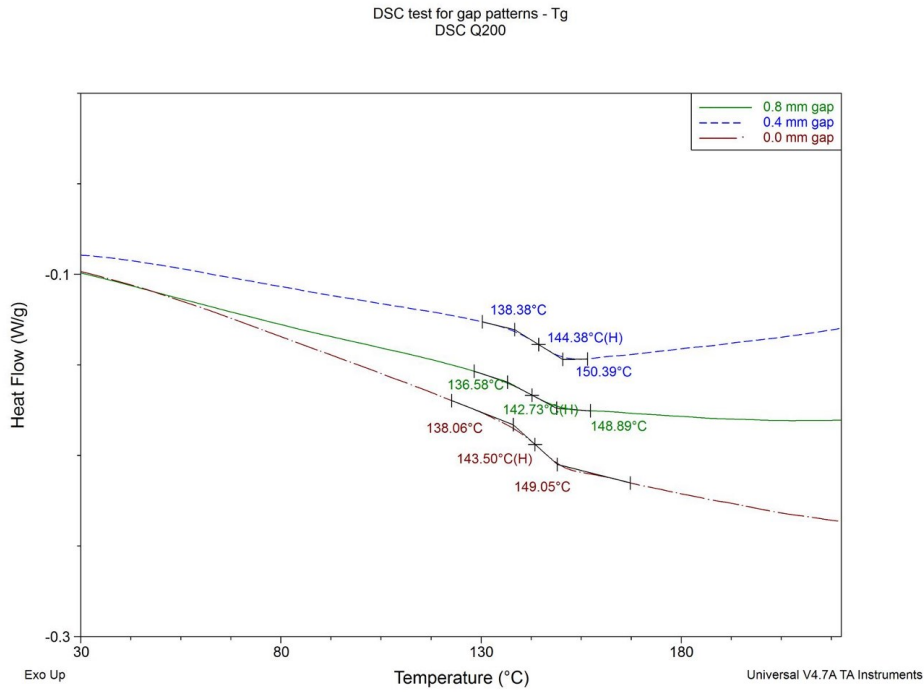
Figure 44. 2nd heat in the DSC result for the three patterns

4.2.3 Results

As it was explained in the DoE section, three laminates without gap (A), with 0.4 mm gap in all layers (B) and with 0.8 mm gap in all layers (C) were fabricated. According to the ASTM D3410, the compression modulus and ultimate compressive stress are calculated using the below equations:

$$F^{cu} = \frac{P^{max}}{A} \tag{12}$$

$$E^{chord} = \frac{\Delta\sigma}{\Delta\varepsilon} \tag{13}$$

In equation 12, F^{cu} is the compressive strength, MPa (psi), P^{max} is the maximum force before failure, N (lbf), and A is the cross-sectional area at the test section. Also, in equation 13, E^{chord} is the compressive (chord) modulus of elasticity, MPa (psi), $\Delta\sigma$ is the difference in applied compressive stress between 1000 and 3000 µε strain points, MPa [psi], and $\Delta\varepsilon$ is the difference in the average compressive strain between 1000 and 3000 µε strain points, absolute strain [44]. Figure 45 illustrates the chord slope in the stress-strain curvature between 1000 and 3000 µε strain for the samples obtained from laminate without gap (pattern A).
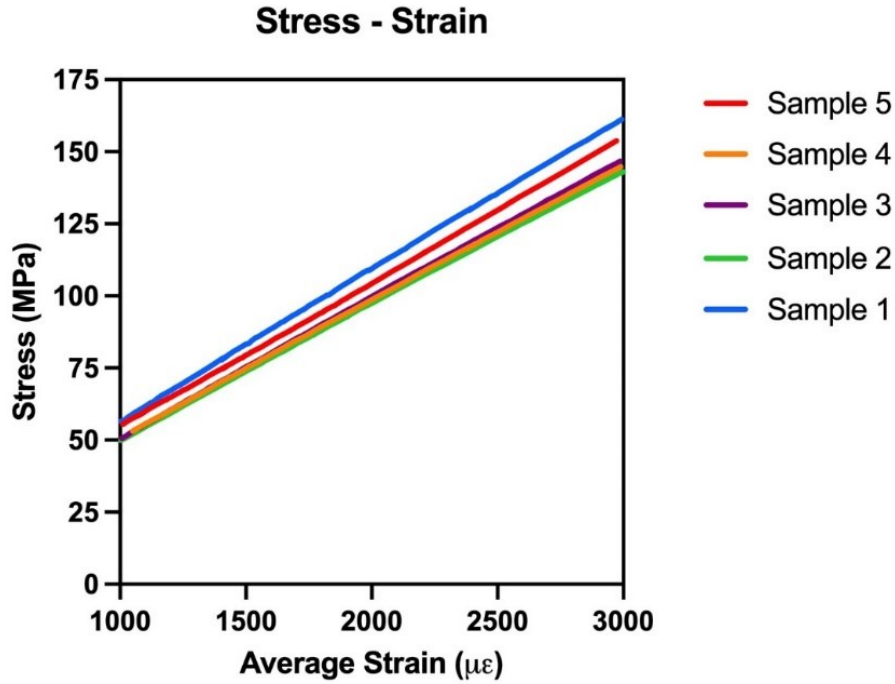
Figure 45. Compressive chord modulus for specimens with 0 mm gap size (A)

Table 19 shows the results obtained from the compression test, including the compressive strength and compressive modulus for three patterns of A, B and C. It can be seen that increasing the gap sizes averagely results in lower compressive strength and modulus, although it significantly reduces the impregnation time of laminates.

Table 19. Compression test detailed result – Compressive Strength

Pattern	A		B		C	
	Strength (MPa)	Modulus (GPa)	Strength (MPa)	Modulus (GPa)	Strength (MPa)	Modulus (GPa)
1	417.5	54.64	317.08	47.58	329.59	47.81
2	443.63	48.44	468.08	47.77	465.38	47.9
3	429.07	49.64	490.71	45.87	419.48	45.99
4	488.39	49.11	406.11	44.91	413.94	45.73
5	399.80	52.25	366.56	49.50	256.91	44.95
Average	435.68	50.82	409.71	47.13	377.06	46.48
SD	30.01	2.31	63.91	1.60	74.36	1.18

Figure 46 shows the relationship between gap size, compressive modulus, and strength. As demonstrated, increasing the gap size, unlike permeability, results in lower modulus and strength. However, in terms of the average modulus, the difference between 0.4- and 0.8-mm gap patterns is insignificant compared to the difference between patterns without and with the gap. Having close gap content compared to pattern C in pattern B may be the main reason which will be explained in the next section.
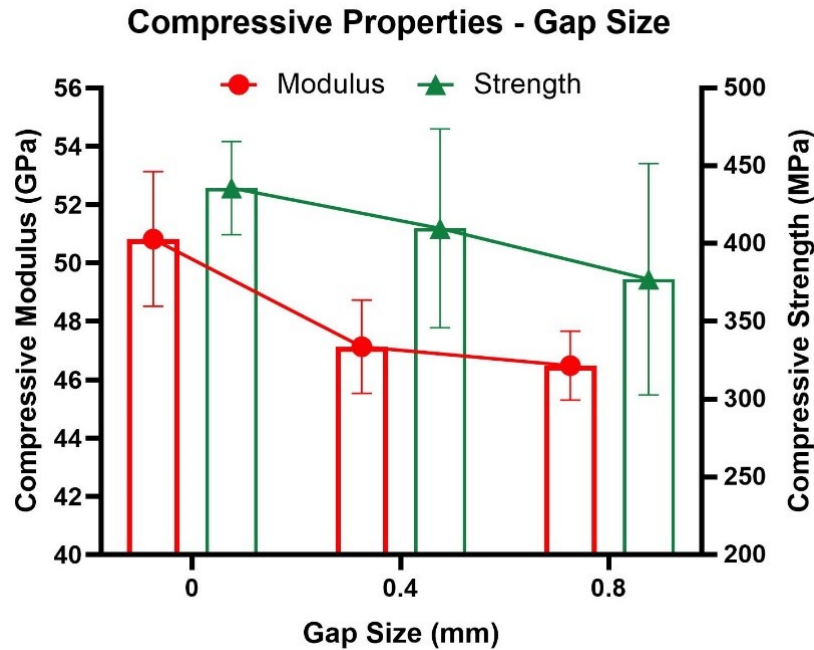
Figure 46. Gap effect on the compressive modulus and strength [37]

4.3 Conclusion

The ADFP provides the ability to introduce the gaps and overlaps into the fiber preform pattern, which influences the fiber volume fraction. While reducing the fiber volume fraction could increase the preform impregnation time, it also affects the mechanical properties of the laminate due to lower fiber content. It has been demonstrated that introducing 0.4 mm and 0.8 mm gaps in all layers increases the out-of-plane permeability about 20 and 50 times compared to the preform without any gap. Also, it has been observed that adding 0.4 mm and 0.8 mm gaps in all layers results in 7.26 % and 8.54 % drops in the compressive modulus and 5.96 % and 13.45 % drops in the compressive strength compared to the laminate without any gap.

Figure 47 illustrates that among the three configurations studied, the optimum gap size is the preform with 0.4 mm gaps in all layers, pattern (B), which provides a significant increase in

the out-of-plane permeability, 20 times greater, and a minimum loss in compressive properties, 7.2 % in modulus and 6 % in strength, compared to the preform without gaps.
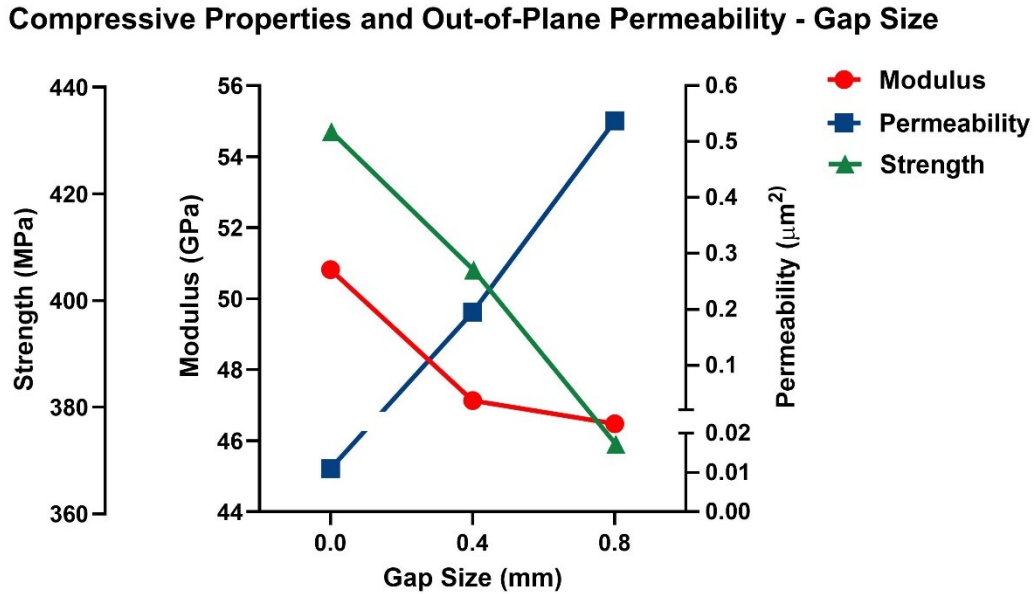
Figure 47. Effect of gap size on the out-of-plane permeability and compressive modulus [37]

Therefore, it can be concluded that introducing gaps in the layup of the preform made by ADFP can solve the impregnation challenge of low permeable dry fibers. However, adding gaps into the layup results in sacrificing the mechanical properties of the laminate as fiber volume content is reduced. It was shown that the loss in mechanical properties, specifically compressive properties, is insignificant compared to the gain in the out-of-plane permeability if an optimum gap size is chosen.

The next chapter will demonstrate how introducing gaps can affect the fabrication of a large-scale fuselage panel with high aerospace quality. In this matter, four fuselage panel demonstrators have been fabricated. Two of them had preforms without gaps, and two preforms with gaps. Preforms with gaps were impregnated in less time, demonstrating higher out-of-plane permeability in which epoxy flew to the bottom layers and resulted in lower void content, specifically, in the last layers.

Chapter 5. Fuselage Panel Demonstrators

Part of this chapter (5.4) is submitted as a paper entitled "Composite Panel Demonstrator Made by Automated Dry Fiber Placement and Resin Infusion" for presentation at Canadian International Conference on Composite Materials in July 2022 [32].

Making composite structures with simple geometries like flat panels using ADFP and VARI has been discussed in other research projects. However, using these processes for manufacturing large complex geometries can raise the interest of manufacturers to use this method as an alternative in the industry.

Benefiting from the AFP machine, dry fibers can be deposited on a curved fuselage panel mold to make preforms. These preforms can then be infused at high temperatures with epoxy using the VARI process. Therefore, to demonstrate the capability of this method, four fuselage panel demonstrators with symmetric quasi-isotropic layup [(90/45/0/-45)]$_s$ were fabricated. Also, a procedure was defined to analyze fabricated laminates' quality, as described in Figure 48.

Distortion	Thickness Variation	Void Content, Vf, Tg, and Waviness

•Analyze Method
  •Visual Inspection
  •Micrometer
 	
•Possible Defects
  •Lift up
  •Twisting
	•Analyze Method
	  •Micrometer
	  •Micrography
	
	•Possible Defects
	  •Non Uniformity
	  •Resin Rich Areas
		•Analyze Method
		  •Micrography
		  •DSC
		  •DMA
		  •TG
		
		•Possible Defects
		  •Significant void content
		  •Resin rich areas
		  •Fiber waviness
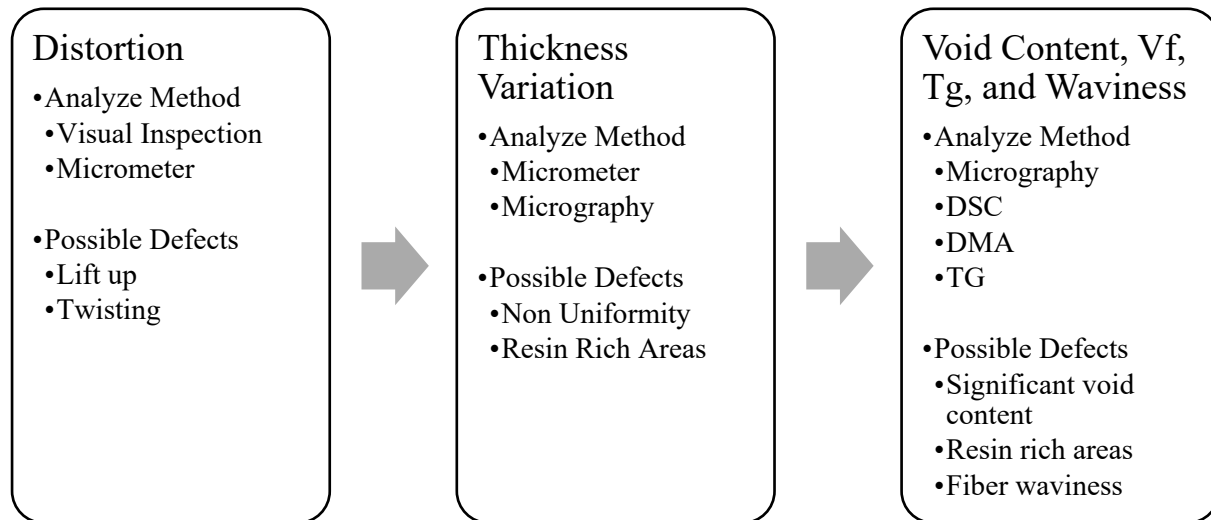
Figure 48. Schematic of quality analysis procedure of demonstrators

Based on the established quality analysis, first, physical features, including dimensions and lift-ups, should be analyzed. The free edges of laminate under the vacuum bag might lift after demolding the part due to spring back effects and causes residual stress, resulting in deformation[47]. Also, the variation of chamber pressure on preform under the vacuum bag influences the thickness variation; thereby, it is critical to measure the thickness variation of laminate. In addition to having local low pressure, bag bridging also creates resin-rich areas that end in non-uniform laminate with major mechanical properties problems.

Second, voids could appear in liquid composite molding due to gas released from the chemical reaction of epoxy and air trap through resin flow [48]. Additionally, local resin-rich areas in the laminate structure could reduce the fiber content and result in reduction in mechanical properties. Finally, laminate made by this developed process should satisfy the standards of the aviation industry in terms of fiber volume fraction, void content and degree of cure.

Moreover, gaps can be tailored into the preform layup to improve the permeability of fuselage panel demonstrators. As explained in Chapter 2, the out-of-plane permeability of fibers is significantly lower than in-plane permeability, making the epoxy impregnation through the thickness more difficult than in-plane flow. Also, in-plane permeability can be increased by increasing the number of flow mesh media. Therefore, the infusion time can be calculated analytically using Darcy's law, equation (1), based on the out-of-plane permeability values obtained in Chapter 4. It is noteworthy that the flow direction is only considered in one direction, thickness direction, as it takes longer for the epoxy to go through the thickness. Using the permeability values calculated for the preforms without gap and preforms with 0.4 mm gap, the estimated time for filling the panel is calculated in Table 20.

Table 20. Estimated 1D infusion time for demonstrator panels

Parameters	μ (Pa.s)	h (mm)	K_z (μm^2)	ΔP (kPa)	Time (s)
Preform without gap	0.02	1.6	0.011	98	29685
Preform with 0.4 mm gap	0.02	1.6	0.195	98	1675

In the above table μ is the viscosity of epoxy, h is the preform thcikness, the distance epxoy travels, K_z is the preform trasnverse permeability, and ΔP is the pressure difference. It can be seen that introducing gaps into the layup of the preform can significantly reduce the filling time. Therefore, two trials were pushed with prefroms without gaps and two were done using preforms with gaps.

5.1 1ˢᵗ Trial

5.1.1 Manufacturing Process
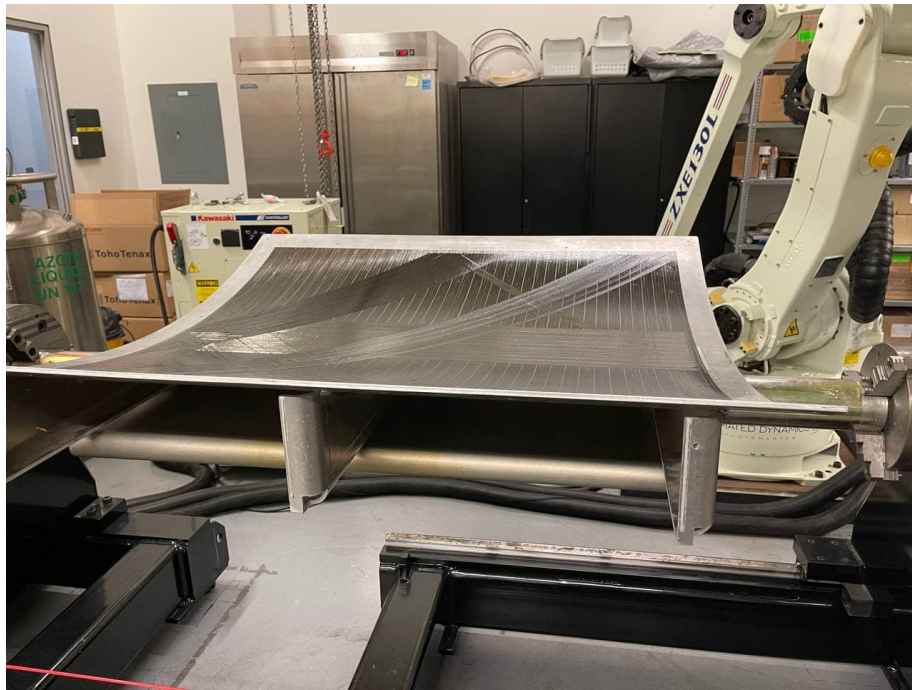
Figure 49. Fuselage panel demonstrator mold

The first trial was done by infusing the preform made by ADFP, Figure 49, using Seemann's composite resin infusion process (SCRIMP) at a high temperature. The SCRIMP setup consisted of different layers as it is described below, see Figure 50.

1. From outside of the setup, the vacuum bag, Airtech Wrightlon WL7400 nylon vacuum bag creates a vacuum chamber for infusion.

2. Omega channel was connected to 2 feet length infusion hosing, which carried the epoxy from the resin pot outside the chamber to the inside.

3. Two layers of glass fiber infusion media, Flexiveil, were laid down underneath the omega channel to increase the in-plane flow rate and make a uniform flow front.

4. A layer of peel ply, Airtech Econolease, is placed on the preform to ease the separation of media from stack-up after infusion. Also, the in-plane permeability of the peel ply is higher than fiber, meaning resin can travel faster inside the peel ply to reach the edges.

5. The preform in dimensions of 91.5 cm by 91.5 cm (36 inches by 36 inches) was placed.

6. Using breather bands around the mold provided uniform vacuum pressure on the panel and resin breakage areas to prevent resin from going through the vacuum port.

7. The bottom layer of the peel ply provides a uniform surface for the vacuum bag to place on the setup.

Materials and process parameters used in both steps are indicated in Table 21.

Table 21. Process parameters for the 1st trial

Process Parameters	
Dry Fiber Material	Solvay TX1100
Layup	[(0/45/90/-45)]S
AFP Parameters	HGT Temp.: 195 and 210 °C HGT Flow: 60 SLPM Compaction Load: 13 lbf Speed Rate: 3in/s Gap Size: no gap
Resin	PRISM EP2400
Dimension	91.4 × 91.4 cm (36 × 36 inch)
Infusion Temperature	100 °C
Curing Temperature	180 °C
Average Thickness	1.488 mm
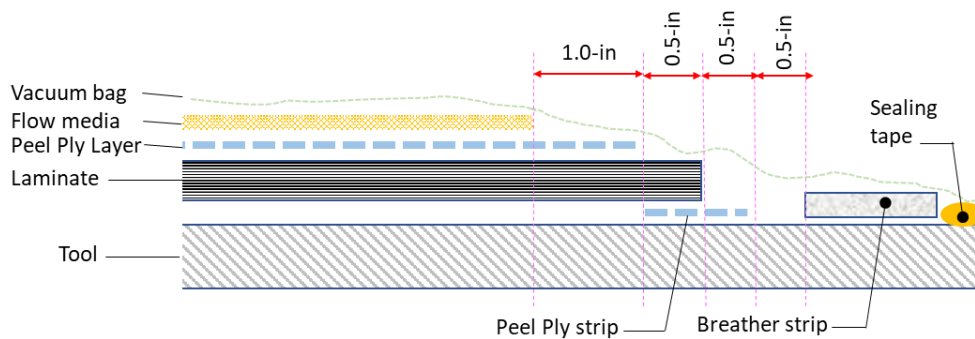
Figure 50. Schematic of the infusion setup for the 1st trial (cross-section)

The infusion procedure is mentioned below:

1. The epoxy resin was degassed for 30 – 45 minutes while heated to 90°C with ABESS equipment at a mixer speed of 60 rpm for 1 hour.

2. Thermocouples were placed one over the stack up, on the bag, and one on the tool side.

3. The tool was preheated to 100 °C.

4. The epoxy was transferred through the infusion Poly Tetra Fluoro Ethylene (PTFE tubes inside the oven and into the part for almost two hours.

5. Once the preform was filled with resin and the inlet (gates) and outlet (vents) were closed, the tool temperature was increased at 2°C/min to 180°C. The oven temperature dwelled at 180°C for 120 minutes.

6. Tool was cooled down to 60°C and below at rate of < 5°C/min before demolding the part from tool.

Figure 51 demonstrates the setup before infusion starts and the setup 2 hours after infusion starts inside the oven. The problem with the infusion at high temperatures is that visual inspection is impossible inside the oven, unlike at room temperature.
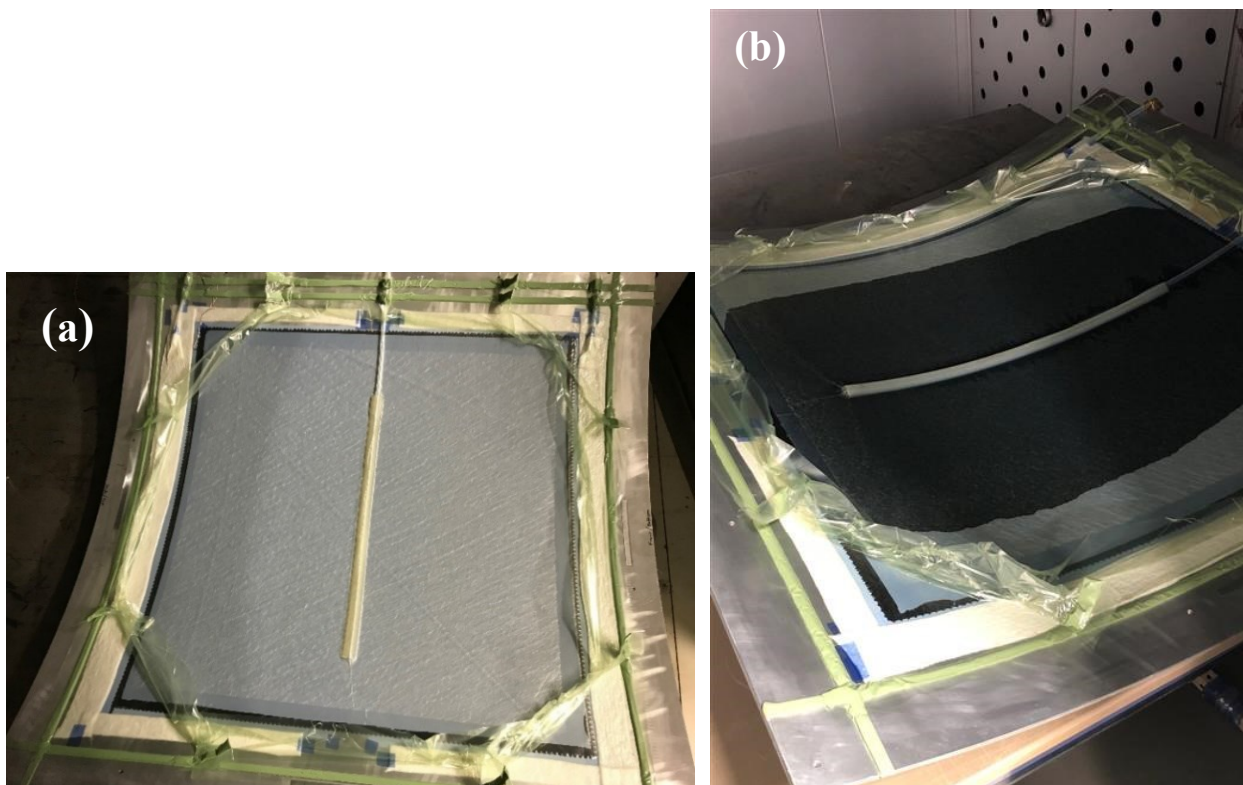
Figure 51. Infusion setup of the 1st trial (a) before infusion (b) after 2 hours

5.1.2 Defects and Challenges

Figure 52 illustrates the 1st fuselage panel demolded after infusion. It is noteworthy that bag bridging about the omega channel also made resin-rich areas. Before depositing any material to make preforms by ADFP, masking tape was used to cover the mold surface to provide stickiness, see Figure 53. In the 1st trial, removing the masking tape from the preform caused the separation of the two first layers. These two layers were added manually to the stack-up, which resulted in an unbalanced layup that caused twisting in the laminate after infusion.
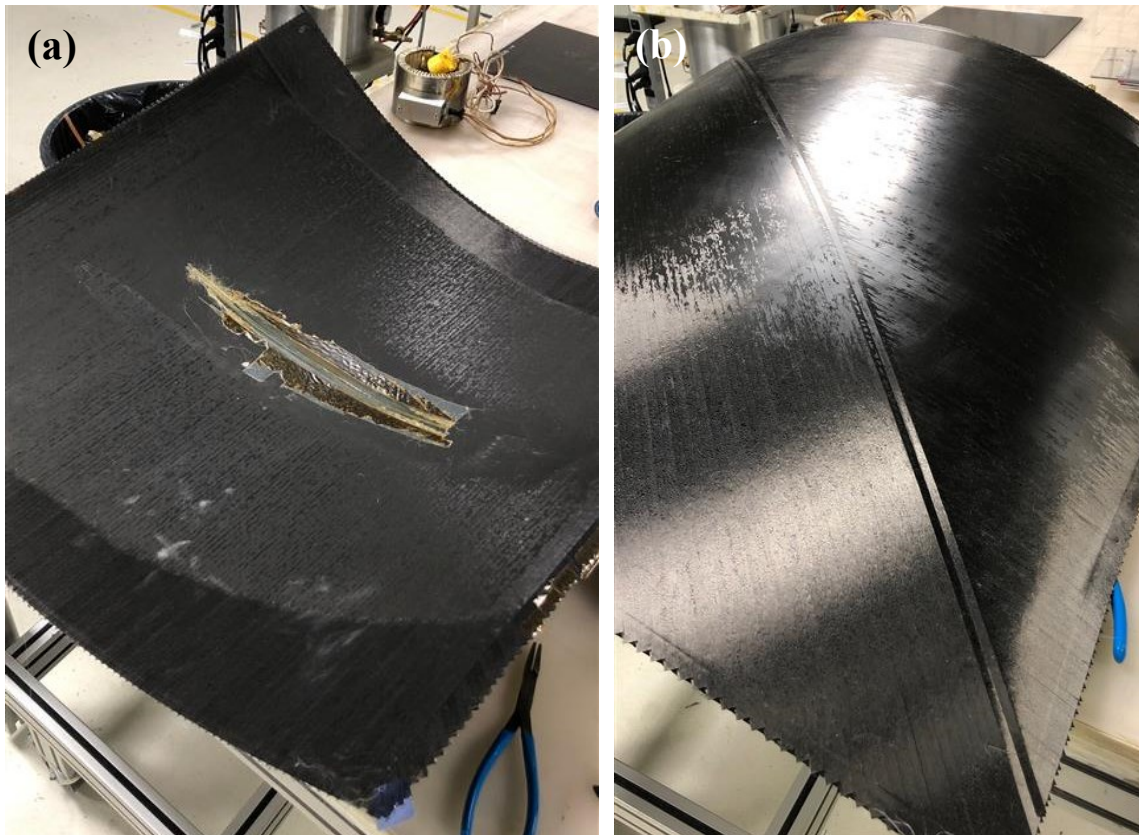
Figure 52. 1st panel after infusion (a) bag side (b) tool side
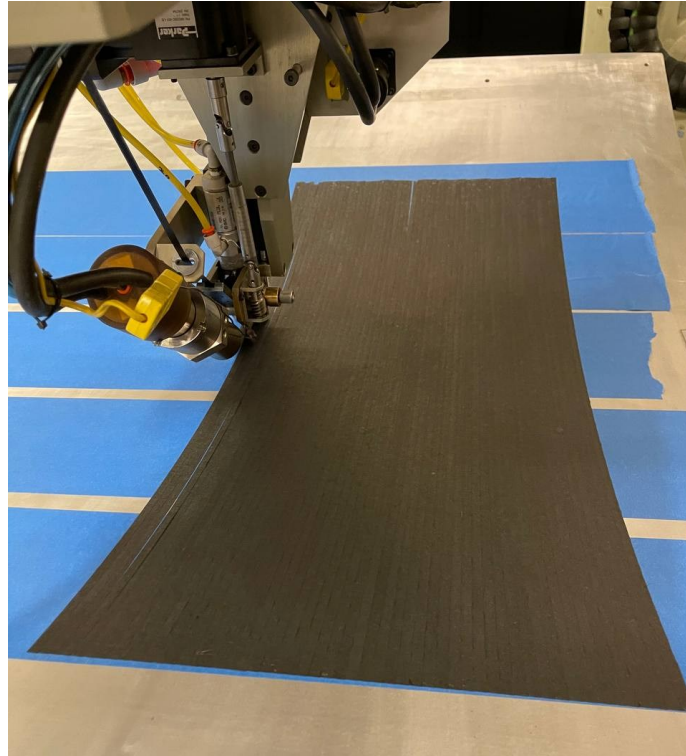
Figure 53. Masking tapes coat on the tool

Additionally, resin shrinkage around the omega channel made a peel-ply imprint on the panel. Moreover, looking at the tool side, the laminate's last layers remained dry for two main reasons.

1. As discussed in Chapter 4, the out-of-plane permeability of the preform without gaps is low.

2. The resin pot was put outside the oven without heating resin in the path to inside the oven. Since the resin viscosity is closely correlated to the temperature, its viscosity increased as the temperature was reduced while transferring the epoxy.

Finally, due to the vacuum sealant unbounding, vacuum pressure was lost, and curing was not completed. As this fuselage demonstrator had not been infused successfully, the quality analysis was not done. However, the lessons learned from 1st trial have been used for the following demonstrators.

5.2 2nd Trial

5.2.1 Manufacturing Process

The second preform, Figure 54, was infused using the same setup used for the 1st trial, SCRIMP, with some modifications in laminate size, heating the hosing and increasing the infusion temperature. A heating line was used for this infusion to heat the hosing while transferring the epoxy inside the oven. Materials and process parameters used in both steps are mentioned in Table 22.
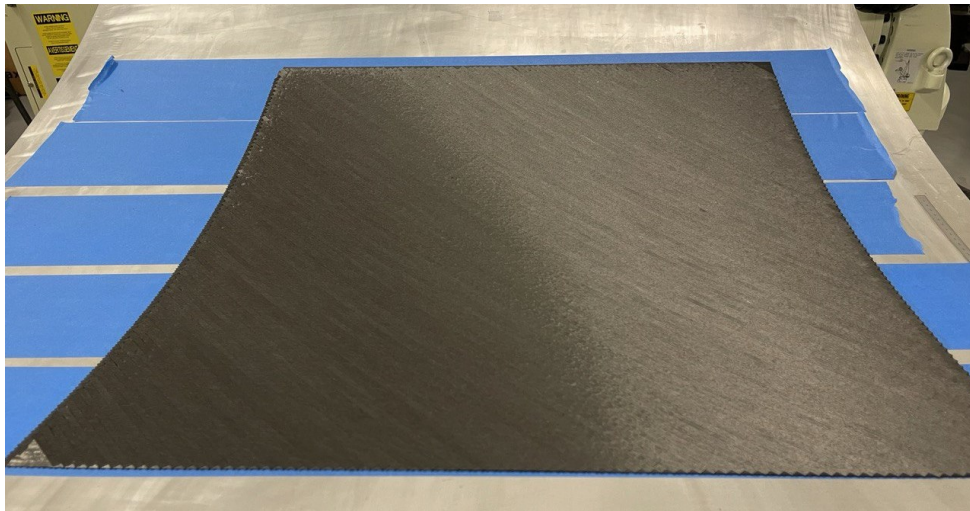
Figure 54. Preform of the 2nd panel

Table 22. Process parameters for the 2nd trial

Process Parameters	
Dry Fiber Material	Solvay TX1100
Layup	[(0/45/90/-45)]S
AFP Parameters	HGT Temp.: 195 and 210 °C
	HGT Flow: 60 SLPM
	Compaction Load: 13 lbf
	Speed Rate: 3in/s
	Gap Size: no gap
Resin	PRISM EP2400
Dimension	76.2 × 76.2 cm (30 × 30 inch)

Infusion Temperature	120 °C
Curing Temperature	180 °C
Void Content Center	0.78 %
Void Content Edge	6.4 %
Average Thickness	1.758mm

The infusion procedure is exactly same with the 1st trial except that the tool was preheated to 120 °C.

5.2.2 Defects and Challenges

First, due to the passing thermal resistance of the peel ply used in the infusion setup, part of the peel ply was melted on the surface, as shown in Figure 55, and made resin-rich areas which acted like a barrier against the resin to flow in-plane. Also, vacuum pressure on the infusion media and hosing created imprints on the bag side of the laminate and compressed the part placed under the hosing, see Figure 56.

Figure 55. 2nd panel after the infusion (bag side)
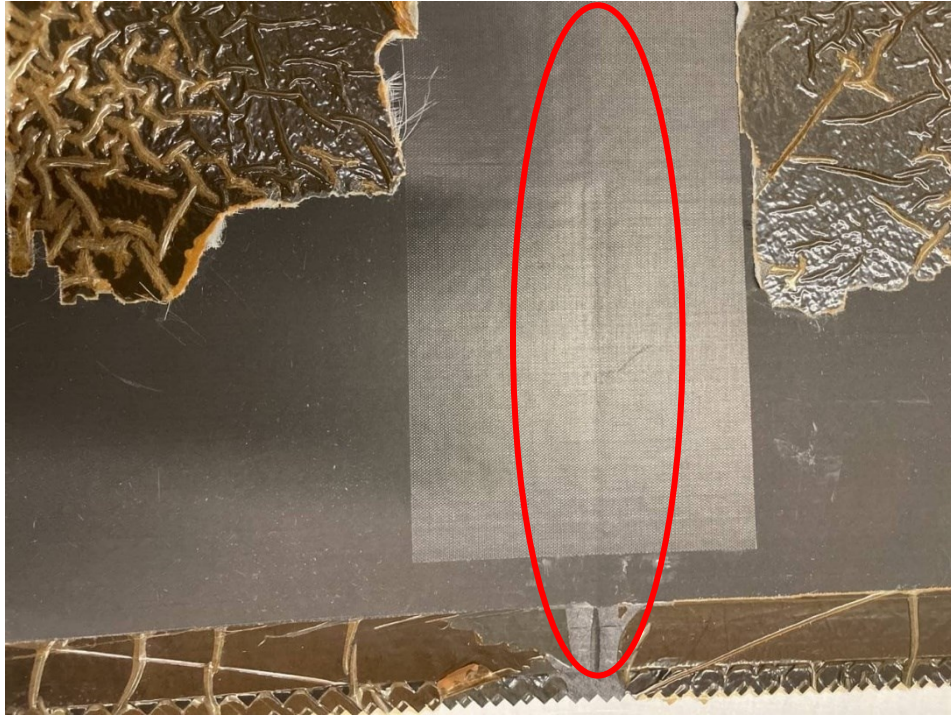
Figure 56. Tube compression on the 2nd panel after infusion

5.2.3 Quality Analysis

Following the procedure defined to analyze the quality of achieved demonstrators, in terms of distortion, Figure 57 demonstrates that edges were lifted approximately 9 mm on one side and 12 mm on the other.
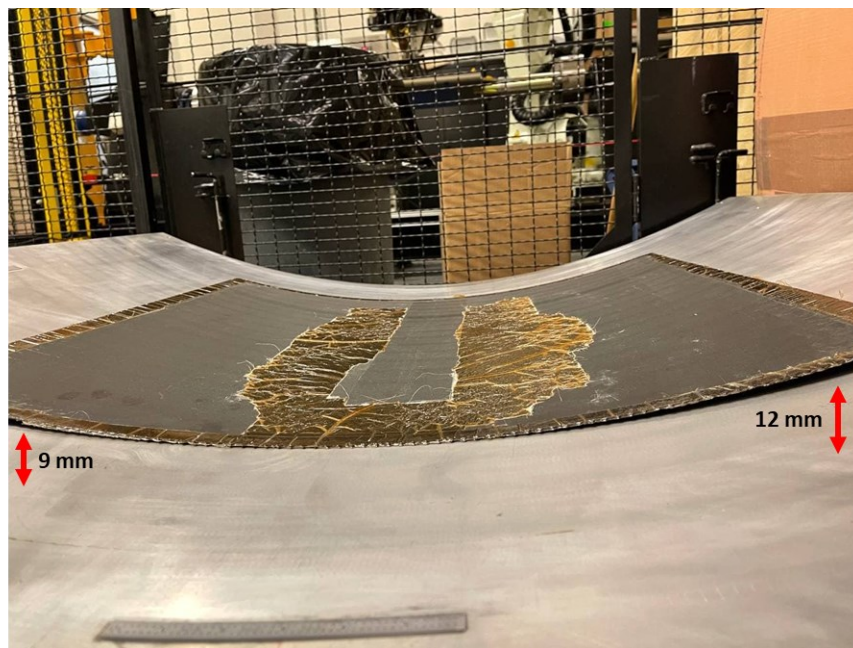
Figure 57. Edge lifts in the 2nd panel (after infusion)

Table 23 describes the result of the thickness uniformity measurement using a 6-inch clamp micrometer for 35 points along the panel.

Table 23. Thickness variation of the 2nd panel

	mm	**in**
Average Thickness	1.758 ± 0.020	0.0692 ± 0.0008
CV %	1.12	1.12
Maximum	1.798	0.0708
Minimum	1.720	0.0677

Regarding microscopic analysis, the panel was trimmed and cut into two parts. As it is illustrated in Figure 58, six bands were taken from one side. In each band, three 25.4 mm by 12.7 mm (1 in by 0.5 in) samples were taken apart for microscopic analysis, which will demonstrate void content and thickness variation using ImageJ software. Figure 58 shows all the bands where three samples were taken for micrography from each band.
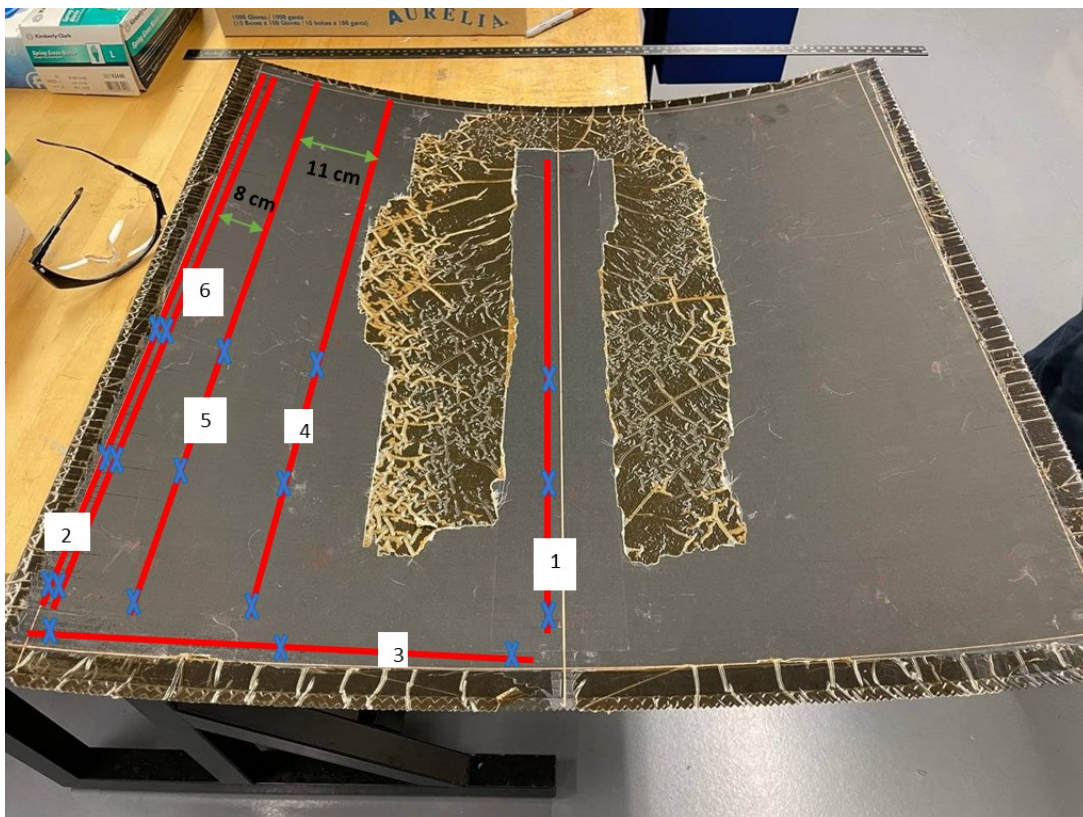
Figure 58. Micrography's samples positions on the 2nd panel

- **Center band (No. 1)**

To clarify the procedure, Figure 59 shows the samples taken from the central band (1). After preparing the samples using the same method described in 4.2.2, void content for each sample was measured using the difference between the contrast of fiber and epoxy with voids. Table 24 shows the achieved void content for each sample.
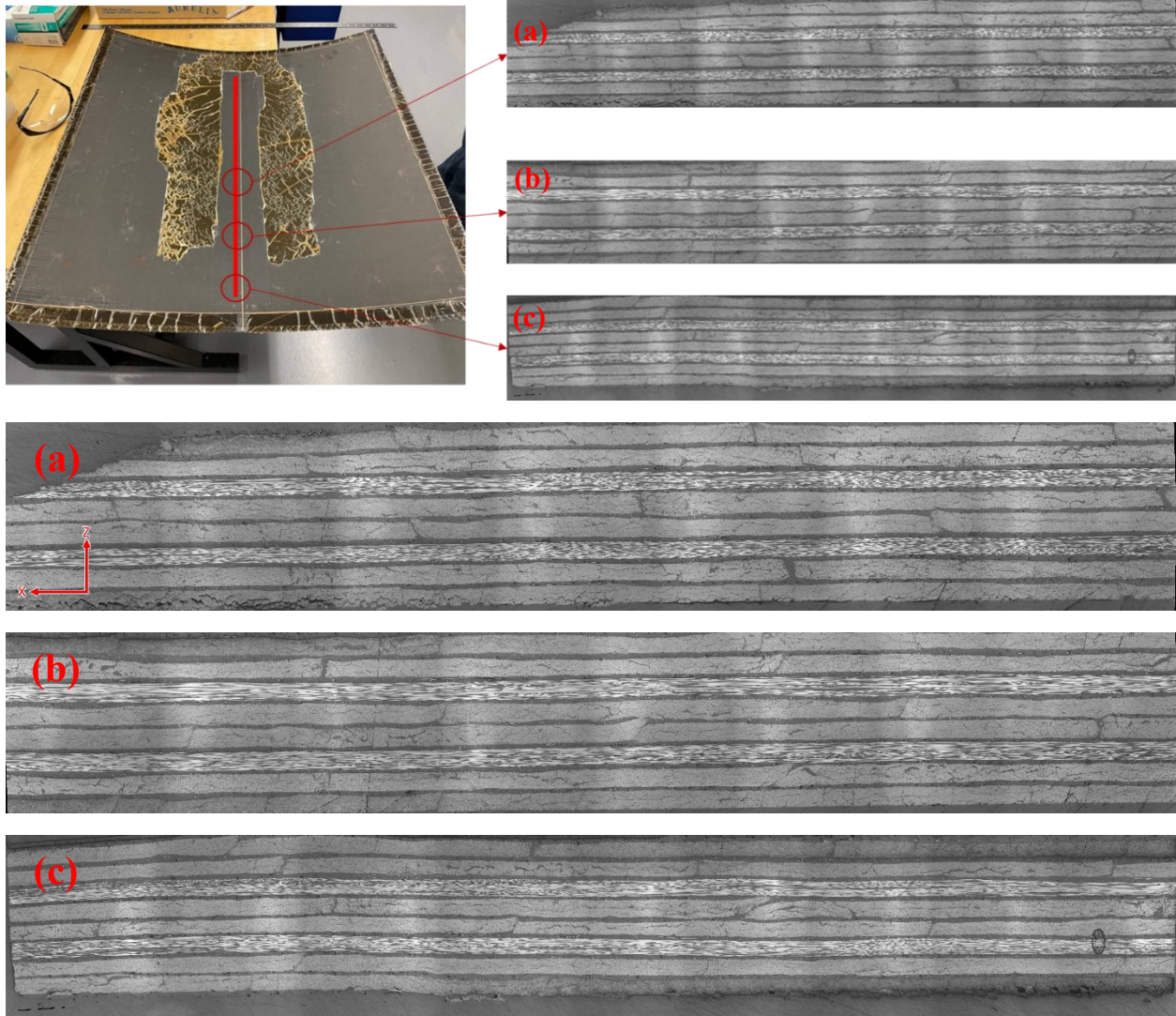
Figure 59. Central band's samples – 2nd panel (a) center sample (b) middle sample (c) edge sample

Table 24. Void content of the 2nd panel

Band Number	Center	Middle	Edge	Average
1	1.026 %	0.213 %	1.033 %	**0.817 %**
2	5.438 %	4.188 %	7.94 %	**5.855 %**
3	6.710 %	1.494 %	0.604 %	**2.756 %**
4	1.611 %	5.420 %	2.910 %	**3.314 %**
5	3.141 %	9.498 %	-	**6.320 %**
6	4.535 %	2.803 %	11.845 %	**6.394 %**
Average (not including band 3)	**3.150 %**	**4.420 %**	**5.930 %**	**-**

Based on the micrography result, there are no wrinkles or fiber disturbances due to the resin flow in the fiber structure. However, since the void fraction in edges is significant, infusion time could be longer to push air outside of the fiber and replace it with epoxy (see Figure 60). Higher void content in the bottom layers confirms the low out-of-plane permeability of preforms made by ADFP using Solvay dry fiber. Due to the low permeability of the preform, the resin flow through the thickness could not wet the last layers thoroughly.
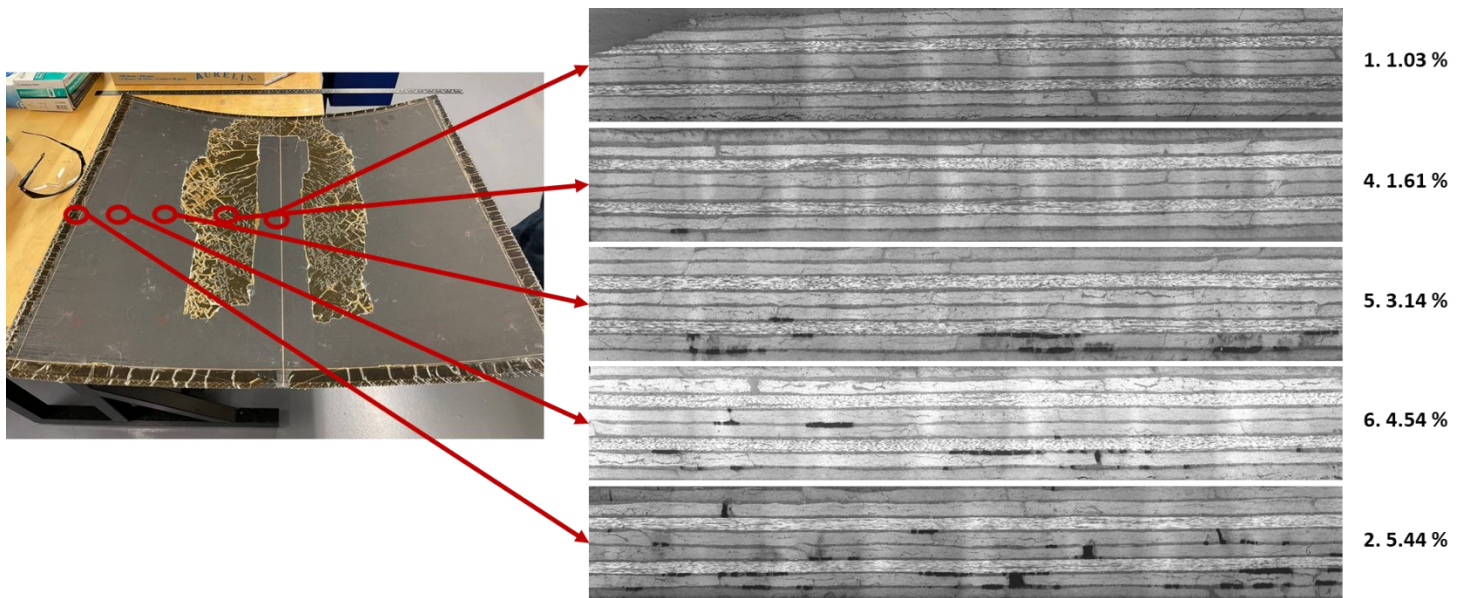
Figure 60. Void development in y direction – 2nd panel

Finally, DSC tests were performed for two samples taken from the panel, one from the center and one from the side, to find the glass transition temperature and degree of cure for the epoxy

system. The test approaches for the two samples were described in Table 25 as heating, cooling, and heating.

Table 25. DSC test's procedure for the 2nd panel

Step	Cycle Type	Cycle Detail
1	Heating	Ramp 10℃/min to 240℃ (center sample)
		Ramp 10℃/min to 200℃ (side sample)
2	Cooling	Ramp 10℃/min to 20℃
3	Heating	Ramp 10℃/min to 240℃ (center sample)
		Ramp 10℃/min to 200℃ (side sample)

Table 26 shows the calculated the degree of cure for the 2nd panel using equation (11) based on the DSC test results (Figure 61 and Figure 62), and it can be seen that the 2nd panel was cured properly. As the total heat of reaction for EP 2400 was not available, the value for the similar epoxy, CYCOM 890 RTM, was used for measuring the degree of cure.

Table 26. DSC test results for the 2nd panel

Sample	Glass Transition Temperature (℃)	Residual Heat of Reaction (J/g)	Total Heat of Reaction (J/g)	Degree of Cure (%)
1	165.70	0.14640	374.7 [49]	99.96
2	156.88	0.07340	374.7	99.98
Average	161.29			99.97
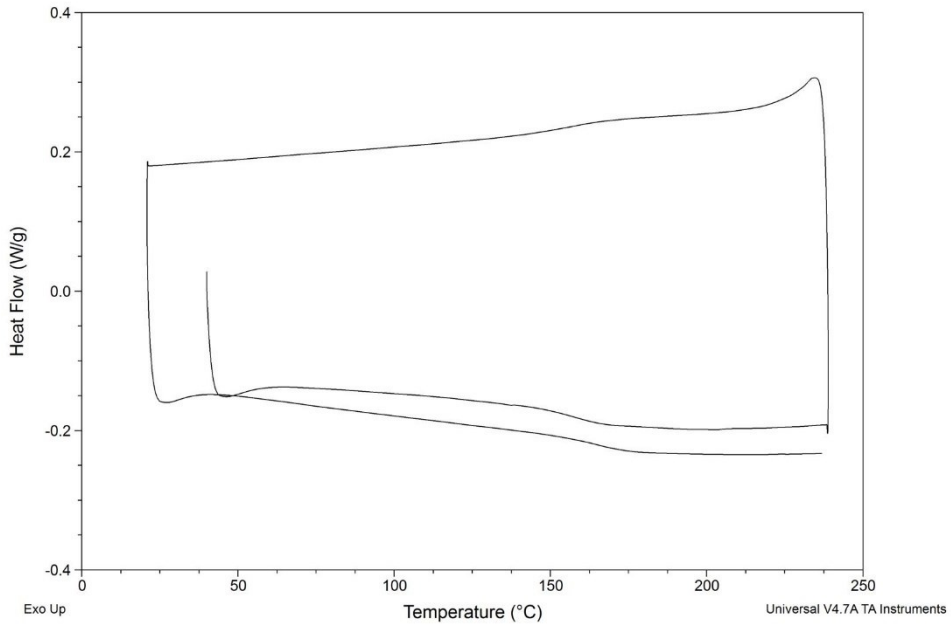
Figure 61. DSC test result for center sample of the 2nd panel
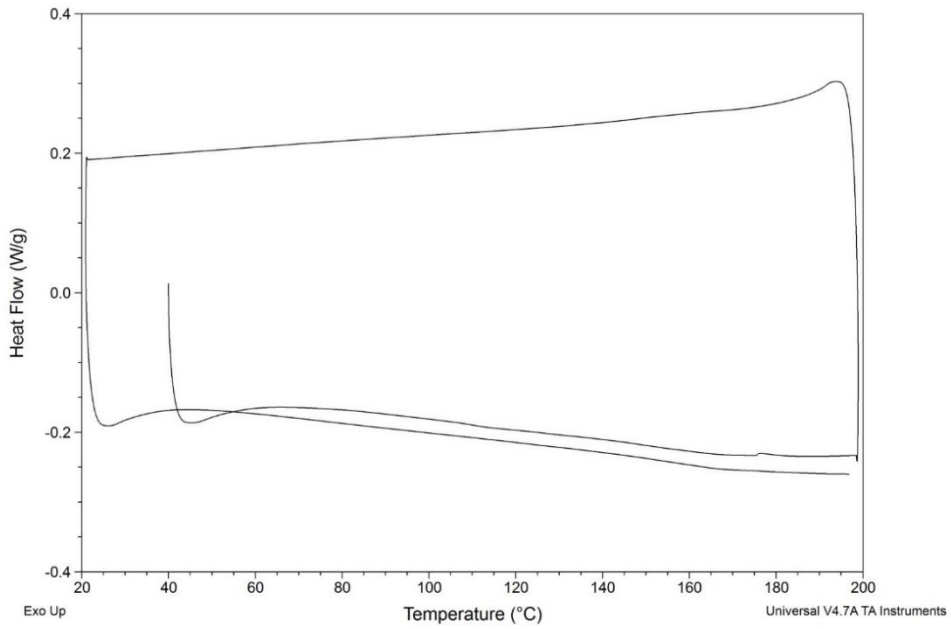
Figure 62. DSC test result for side sample of the 2nd panel

5.3 3rd Trial

5.3.1 Manufacturing Process

Unlike the two first trials, the vacuum-assisted process with the membrane (VAP) was used to infuse the preform in the 3rd trial. In this infusion method, a layer of membrane is operated to make a resin barrier chamber, which keeps the resin inside the chamber, and lets gases go outside the panel through the membrane. As shown in Chapter 4, introducing gaps into the preform layup can increase the permeability by creating channels for the resin to flow through the thickness. Thus, dry fiber tows with 0.2 mm gaps were deposited adjacent using the AFP machine controller. Materials and process parameters used in both steps are indicated in Table 27.
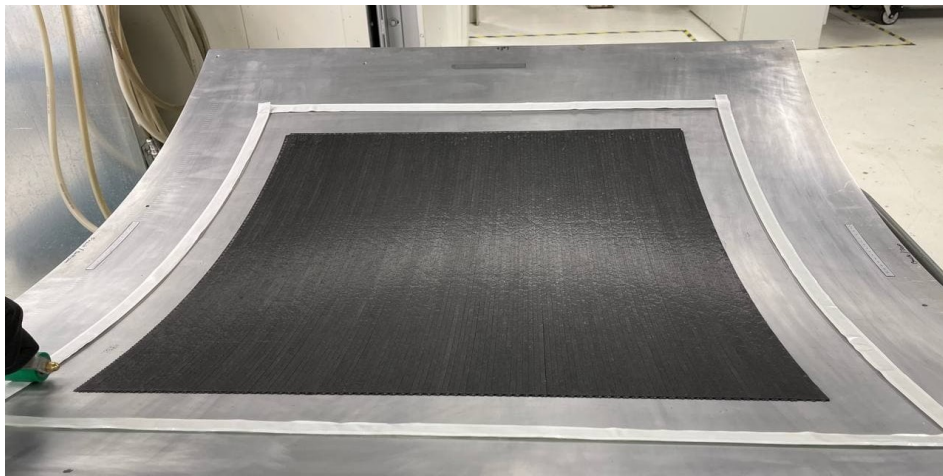
Figure 63. Preform of the 3rd panel

In the vacuum-assisted process with membrane (VAP) setup, Figure 64, the below sequence was followed from outside of the setup;

1. A layer of the vacuum bag, Airtech Wrightlon WL740, was used to create the outer chamber.
2. A breather layer, Airweave 1332, was placed to provide uniform pressure on the setup.
3. A layer of VAP membrane, Dahltexx SP-2, was used to construct the second chamber, which keeps the resin inside.
4. An omega channel connected to a PTFE tube was put in, carrying the epoxy from the resin pot outside the chamber to the inside.
5. Two layers of glass fiber infusion media, Flexiveil, were laid down underneath the omega channel to increase the in-plane flow rate and make a uniform flow front.

6. A layer of Teflon peel ply followed by media, Airtech Release Ease 234 TFP, is placed on the preform to ease the separation of media from stack-up after infusion. Also, the in-plane permeability of the peel ply is higher than fiber, meaning resin can travel faster inside the peel ply to reach the edges.

7. The preform with dimensions 76 cm by 76 cm (30 inches by 30 inches) was placed.

Table 27. Process parameters of the 3rd trial

Process Parameters	
Dry Fiber Material	Solvay TX1100
Layup	[(90/45/0/-45)]S
AFP Parameters	HGT Temp.: 215 and 230 °C
	HGT Flow: 60 SLPM
	Compaction Load: 10 and 13 lbf
	Speed Rate: 3in/s
	Gap Size: 0.2 mm gap size
Resin	PRISM EP2400
Dimension	76.2 × 76.2 cm (30 × 30 inch)
Infusion Temperature	120 °C
Curing Temperature	180 °C
Void Content Center	1.79 %
Void Content Edge	1.713 %
Average Thickness	1.56 mm
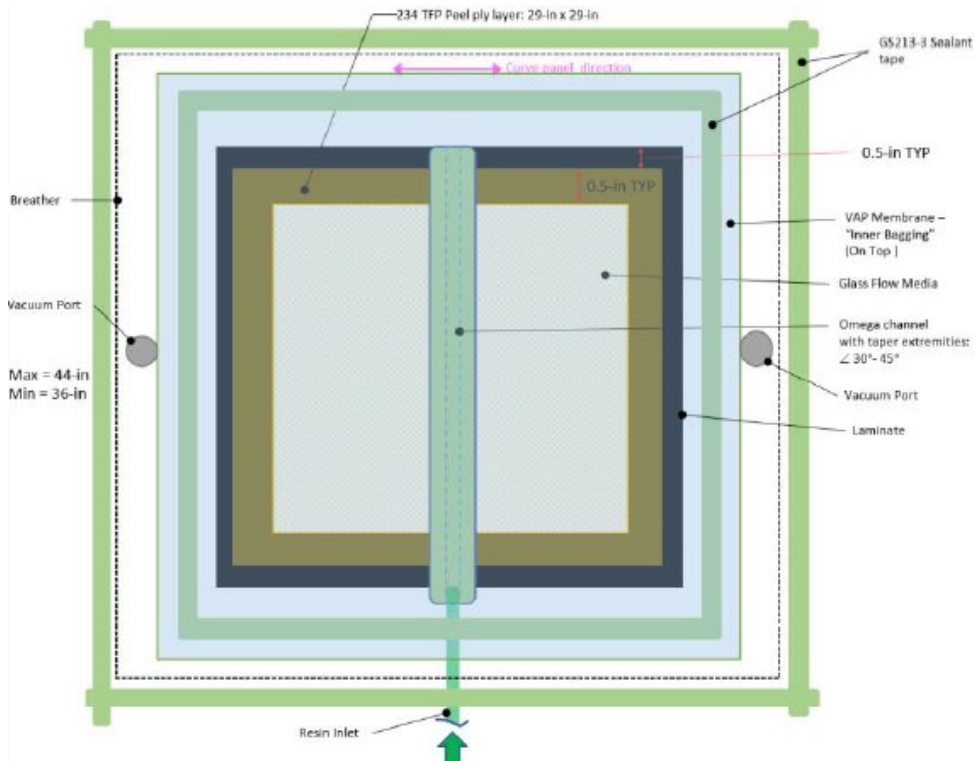
Figure 64. Schematic of the infusion setup for the 3rd trial [50]

The infusion procedure is described below:

1. The resin was preheated to 60°C in its container for transfer to the resin pot.

2. The epoxy resin was degassed for 30 – 45 minutes while heated to 90°C with ABESS equipment at a mixer speed of 60 rpm for 1 hour.

3. Thermocouples were placed one over the stack up, on the bag, and one on the tool side.

4. The tool was preheated to 120 °C.

5. The epoxy was transferred through the infusion PTFE tubes which were placed in the heating line to the inside of the oven.

6. The infusion was carried out for almost one hour and a half.

7. Once the preform was filled with resin and the inlet (gates) and outlet (vents) were closed, the tool temperature was increased at 2°C/min to 180°C. The oven temperature dwelled at 180°C for 120 minutes.

8. Tool was cooled down to 60°C and below at rate of < 5°C/min before demolding the part from tool.

5.3.2 Defects and Challenges

As illustrated in Figure 65, unlike the 2nd panel, the resin travelled poorly in-plane. 4-inch less, through the non-woven glass flow media. Also, the Teflon-based peel ply permeability was lower than the nylon peel ply fabric used in the last two trials. Therefore, resin flow through the laminate was weaker. The area showing white spots on the bag side of the laminate illustrates the laminate contamination with small particles of the barrier side of the VAP Membrane, mainly due to the membrane dissolving by resin flow. The vacuum pressure also caused the housing imprint on the bag side of the laminate.
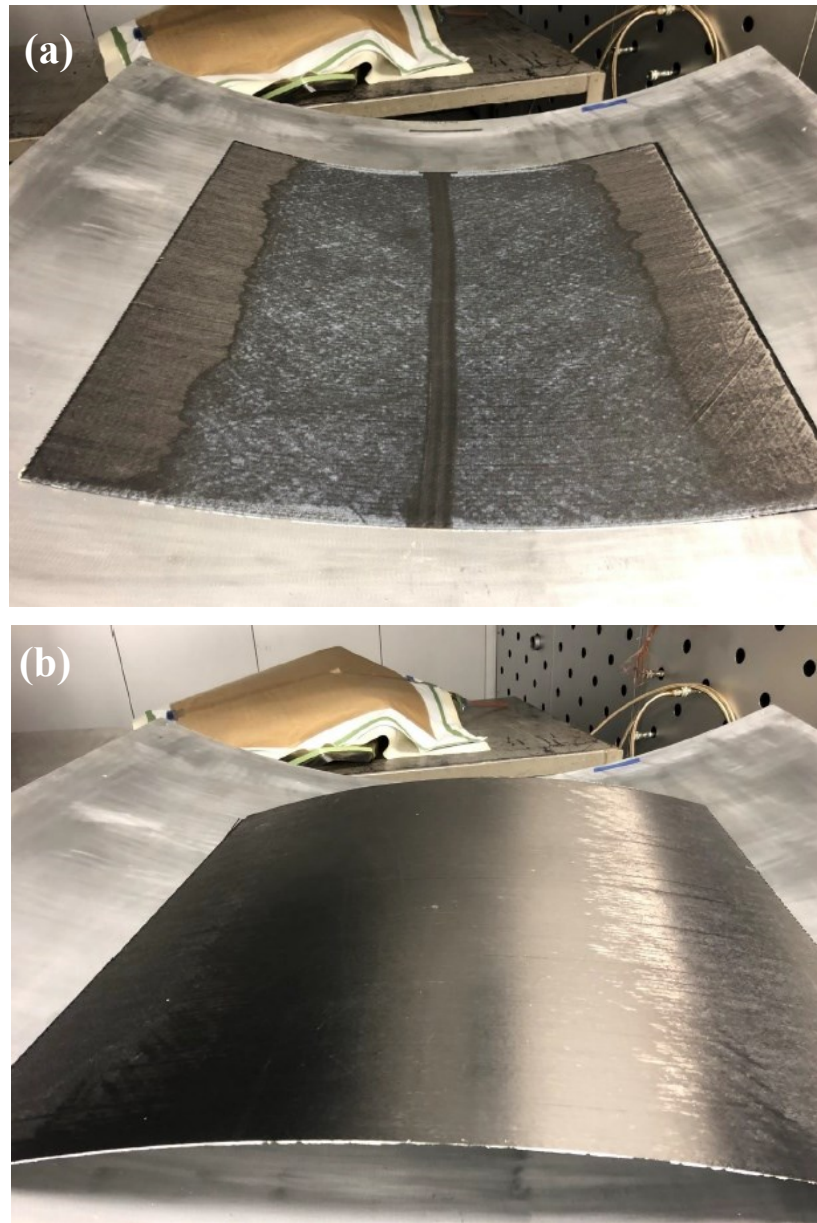
Figure 65. 3rd panel after infusion (a) bag side (b) tool side

After removing the mold from the oven, the resin passed through the membrane during curing and wetted some parts of the breather, like bridging areas (e.g., around the flow channel). Visual inspection at various times during the curing sequence confirms that resin leakage happened during the later stage of the 180°C in the curing cycle, see Figure 66. One possible reason is that the stretching of the membrane caused the extension of the micro holes in the barrier layer and provided escape routes for the resin.

Figure 66. Membrane leakage in the 3rd trial

5.3.3 Quality Analysis

In terms of distortion, the only observed distortion was the inlet imprint on the bag side due to the resin shrinkage. As the panel was not fully impregnated, microscopic analysis was run only for the infused sections. The bands taken from laminate for micrography are shown in Figure 67. Following the micrography, results showed neither significant wrinkle nor fiber disturbance due to the resin flow in the fiber structure, see Figure 68 and Figure 69. As the edge of the panel remained dry, the DSC test was not done in this trial.
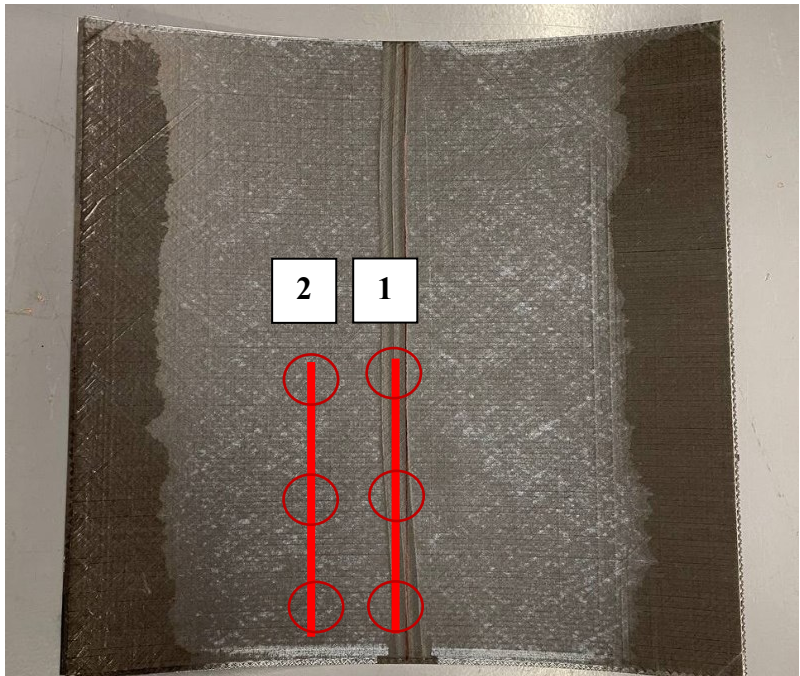
Figure 67. Micrography's samples positions on the 3rd panel

- **Center band (No. 1)**
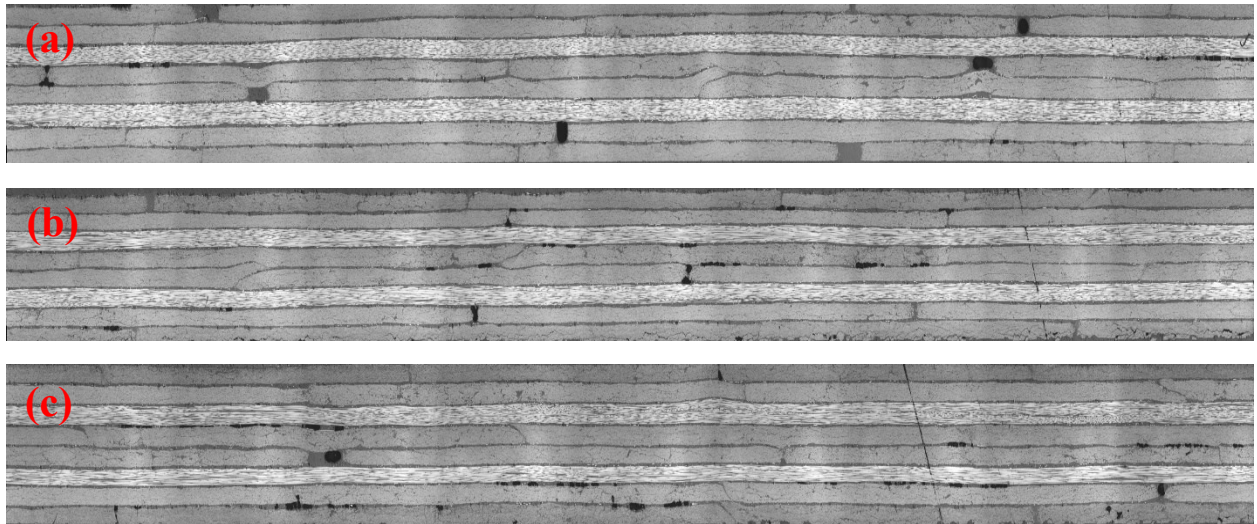
Figure 68. Central band's samples – 3rd panel (a) center sample (b) middle sample (c) edge

- **Middle band (No. 2)**
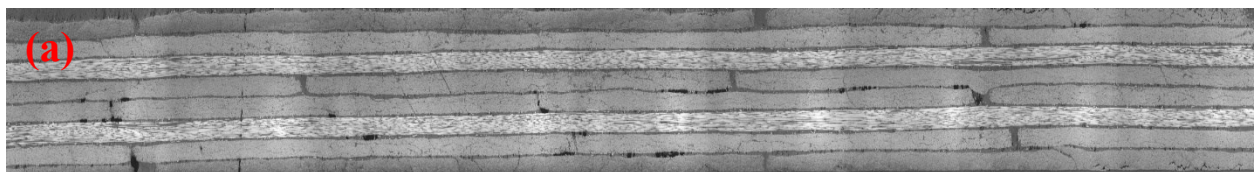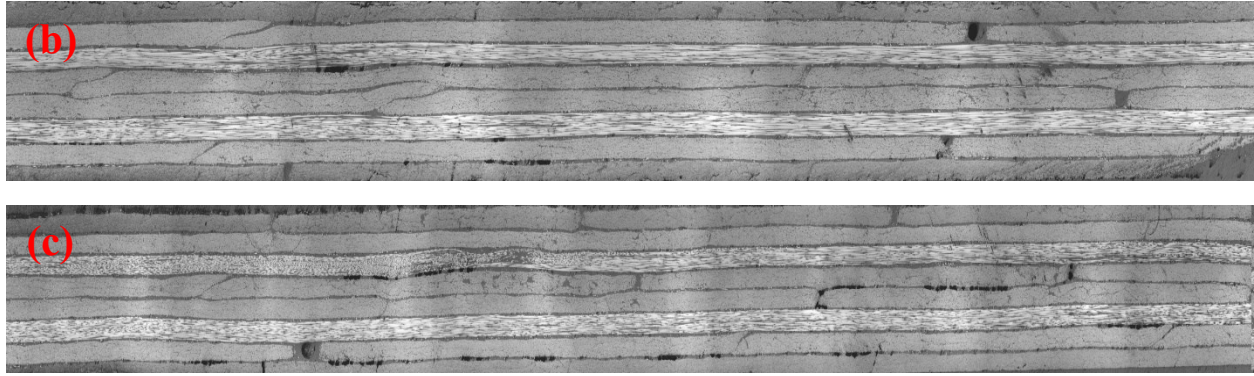
Figure 69. Middle band's samples – 3rd panel (a) center sample (b) middle sample (c) edge sample

Regarding the void content, Table 28 demonstrates that, unlike the 2nd demonstrator, the void content in this demo is almost uniform which can explain this setup had more uniform flow than the previous one.

Table 28. Void content of the 3rd panel

Band Number	Center	Middle	Edge	Average
1	1.976 %	0.956 %	2.424 %	**1.785 %**
2	0.969 %	1.048 %	3.121 %	**1.713 %**

Table 29 shows that the 2nd panel had higher void content at the same distance from the center (middle band) compared to the 3rd panel, which can explain why introducing gaps improves the permeability in the 3rd trial. However, replacing the nylon peel ply with Teflon peel ply reduces the in-plane flow rate, and it needs to be improved by increasing the number of flow mesh.

Table 29. Void content comparison of the 2nd and 3rd panels

Band Position	2nd	3rd
Center	0.78 %	1.79 %
Middle	3.04 %	1.71 %

5.4 4th Trial - Demonstrator

For the 4th panel, using PAM RTM 2017 software [51], 3D simulation was performed for the infusion process of the same geometry panel, 76.2 × 76.2 cm (30 × 30 in), with two omega channels with dimensions of 1.27 × 0.76 × 76.2 cm. The cross-section of omega channels was converted to a rectangular shape as an assumption to ease the geometry modelling. The simulation was conducted to estimate the filling time of the fuselage panel demonstrator using the experimental out-of-plane permeability measurement. In addition to the out-of-plane permeability,

in-plane permeabilities of Solvay TX1100 dry fiber were obtained from Ref. [24]. The governing equations used for the simulation in the software are Darcy's law and Kamal's equation. The cure kinetic model of the epoxy was obtained from Ref. [24] based on Kamal's equation. Although the viscosity model was developed in the literature, the viscosity was assumed constant (20 cP) as the infusion time was expected to be lower than 1 hour, and there is no significant change in the viscosity below 100 minutes based on the isothermal viscosity profiles, Figure 31. Figure 70 shows the element face of tetrahedral meshes chosen for meshing the geometry with an element size of 9.88 mm (0.39 in).
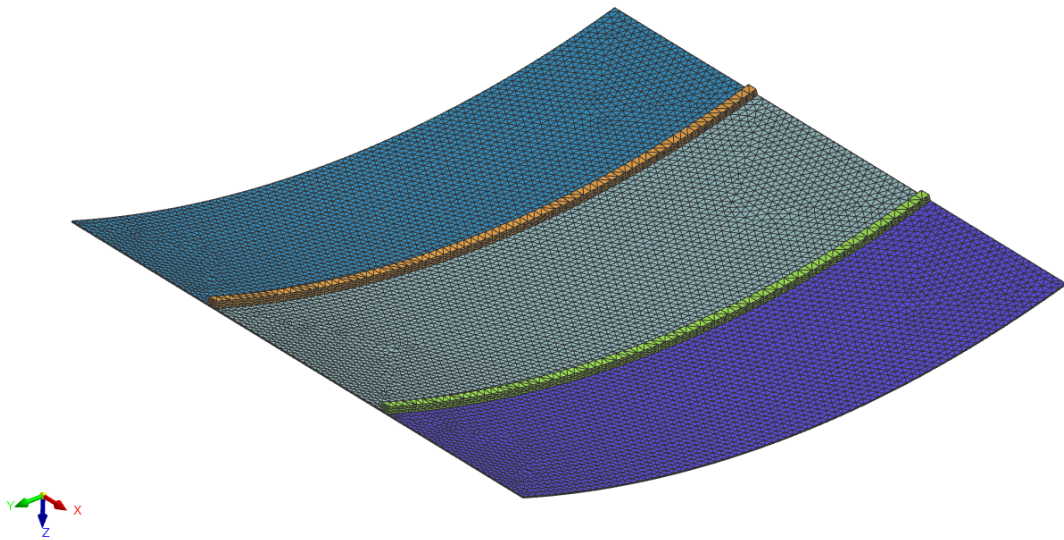
Figure 70. Meshed geometry model for the fuselage panel demonstrator

Figure 71 illustrates the setup's resin inlets, vacuum ports, and omega channel configuration. Although vacuum ports were placed outside the preform in the infusion setup, using a breather layer provides uniform vacuum pressure on the preform. Therefore, all the edges of the preforms were considered with the vacuum lines in the simulation. The initial condition was resin temperature of 100℃, and boundary conditions were atmospheric pressure at the inlet, 100 kPa, vacuum pressure at the vacuum lines, and preform temperature of 120℃. The in-plane and out-of-plane permeabilities of the omega channels were calculated using the equation provided by PAM RTM. Table 30 shows the permeability values used for the preform textile and omega channel.

Table 30. Permeability values for the preform and omega channels

	K_x (µm²)	K_y (µm²)	K_z (µm²)
Preform without gaps	2.81	0.38	0.011
Preform with 0.4 mm gaps			0.195
Omega Channel	2.05E7	2.05E7	2.05E7
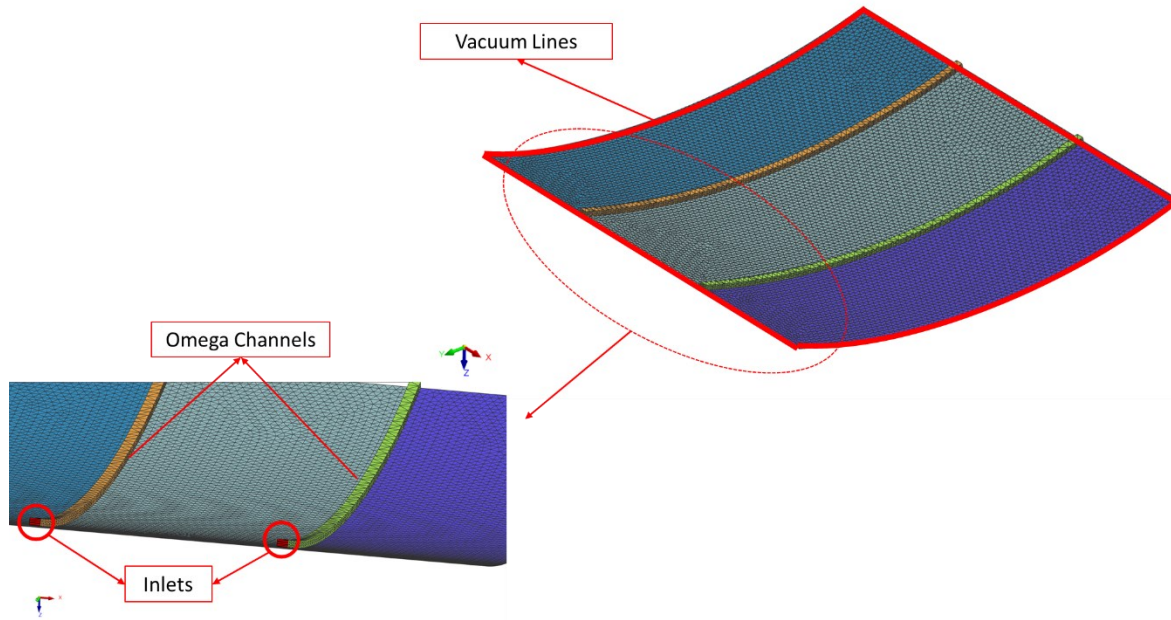
Figure 71. Resin inlet, vacuum lines, and omega channels position

The different filling sections are shown in Figure 72 for the infusion of the fuselage panel demonstrator with out-of-plane permeability of 0.195 µm² at the temperature of 120 ℃ and pressure difference of 100 kPa. In each contour, the magenta color represents a fully filled location, the blue color represents an empty location, and the grey color represents dry fibers. Obliviously, the flow started through the omega channel, which has higher permeability and then flew through the fiber architecture. Also, as was expected, the flow front on the vacuum side was wider than the flow front on the tool side in the beginning due to the difference between out-of-plane and in-plane permeabilities.

Finally, the estimated time of infusion is compared with the estimated time using analytical calculation, see Table 31.
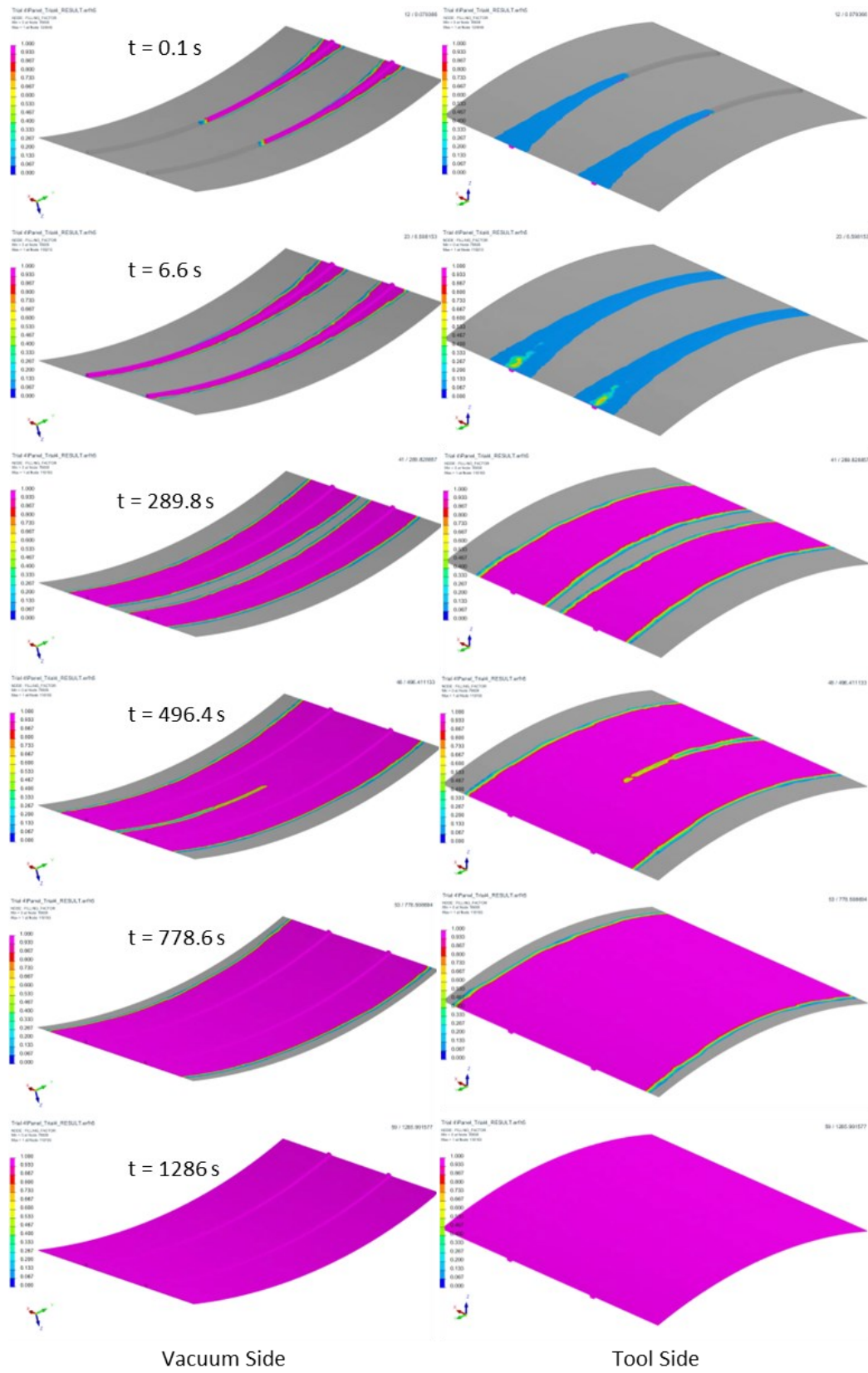
Figure 72. Different filling steps for the preform with 0.4 mm gap

Table 31. Estimated time of infusion obtained from analytical calculation and simulation

Estimated Time	Analytical (s)	Simulation (s)
Preform without gaps	29685	1426
Preform with 0.4 mm gaps	1675	1286

It can be seen that simulation estimated the infusion time for the preform without any gap faster than the analytical solution. The reason is that the resin flow was only considered in the z-direction in the analytical solution, which means the interaction of flow direction (interaction of permeabilities) was neglected, see Figure 73 (a). However, the interaction of flow directions was considered in the simulation as in-plane permeabilities were defined, see Figure 73 (b). So, the interaction of in-plane and through the thickness flow may help to estimate the time more precisely than neglecting them in the case of preforms without the gaps, as the out-of-plane permeability is too low in preforms without gaps. On the other hand, interaction in preforms with gaps has no significant difference as out-of-plane permeability is high enough, allowing the resin to flow easily.
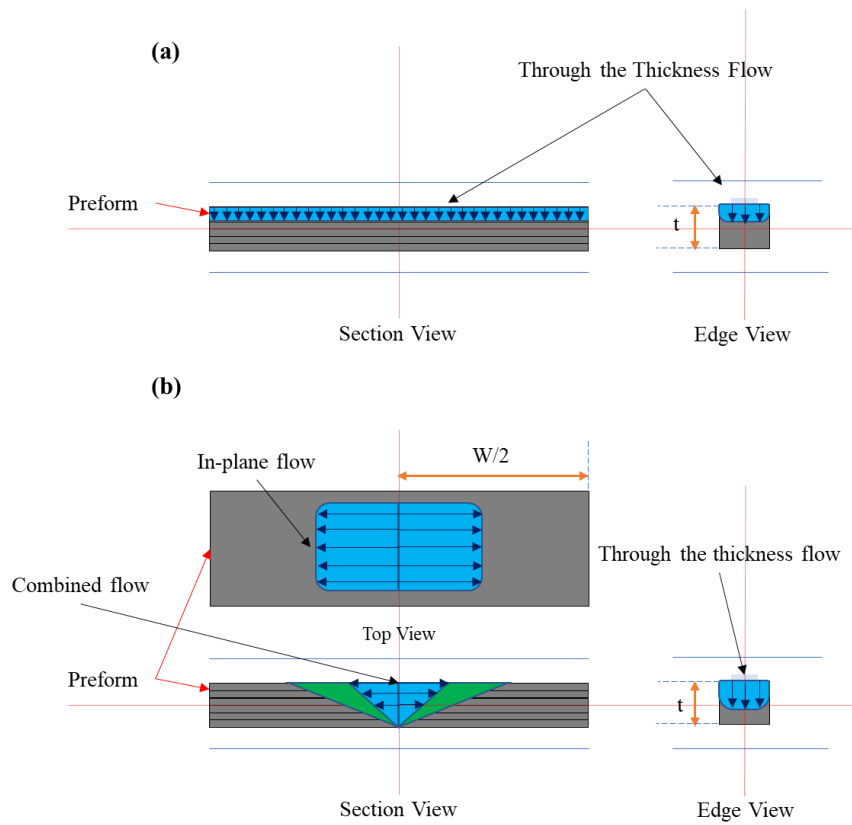
Figure 73. Schematic of flow in (a) analytical solution (b) simulation

5.4.1 Manufacturing Process

Like the 3rd trial, the vacuum-assisted process with the membrane (VAP) was operated to infuse the last panel. However, some modifications were applied to the setup to improve the outcome and solve the previous challenges as explained in the following paragraph. Also, 0.3 mm gaps were introduced to the layup. Materials and process parameters used in both steps are indicated in Table 32.

Table 32. Process parameters of the 4th demonstrator

Process Parameters	
Dry Fiber Material	Solvay TX1100
Layup	[(90/45/0/-45)]S
AFP Parameters	HGT Temp.: 215 and 230 °C
	HGT Flow: 60 SLPM
	Compaction Load: 10 and 13 lbf
	Speed Rate: 3in/s
	Gap Size: 0.3 mm gap size
Resin	PRISM EP2400
Dimension	76.2 × 76.2 cm (30 × 30 inch)
Infusion Temperature	120 °C
Curing Temperature	180 °C
Void Content Center	0.303 %
Void Content Edge	0.184 %
Average Thickness	1.503 mm

Based on the obtained result from the 3rd trial, five layers of glass fiber infusion media, Flexiveil, were used instead of two to increase the in-plane speed. In addition to increasing the media layers, one line of omega channel was added too. Other infusion parameters were kept the same as in the previous experiment, which helped us to understand the effect of the applied modification, see Figure 74.
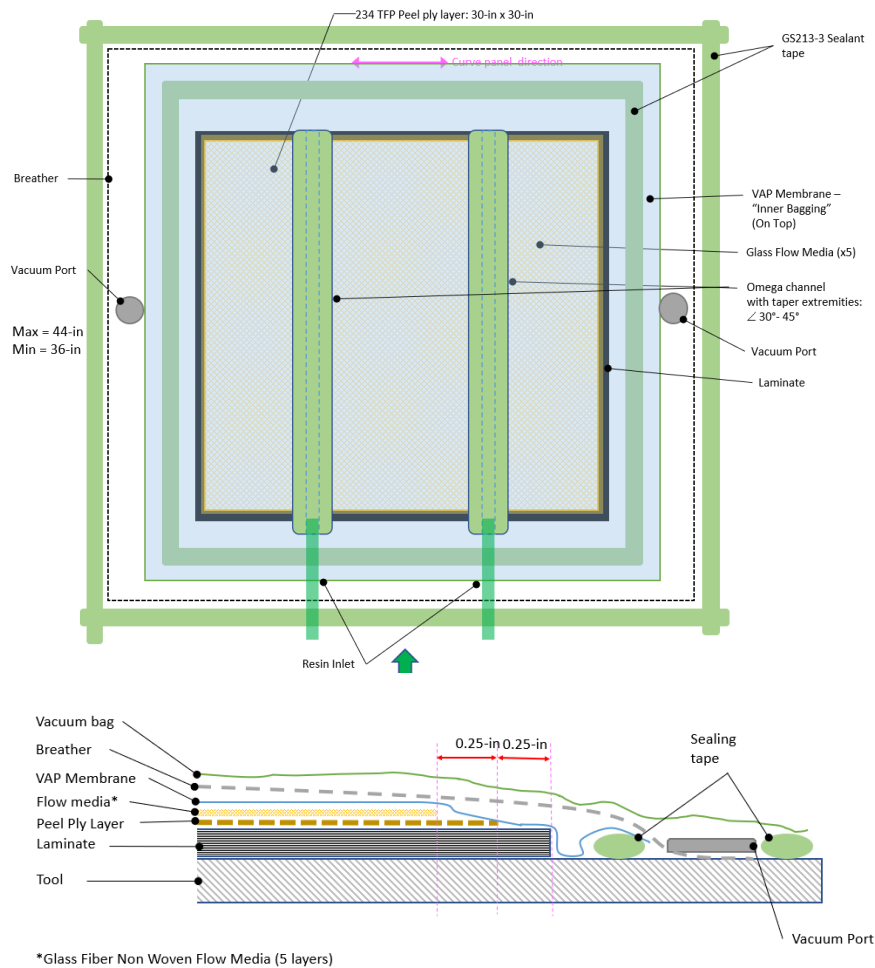
Figure 74. Schematic of the infusion setup for the 4th trial [50]

The infusion procedure for the 4th trial is the same as the 3rd one except that the infusion time only took 1 hour.

5.4.2 Defects and Challenge

Figure 75 shows that no edge lift-up appeared after curing in the oven for the 4th fuselage panel. The only defect which can be negligible is the tube imprint which caused the 0.356 mm (0.014 in) lift-up around the imprint, see Figure 76.
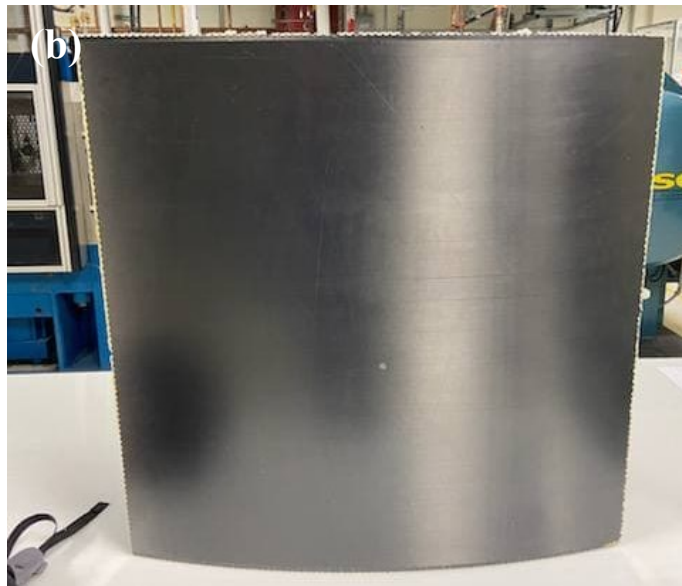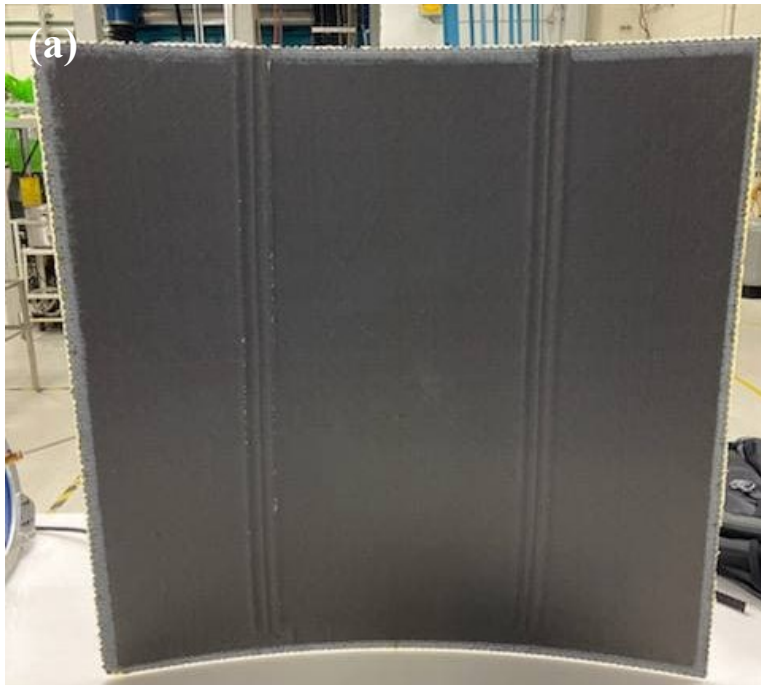
Figure 75. 4th panel after infusion (a) bag side (b) tool side (c) cross-section

Figure 76. Omega channel imprint on the bag side of the 4th panel

5.4.3 Quality Analysis

The 6-inch clamp micrometer was employed to measure thickness for 37 points, see Figure 77, around the panel, and the result is mentioned in Table 33.

Table 33. Thickness variation of the 4th panel

	mm	in
Average Thickness	1.503 ± 0.025	0.059 ± 0.001
CV %	1.69	1.69
Maximum	1.595	0.063
Minimum	1.473	0.058
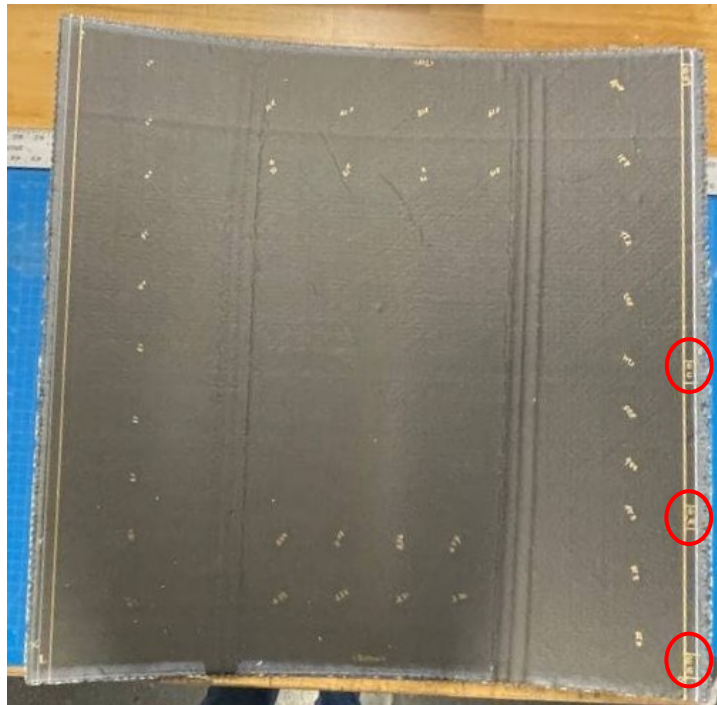
Figure 77. Micrography sample positions on the 4th panel
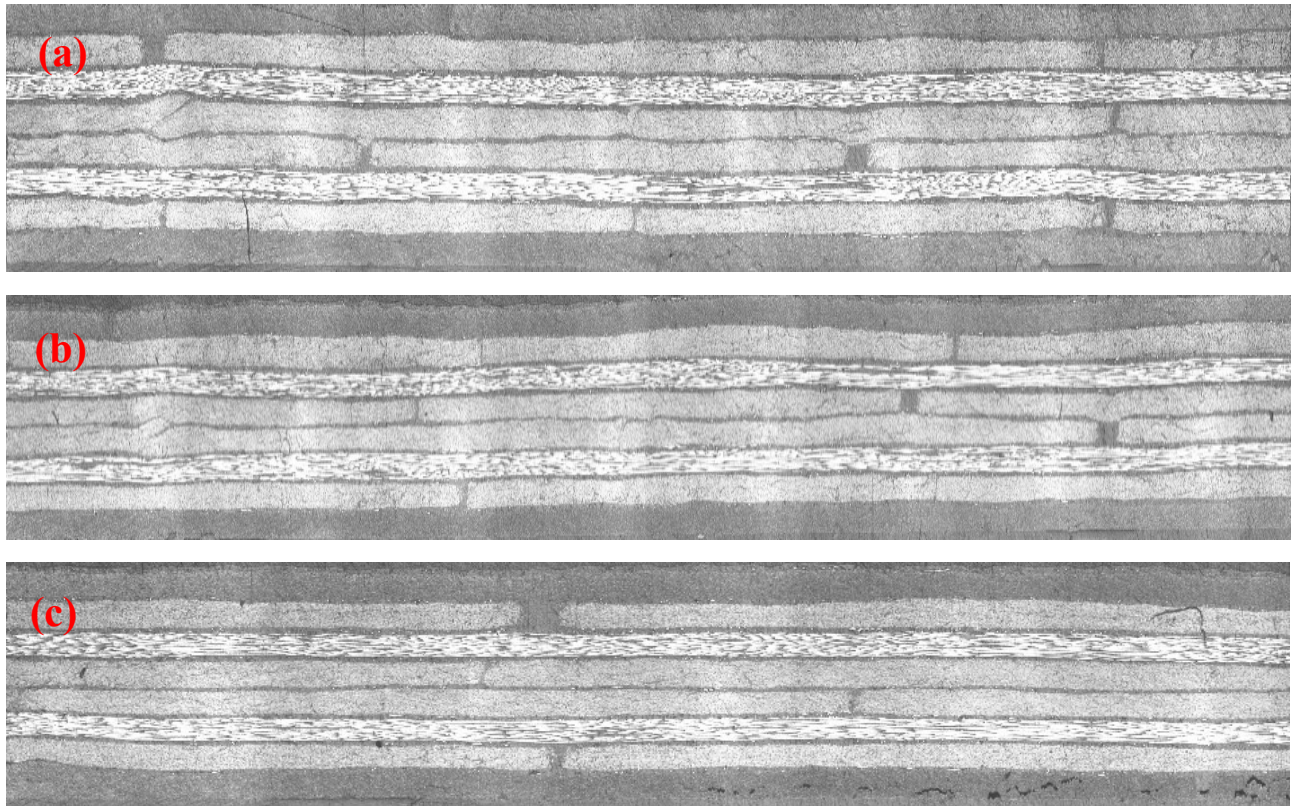
Figure 78. Edge band's samples – 4th panel (a) center sample (b) middle sample (c) edge sample

The void content was measured for each sample using micrographs taken from laminate, Figure 78, as described in Table 34.

Table 34. Void content of the 4th panel (central band)

	Center	Middle	Edge	Average
Void Content	0.303 %	0.184 %	0.445 %	**0.311 %**

Compared to the 2nd fuselage panel's microscopic analysis, the void fraction in edges had considerably dropped from 5.86 % to 0.311 %. Accordingly, it can demonstrate the effect of using a membrane which provides uniform vacuum pressure inside the chamber. The chamber under consistent pressure improves the flow rate in the thickness direction. In addition, by comparing the microscopic analysis of the 3rd and 4th fuselage panels, it is seen that resin travelled further in-plane in the 4th panel. Although void content in the middle band of the 3rd panel, about 25.4 cm from the edge, was 1.713 %, the void content of the 4th panel's edge was noticeably lower. Therefore, increasing the number of distribution media refines the in-plane flow. Moreover, considering gaps between tows by AFP machine improves not only out-of-plane permeability but also in-plane.

Two methods were used to analyze the fiber content: 1- thermogravimetric analyzer test and 2- microscopic images of samples taken from laminate. The thermogravimetric analyzer test (TGA) was run with a ramp cycle up to 600 °C followed by isothermal for 10 minutes. According to the TGA test result (Figure 79), the sample weight loss is 23.17 %, and it can be estimated that 76.83 % of the sample weight is fiber. Moreover, either the acid digestion test or microscopic analysis can verify this result, which microscopic analysis was chosen due to digestion's high hazardous effects.
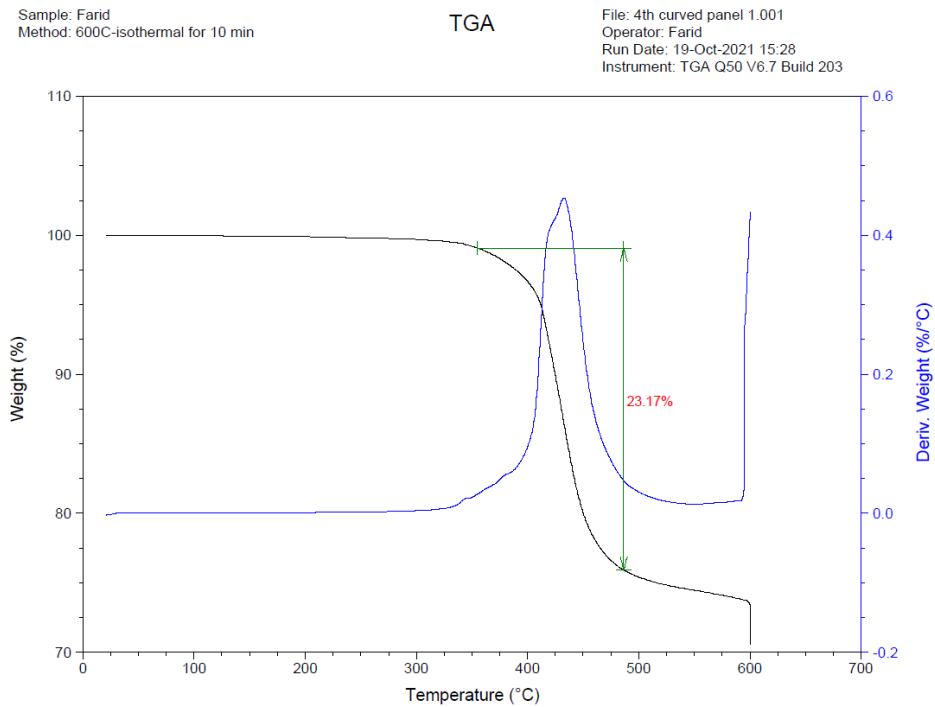
Figure 79. TGA test results of 4th demonstrator

As the layup sequence is symmetric quasi-isotropic with eight layers, cross-sections of taken samples are visible in the first and last layers, the 90° layers, see Figure 80. Based on computing the fiber content for different regions in these two layers, the average fiber content is 60.02 ± 2.8 % which is 16.81 % lower than the TGA result. Mainly, two reasons could result in this difference between fiber content calculated by micrographs and TGA. First, epoxy might not burn completely in the TGA test. Second, fiber volume content might be different in other layers as only two were considered for fiber volume fraction using micrographs. Using equation (3) to estimate the fiber volume fraction, it can be observed that the microscopic method gives a more realistic result than TGA.
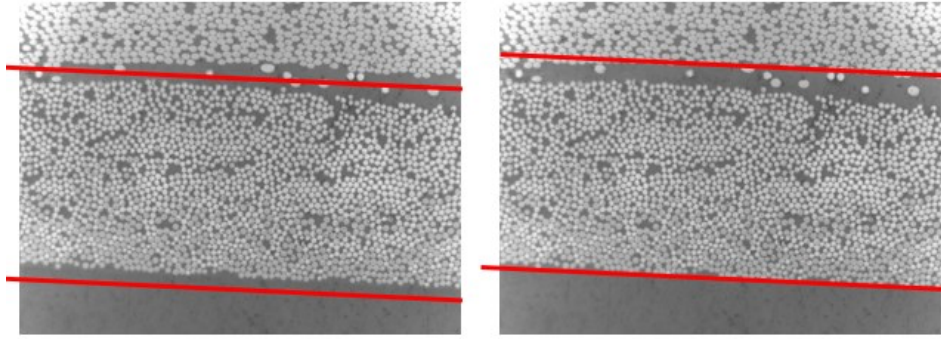
Figure 80. Microscopic measurement of the fiber content for the 4th demonstrator [32]

Both differential scanning calorimetry test (DSC) and dynamic mechanical analyzer (DMA) were used to estimate the epoxy system's glass transition temperature and degree of cure. In each of these tests, the glass transition temperature is derived by measuring changes in specific material properties, specifically, heat capacity in DSC and mechanical strength in DMA. As shown in Figure 80, the DSC test approach was heating to 200 ℃, cooling to 20 ℃, and heating to 200 ℃ with a rate of 10 ℃/min. Based on the DSC test result, the unreacted portion in the above DSC curve describes the residual heat of the reaction. Table 35 shows the calculated degree of cure using Equation (11) and the total heat of reaction for similar epoxy (i.e., CYCOM 890 RTM) obtained from Ref [49]. Based on the obtained degree of cure, the epoxy followed the right curing cycle, and it can be considered cured. Consequently, the average glass transition temperature obtained from several samples is approximately 145 ℃.

Table 35. DSC test result for the 4th panel

Sample	Glass Transition Temperature (℃)	Residual Heat of Reaction (J/g)	Total Heat of Reaction (J/g)	Degree of Cure (%)
1	144.78	0.2071	374.7 [49]	99.98

Using the DMA test and measuring the loss modulus and peak temperature, the average Tg was computed at 160.25 °C, see Table 36. The difference between DMA and DSC results explains the difference between the mechanism of these tests. As a metallic fixture is used in DMA, the measured temperature could be affected as the fixture acts as a heat sink. So, there might be a difference between DMA and DSC results.
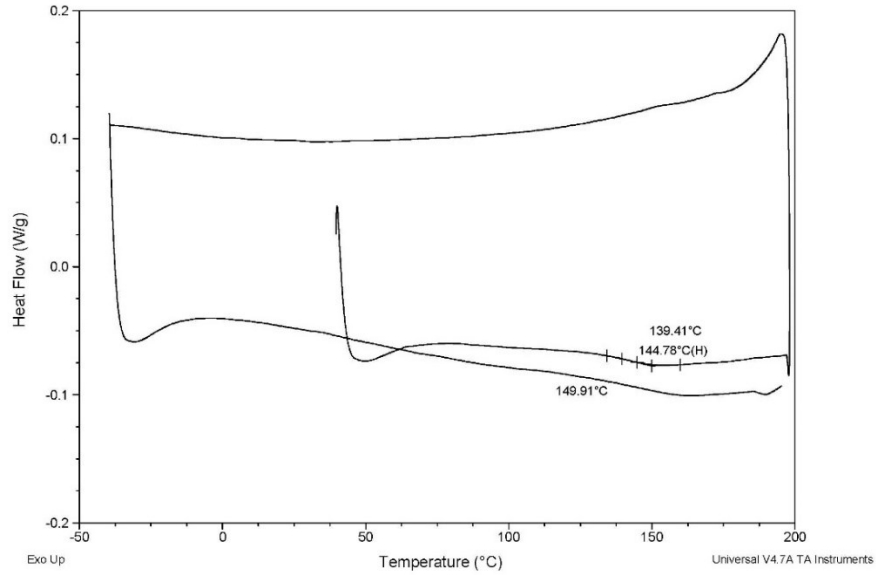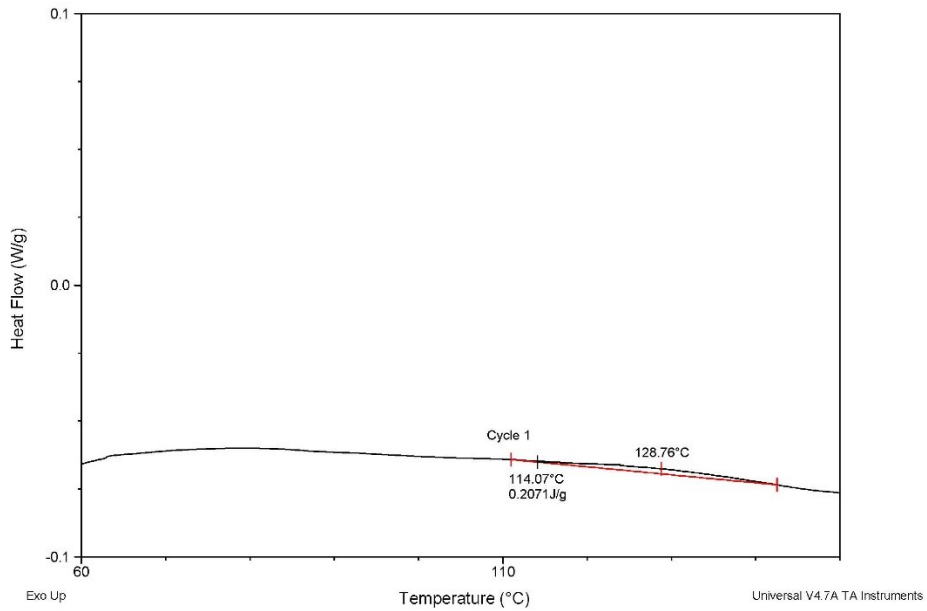
Figure 81. 4th demonstrator DSC test result

Sample: Farid_4th_Cured_Panel1
Size: 35.0000 x 11.7200 x 1.4650 mm
Method: Temperature Ramp

DMA

File: C:...\DMA\Farid\4th_cured_Panelnew.001
Operator: Farid
Run Date: 07-Oct-2021 10:48
Instrument: DMA Q800 V20.24 Build 43

(1)

161.09°C

Universal V4.7A TA Instruments
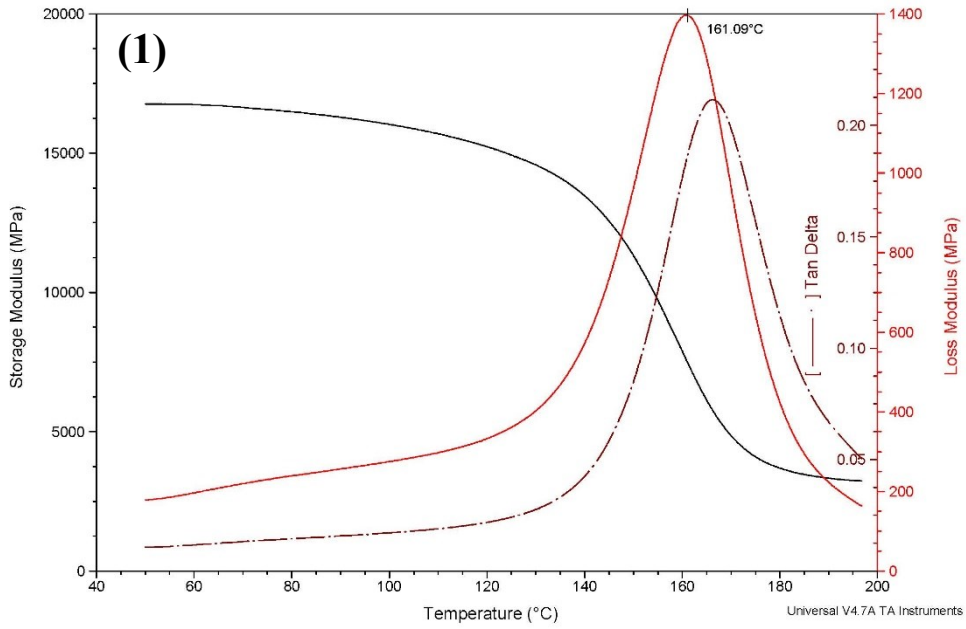
Sample: Farid_4th_Cured_Panel1
Size: 35.0000 x 11.7000 x 1.4650 mm
Method: Temperature Ramp

DMA

File: C:...\DMA\Farid\4th_cured_Panelnew.002
Operator: Farid
Run Date: 07-Oct-2021 16:21
Instrument: DMA Q800 V20.24 Build 43

(2)

159.55°C

Universal V4.7A TA Instruments
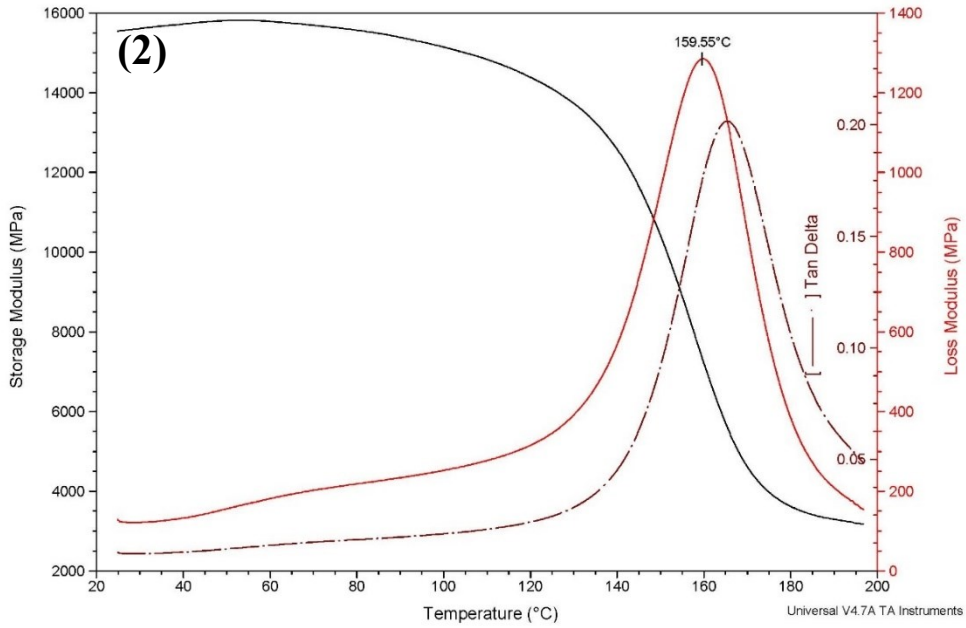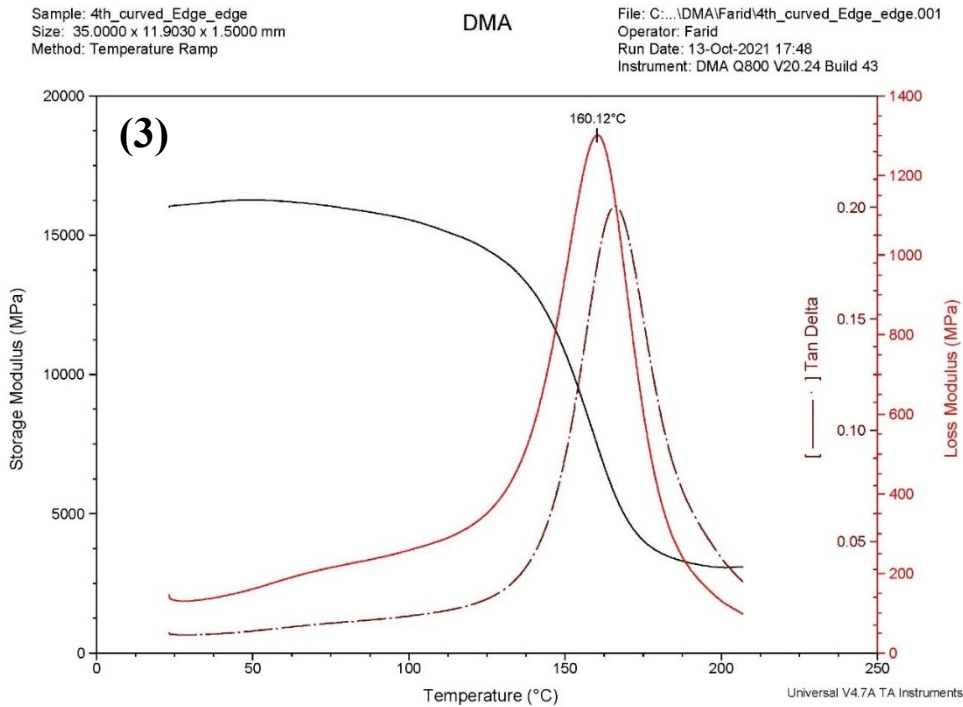
Figure 82. DMA test results – 4th demonstrator

Table 36. DMA test result summary – 4th demonstrator [32]

	1	2	3	Average	Datasheet
Tg	161.09 °C	159.55 °C	160.12 °C	160.25 °C	*163, 179 °C

*There are two glass transition temperatures (Tg) in the datasheet of EP2400 depending on specimen conditioning. For room temperature and dry is 179 °C (354 °F) and for wet and 48-hour water boil is 163 °C (325 °F).

5.5 Conclusion

In this chapter, automated dry fiber placement (ADFP) preforms were impregnated with vacuum-assisted resin infusion (VARI) to show the capability of this method to manufacture a sizable demonstrator that reaches high standards in terms of thickness uniformity, void content, and degree of cure. Firstly, two different infusion methods were operated at high temperatures. Secondly, defects and challenges for each infusion setup were discussed to understand the effect of the setup's components on the result. Thirdly, the impact of introducing gaps into the layup on manufacturing a large-scale fuselage was demonstrated.

As a comparison between 2nd and 3rd panels, see Figure 83, micrographic study of the center band shows that void content in the last layers of the 3rd panel is better than 2nd panel which can be used to explain that introducing gaps, improves the out-of-plane permeability of the 3rd panel.
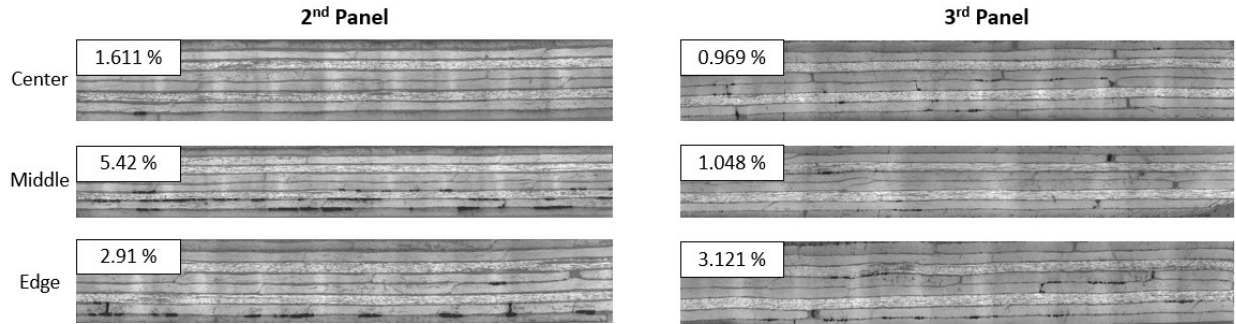
Figure 83. 2nd and 3rd fuselage panels micrography comparison

Also, comparing the 2nd and 4th panels' micrography in the edge band, introducing the 0.3 mm gaps in all layers improved not only the flow through the thickness, but also in-plane flow as the flow front reached the edges of the panel. Figure 84 shows that introducing a larger gap size, demonstrated by red squares, and adding one more infusion line enhanced the in-plane flow as lower void content reached the 4th-panel edge. Also, void development in the last layers cannot be observed in the 4th panel bottom layers which approves the higher out-of-plane permeability.
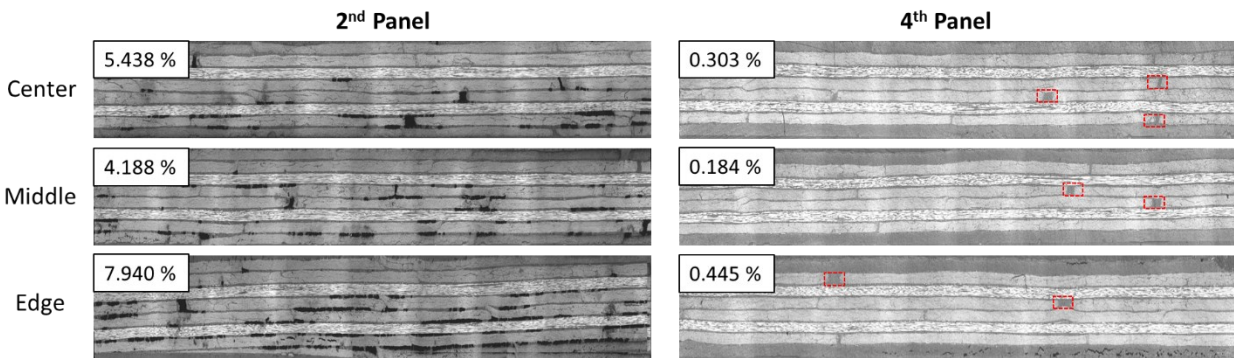
Figure 84. 2nd and 4th fuselage panels micrography comparison

As a result, the fabricated demonstrator panel with [(90/45/0/-45)]$_s$ layup has a uniform thickness of 1.503 ± 0.025 mm, low void content of 0.311%, and fully cured.

Chapter 6. Conclusion, Contribution and Future Outlook

6.1 Conclusion

Developing composite manufacturing techniques in the aviation industry, such as automation, has improved the production rate and reliability and reduced material waste. New methods should be analyzed precisely to see whether they can manufacture structures in the aerospace industry scale. Automated Fiber Placement provides possibilities to manufacture composite structures in complex geometries. This thesis focused on combining Automated Dry Fiber Placement, using AFP machine with HGT, and Resin Vacuum Assisted Infusion at high temperatures to manufacture carbon/epoxy composite structures with aerospace quality. This method can provide a higher production rate compared to the manual hand lay-up process and lower manufacturing cost compared to conventional prepreg/autoclave.

Dry fiber materials developed for the Automated Dry Fiber Placement must be bonded with the substrate during the deposition process and then impregnated with the infusion. Suppliers use different methods to add a binder to increase the bonding between fiber layers. Binder and AFP machine's compaction load on the substrate would decrease the permeability of preforms by closing the infiltration channels. AFP machines can fabricate preforms with different patterns, including laying tows with overlaps and gaps in different sizes and angles, influencing the preform permeability.

Some of the available dry fiber materials from different suppliers were introduced in Chapter 3. Process parameters for ADFP and VARI were presented. Using a trial and error approach based on the process parameters, challenges of fabrication preforms using AFP machine with HGT and solutions to overcome these defects were proposed. Moreover, this chapter investigated epoxy systems and infusion setups used in this dissertation and the correlated challenges.

In Chapter 4, this dissertation developed a comparative study to compare the effect of introducing gaps on the preform's out-of-plane permeability. Although introducing gaps reduces the fiber content, considering an optimized gap pattern can result in high permeability and increase the epoxy impregnation. While introducing gaps into the layers of preform increases the out-of-plane permeability and reduces the impregnation time, it should be noticed that reducing the fiber content also affects the mechanical properties of laminates. Therefore, the effect of introducing gaps to the layup on mechanical properties has been analyzed. This study considered compressive

properties as demonstrators for mechanical properties as it illustrates the bonding between the epoxy and fibers. The results show that the introduction of the gaps enhances the permeability while decreasing the compressive properties. There exists a gap size (0.4 mm) where a significant increase in permeability (20 times) with a slight reduction in compressive modulus (7.26%), as compared to the case of no gap, is observed.

Finally, large-scale fuselage panel demonstrator with [(90/45/0/-45)]s layup was manufactured using ADFP to make the 30 inches by 30 inches preform and VAP VARI at a high temperature to infuse the preform. In Chapter 5, in addition to process parameters used for each fuselage panel, the effect of using an AFP machine to control the fiber volume content, introducing gaps between tows in the preform lay-up, was also demonstrated. The last fuselage panel demonstrator has a uniform thickness of 1.503 ± 0.025 mm, low void content of 0.311%, and degree of cure above 99.5 %.

6.2 Contributions

Some of the major contributions achieved in this dissertation are described as follows:

— Process parameters for depositing dry fibers using the AFP machine equipped with HGT and thermoplastic head are identified.

— Correlated challenges in using dry fiber with AFP are introduced and overcame.

— Effects of using different VARI setups on the infusion to identify the challenges in this process are studied.

For the first time

— Using a comparative study, the effect of introducing gaps in the lay-up on the out-of-plane permeability of the preform made by ADFP is investigated experimentally.

— Using comparative study, the effect of introducing gaps in the lay-up on the compressive properties of the laminate, infused using high-temperature SCRIMP, is investigated experimentally.

— A large-scale fuselage panel demonstrator (30 inches by 30 inches) using ADFP and VARI in high temperature is manufactured.

— Analyzing the quality of the demonstrator shows less than 0.5 % void content with a fiber volume fraction above 60%, which are within the acceptable ranges of the aerospace industry.

In addition to the above contributions, there are also two publications:

1. Ehsani F, Rosca D, Dubreuil H, Gordon S, Dube R, Hoa SV, Shadmehri F, Composite Panel Demonstrator Made by Automated Dry Fiber Placement and Resin Infusion, Canadian International Conference on Composite Materials, Fredericton, July 2022.

2. Ehsani F, Hoa SV, Shadmehri F, Out-of-Plane Permeability of Preforms made by Automated Dry Fiber Placement (Poster), Colloque Étudiant CREPEC 2022, Montreal, September 2022.

3. Ehsani F, Hoa SV, Shadmehri F, Effect of gaps on preform and laminate made by automated dry fiber placement and resin infusion, submitted for Composites Part A, October 2022.

6.3 Future Outlook

Completing this dissertation opens doors to opportunities for research in automated dry fiber placement and vacuum-assisted resin infusion. Although large-scale demonstrators were manufactured using ADFP, fabricating laminates without free edges still needs to be addressed with this method. Therefore, the following recommendations are proposed for further research in this area:

– Identification of the process parameters of AFP machines with different type of heat sources can result in finding the optimum heating system to deposit dry fiber material.

– In identifying process parameters, tows were deposited without any steering. However, process parameters can be effective in the tow buckling of steered tows. Therefore, developing this method for steering in complex geometries should be studied. Different cutout patterns can be fabricated using this method.

– Comparing the mechanical performance of laminates made by this method with those made by conventional prepreg-autoclave can be studied considering similar fiber and matrix for both methods. In this way, cost and energy can also be compared.

– The comparative study presented in this thesis is narrowed down to out-of-plane permeability, however, the effect of tailored gaps on the in-plane permeability can also be considered.

References

[1] Aero Montreal, "Aero Montreal; Aerospace sector." https://www.aeromontreal.ca/aerospace.html (accessed Sep. 14, 2021).

[2] International Trade Administration of Unites States of America, "Canada - Country Commercial Guide; Aerospace and Defense," Aug. 03, 2022. https://www.trade.gov/country-commercial-guides/canada-aerospace-and-defense (accessed Sep. 14, 2022).

[3] Y. Xu, J. Zhu, Z. Wu, Y. Cao, Y. Zhao, and W. Zhang, "A review on the design of laminated composite structures: constant and variable stiffness design and topology optimization," *Advanced Composites and Hybrid Materials*, vol. 1, no. 3. Springer Science and Business Media B.V., pp. 460–477, Sep. 01, 2018. doi: 10.1007/s42114-018-0032-7.

[4] Ginger Gardiner, "Composites World; A350 XWB update - Smart manufacturing," Jan. 09, 2011. https://www.compositesworld.com/articles/a350-xwb-update-smart-manufacturing (accessed Sep. 14, 2021).

[5] Jeff Sloan, "Large, high-volume, infused composite structures on the aerospace horizon," *Composites World*, 2019. Accessed: Nov. 20, 2022. [Online]. Available: https://www.compositesworld.com/articles/large-high-volume-infused-composite-structures-on-the-aerospace-horizon

[6] R. A. Witik, F. Gaille, R. Teuscher, H. Ringwald, V. Michaud, and J. A. E. Månson, "Economic and environmental assessment of alternative production methods for composite aircraft components," *J Clean Prod*, vol. 29–30, pp. 91–102, Jul. 2012, doi: 10.1016/j.jclepro.2012.02.028.

[7] Y. N. Liu, C. Yuan, C. Liu, J. Pan, and Q. Dong, "Study on the resin infusion process based on automated fiber placement fabricated dry fiber preform," *Sci Rep*, vol. 9, no. 1, Dec. 2019, doi: 10.1038/s41598-019-43982-1.

[8] G. Dell'Anno *et al.*, "Automated manufacture of 3D reinforced aerospace composite structures," *International Journal of Structural Integrity*, vol. 3, no. 1, pp. 22–40, 2012, doi: 10.1108/17579861211209975.

[9]   S. van Oosterom, T. Allen, M. Battley, and S. Bickerton, "An objective comparison of common vacuum assisted resin infusion processes," *Compos Part A Appl Sci Manuf*, vol. 125, Oct. 2019, doi: 10.1016/j.compositesa.2019.105528.

[10]   S. v. Hoa, *Principles of the Manufacturing of Composite Materials*. DEStech Publications, 2009.   Accessed: Nov.   09,   2020.   [Online].   Available: https://books.google.ca/books/about/Principles_of_the_Manufacturing_of_Compo.html?id =BiplTS70dw0C&redir_esc=y

[11]   A. Brasington, C. Sacco, J. Halbritter, R. Wehbe, and R. Harik, "Automated fiber placement: A review of history, current technologies, and future paths forward," *Composites Part C: Open Access*, vol. 6. Elsevier B.V., Oct. 01, 2021. doi: 10.1016/j.jcomc.2021.100182.

[12]   E. Oromiehie, B. G. Prusty, P. Compston, and G. Rajan, "Automated fibre placement based composite structures: Review on the defects, impacts and inspections techniques," *Composite Structures*, vol. 224. Elsevier Ltd, Sep. 15, 2019. doi: 10.1016/j.compstruct.2019.110987.

[13]   M. B. Gruber, M. A. Lamontia, and B. J. Waibel, "Automated fabrication processes for large composite aerospace structures: A trade study," *Materials Science*, 2007, Accessed: Nov.   09,   2021.   [Online].   Available: https://www.researchgate.net/publication/237240904_Automated_fabrication_processes_f or_large_composite_aerospace_structures_A_trade_study

[14]   F. C. Campbell, *Manufacturing Processes for Advanced Composites*. Elsevier, 2004. [Online].   Available: https://app-knovel-com.lib-ezproxy.concordia.ca/hotlink/khtml/id:kt009ADCP5/manufacturing-processes/introduction-composite

[15]   D. H. J. A. Lukaszewicz, C. Ward, and K. D. Potter, "The engineering aspects of automated prepreg layup: History, present and future," *Compos B Eng*, vol. 43, no. 3, pp. 997–1009, Apr. 2012, doi: 10.1016/j.compositesb.2011.12.003.

[16]   M. B. Gruber, M. A. Lamontia, and B. J. Waibel, "Automated fabrication processes for large composite aerospace structures: A trade study," *Materials Science*, 2007, Accessed: Nov.   09,   2021.   [Online].   Available:

https://www.researchgate.net/publication/237240904_Automated_fabrication_processes_for_large_composite_aerospace_structures_A_trade_study

[17] L. Veldenz, "Automated Dry Fibre Placement and Infusion Process Development for Complex Geometries," PhD Thesis, University of Bristol, Bristol, 2019. Accessed: Sep. 14, 2022. [Online]. Available: https://research-information.bris.ac.uk/en/studentTheses/automated-dry-fibre-placement-and-infusion-process-development-fo

[18] L. Veldenz, M. di Francesco, P. Giddings, B. C. Kim, and K. Potter, "Material selection for automated dry fiber placement using the analytical hierarchy process," *Advanced Manufacturing: Polymer and Composites Science*, vol. 4, no. 4, pp. 83–96, Oct. 2018, doi: 10.1080/20550340.2018.1545377.

[19] L. Veldenz, S. Astwood, G. Dell, B. Chul Kim, M. di Francesco, and K. Potter, "Characteristics and Processability of Bindered Dry Fibre Material for Automated Fibre Placement," in *ECCM17 - 17th European Conference on Composite Materials*, 2016. Accessed: Nov. 09, 2022. [Online]. Available: https://www.researchgate.net/publication/304896784_CHARACTERISTICS_AND_PROCESSABILITY_OF_BINDERED_DRY_FIBRE_MATERIAL_FOR_AUTOMATED_FIBRE_PLACEMENT

[20] M. Belhaj *et al.*, "Dry fiber automated placement of carbon fibrous preforms," *Compos B Eng*, vol. 50, pp. 107–111, Jul. 2013, doi: 10.1016/j.compositesb.2013.01.014.

[21] R. Agogue, N. Chebil, M. Deleglise-Lagardere, P. Beauchene, and C. H. Park, "Efficient Permeability Measurement and Numerical Simulation of the Resin Flow in Low Permeability Preform Fabricated by Automated Dry Fiber Placement," *Applied Composite Materials*, vol. 25, no. 5, pp. 1169–1182, Oct. 2018, doi: 10.1007/s10443-017-9659-8.

[22] A. R. Aziz, M. A. Ali, X. Zeng, R. Umer, P. Schubel, and W. J. Cantwell, "Transverse permeability of dry fiber preforms manufactured by automated fiber placement," *Compos Sci Technol*, vol. 152, pp. 57–67, Nov. 2017, doi: 10.1016/j.compscitech.2017.09.011.

[23] A. X. H. Yong *et al.*, "Out-of-plane permeability measurement for reinforcement textiles: A benchmark exercise," *Compos Part A Appl Sci Manuf*, vol. 148, Sep. 2021, doi: 10.1016/j.compositesa.2021.106480.

[24] F. Lionetto, A. Moscatello, G. Totaro, M. Raffone, and A. Maffezzoli, "Experimental and numerical study of vacuum resin infusion of stiffened carbon fiber reinforced panels," *Materials*, vol. 13, no. 21, pp. 1–17, Nov. 2020, doi: 10.3390/ma13214800.

[25] William H. Seemann, "Plastic transfer molding techniques for the production of fiber reinforced plastic structures," Feb. 20, 1990 Accessed: Sep. 25, 2022. [Online]. Available: https://patents.google.com/patent/US4902215A/en

[26] J. Glancey, "Vacuum-Assisted Resin Transfer Molding," 2010, pp. 531–544. doi: 10.1201/b10386-19.

[27] P. Hubert, R. Byron Pipes, and B. W. Grimsley, "Variability Analysis in Vacuum Assisted Resin Transfer Molding," *NASA Technical Reports Server*, 2002, Accessed: Sep. 25, 2022. [Online]. Available: https://ntrs.nasa.gov/citations/20030015404

[28] N. Gharabegi, "Composite Laminates Made by Automated Fiber Placement of Dry Fibers and Vacuum Assisted Resin Transfer Molding," Masters thesis, Concordia University, Montreal, 2018. Accessed: Nov. 13, 2022. [Online]. Available: https://spectrum.library.concordia.ca/id/eprint/983680/

[29] Concordia University, "Concordia Centre for Composites (CONCOM)." https://www.concordia.ca/research/composites.html (accessed Nov. 09, 2022).

[30] O. Aghababaei Tafreshi, S. van Hoa, F. Shadmehri, D. M. Hoang, and D. Rosca, "Determination of convective heat transfer coefficient for automated fiber placement (AFP) for thermoplastic composites using hot gas torch," *Advanced Manufacturing: Polymer and Composites Science*, vol. 6, no. 2, pp. 86–100, Apr. 2020, doi: 10.1080/20550340.2020.1764236.

[31] F. Ehsani, F. Shadmehri, S. v. Hoa, D. Rosca, and Gordon S, "Study of Automated Dry Fiber Placement process carries out with Vacuum Assist Resin Transfer Molding," Montreal, Nov. 2020.

[32] Ehsani F *et al.*, "Composite Panel Demonstrator made by Automated Dry Fiber Placement and Resin Infusion," in *The 12th Canadian-International Conference on Composites, CANCOM 2022*, Jul. 2022.

[33]   F. Lionetto, A. Moscatello, and A. Maffezzoli, "Effect of binder powders added to carbon fiber reinforcements on the chemoreology of an epoxy resin for composites," *Compos B Eng*, vol. 112, pp. 243–250, Mar. 2017, doi: 10.1016/J.COMPOSITESB.2016.12.031.

[34]   Cytec Solvay, "CYCOM ® 7720 RTM Preform Binder," 2010. [Online]. Available: www.cytec.com

[35]   J. Vilà, C. González, and J. Llorca, "Fabric compaction and infiltration during vacuum-assisted resin infusion with and without distribution medium," *J Compos Mater*, vol. 51, no. 5, pp. 687–703, Mar. 2017, doi: 10.1177/0021998316649783.

[36]   Airtech, "DAHLTEXX SP-2 - Air permeable resin barrier material," 2016. Accessed: Jul. 03, 2021. [Online]. Available: https://airtechintl.com/

[37]   F. Ehsani, S. van Hoa, and F. Shadmehri, "Effect of gaps on preform and laminate made by automated dry fiber placement and resin infusion (submitted)," *Composites Part A*, Oct. 2022.

[38]   A. J. Comer, D. Ray, G. Clancy, W. Obande, and W. Stanley, "Effect of Moisture on the Mechanical Properties of Composite Laminates Manufactured Using Benzoxazine Resin Systems for Aerospace Applications," in *SETEC 14 Tampere Conference & Table Top Exhibition*, Nov. 2014. doi: 10.13140/2.1.2616.7041.

[39]   Ginger Gardiner, "Semipermeables: Next trend in infusion?," *Composites World*, 2014. Accessed: Oct. 31, 2022. [Online]. Available: https://www.compositesworld.com/articles/semipermeables-next-trend-in-infusion

[40]   Huntsman, "Araldite ® LY 8601 Aradur ® 8602 System Advanced Materials Araldite ® LY 8601 / Aradur ® 8602 System EPOXY RESIN SYSTEM," 2010.

[41]   Hexion, "Technical Data Sheet of EPON^{TM} Resin 862." Accessed: Mar. 06, 2022. [Online]. Available: https://www.hexion.com/CustomServices/PDFDownloader.aspx?type=tds&pid=1acdf63b -5814-6fe3-ae8a-ff0300fcd525

[42]   Solvay, "PRISM^{TM} EP2400." https://www.solvay.com/en/product/prism-ep2410-resin-system (accessed Apr. 03, 2022).

[43]   N. Saba, M. Jawaid, and M. T. H. Sultan, "An overview of mechanical and physical testing of composite materials," in *Mechanical and Physical Testing of Biocomposites, Fibre-*

Reinforced Composites and Hybrid Composites, Elsevier, 2018, pp. 1–12. doi: 10.1016/B978-0-08-102292-4.00001-1.

[44] ASTM, "Standard Test Method for Compressive Properties of Polymer Matrix Composite Materials with Unsupported Gage Section by Shear Loading, ASTM D3410".

[45] R. Shanku, J. G. Vaughan, and J. A. Roux, "Rheological characteristics and cure kinetics of EPON 862/W epoxy used in pultrusion," *Advances in Polymer Technology*, vol. 16, no. 4, pp. 297–311, Nov. 1997, doi: https://doi.org/10.1002/(SICI)1098-2329(199711)16:4<297::AID-ADV4>3.0.CO;2-Q.

[46] CKN Knowledge in Practice Centre contributors, "Degree of cure (A104)," Apr. 23, 2021. https://compositeskn.org/KPC/index.php?title=A104&oldid=5698 (accessed Nov. 16, 2022).

[47] M. Thor, M. G. R. Sause, and R. M. Hinterhölzl, "Mechanisms of origin and classification of out-of-plane fiber waviness in composite materials — A review," *Journal of Composites Science*, vol. 4, no. 3, 2020, doi: 10.3390/jcs4030130.

[48] X. Li, S. R. Hallett, and M. R. Wisnom, "Modelling the effect of gaps and overlaps in automated fibre placement (AFP)-manufactured laminates," *Science and Engineering of Composite Materials*, vol. 22, no. 2, pp. 115–129, Mar. 2015, doi: 10.1515/secm-2013-0322.

[49] J. H. Chen, M. A. Octeau, M. Hojjati, and A. Yousefpour, "Cure cycle optimisation for composite panels fabricated by RTM using dielectric sensors," in *17th International Conference on Composite Materials, ICCM-17*, 2009. Accessed: Nov. 21, 2022. [Online]. Available: http://iccm-central.org/Proceedings/ICCM17proceedings/Themes/Manufacturing/COMPOSITES%20FORMING/INT%20-%20COMPOSITES%20FORMING/IC1.3%20Chen.pdf

[50] H. Dubreuil, S. Gordon, and F. Ehsani, "Infusion Process at Elevated Temperature for Curved Large Panel (Report)," Montreal, 2021.

[51] Pacific Engineering Systems International, "PAM-RTM." Accessed: Nov. 16, 2022. [Online]. Available: https://www.esi.com.au/software/pamrtm/